

DOKUZ EYLÜL UNIVERSITY
GRADUATE SCHOOL OF NATURAL AND APPLIED SCIENCES

**MODELING AND CONTROL OF RAW
EMISSIONS OF A DIESEL ENGINE UNDER
PRACTICAL CONDITIONS**

by
Emrah Cihan ÇEBİ

November, 2012

İZMİR

MODELING AND CONTROL OF RAW EMISSIONS OF A DIESEL ENGINE UNDER PRACTICAL CONDITIONS

**A Thesis Submitted to the
Graduate School of Natural and Applied Sciences of Dokuz Eylül University
In Partial Fulfillment of the Requirements for the Degree of Doctor of
Philosophy in Mechatronics Engineering, Mechatronics Engineering Program**

**by
Emrah Cihan ÇEBİ**

November, 2012

İZMİR

to my grandfather, Kemal Aydın (1933-2011)

for all that he has given me and our family

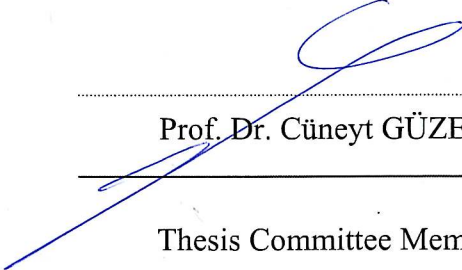
PH.D. THESIS EXAMINATION RESULT FORM

We have read the thesis entitled “**MODELING AND CONTROL OF RAW EMISSIONS OF A DIESEL ENGINE UNDER PRACTICAL CONDITIONS**” completed by **EMRAH CİHAN ÇEBİ** under supervision of **PROF. DR. EROL UYAR** and we certify that in our opinion it is fully adequate, in scope and in quality, as a thesis for the degree of Doctor of Philosophy.




Prof. Dr. Erol UYAR

Supervisor




Prof. Dr. Cüneyt GÜZELİŞ

Thesis Committee Member



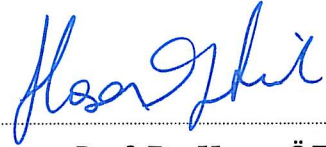
Assoc. Prof. Dr. Zeki KIRAL

Thesis Committee Member



Assist. Prof. Dr. Osman Akın KUTLAR

Examining Committee Member



Assoc. Prof. Dr. Hasan ÖZTÜRK

Examining Committee Member



Prof. Dr. Mustafa SABUNCU

Director

Graduate School of Natural and Applied Sciences

ACKNOWLEDGEMENTS

This work has been carried out at Daimler AG, Group Research and Advanced Engineering, Powertrain Control Dept. (GR/AKP) in Stuttgart, Germany and supported by Dokuz Eylül University, Izmir, Turkey and Esslingen University of Applied Sciences, Esslingen, Germany.

I would like to thank Josef Steuer, Michael Mladek, Christian Dengler, Johan Eldh, Simon Binder, Matthias Schmidt and Werner Mayer for their constructive suggestions during the many discussions we had and for their support throughout the work. Moreover thanks to Yuriy Bogachik for his help in measurement data allocation. Not to forget, thanks to Onur Nihat Demirer, Hannes Lay and Mahmut Özel for their valuable contributions during their internships at Daimler AG.

My sincere thanks goes to my professors Erol Uyar and Gregor Rottenkolber for the supervision of this work and their flexibility, Zeki Kırıl, Cüneyt Güzeliş for their support and advice during our thesis meetings and also Peter Schmid for making this cooperation possible at the first place. Moreover, I would like to express my gratitude to Zuhale Temiz for making life easier with student affairs formalities.

Further appreciation goes to my friends Kadir Burak Keskinliç, Okan Tiritiođlu, Nils Brinkert, Salih Kerem Tüfekçi and Merdan Başaran for their suggestions and support regarding my thesis.

Above all, I can't thank my beloved family enough for standing by my side under all circumstances throughout my entire life. My deepest gratitude goes to them, my father Ramis Çebi, my mother Nurten Çebi and my brother Yusuf Ateş Çebi.

Emrah Cihan Çebi

MODELING AND CONTROL OF RAW EMISSIONS OF A DIESEL ENGINE UNDER PRACTICAL CONDITIONS

ABSTRACT

A real-time capable in-cylinder pressure based diesel engine-out PM estimator has been developed. Using the ECU signals and in-cylinder pressure data new variables have been derived and used as inputs for an exponential zero dimensional modeling approach. This approach required little computational effort making the ECU capable of cycle based PM emissions calculation, significantly faster than in real-time. Along with the PM estimator an accurate NO_x emissions model has been utilized in a MIMO feedback controller motivated by the gain scheduling concept. Two types of experimental passenger car DI diesel engines, equipped with in-cylinder pressure sensors have been used. Measurements have been taken during steady state and transient operation on engine test benches for development work. Implementation of the emission models and the controller has been done on a test vehicle and tests were carried out on the test track and vehicle test bench. Good correlation between the estimated and measured PM has been achieved for various experiments, not only at steady state operation but also for transient states. Particularly, the model delivers good qualitative results in general, as well as good quantitative results in some regions. PM emission gradients between operating points are represented successfully. The raw emissions controller – despite further need for optimization – has been successful in controlling PM and NO_x emissions simultaneously over EGR and pilot injection quantity. Gain scheduling has eliminated the need for an inverse combustion model. EGR and injector actuators were manipulated in a cascaded controller structure where the designed PI controllers altered reference values of the actual EGR and pilot injection quantity controllers that were already present in the system.

Keywords: Particulate matter, soot, nitrogen oxides, emissions control, in-cylinder pressure, empirical modeling, gain scheduling, diesel engine.

BİR DİZEL MOTORUN HAM EMİSYONLARININ SAHA KOŞULLARINDA MODELLENMESİ VE KONTROLÜ

ÖZ

Bir dizel motorun ham partikül madde emisyonlarının hesaplanması için gerçek zamanlı silindir içi basınca dayalı bir model geliştirilmiştir. Motor kontrol ünitesi ve silindir içi basınç verileri kullanılarak yeni değişkenler türetilmiş ve değişkenlerin üstel çarpımlarını esas alan sıfır boyutlu bir yöntem kullanılmıştır. Bu yaklaşım düşük hesap gücüne ihtiyaç duyarak motor kontrol ünitesinin partikül madde emisyonlarını devir bazlı hesaplayabilmesine olanak sağlamıştır. Partikül madde modeli, halihazırdaki bir azot oksit emisyon modeli ile birlikte çok girişli çok çıkışlı, kazanç ayarlama yöntemini kullanan, kapalı çevrim kontrol sisteminde kullanılmıştır. Çalışma silindir içi basınç ölçüm sensörleriyle donatılmış iki çeşit deneysel direk enjeksiyonlu dizel binek araç motoru üzerinde yapılmıştır. Geliştirme sırasında motor test düzeneğinde elde edilen kararlı ve geçici rejim ölçüm verilerine başvurulmuştur. Model ve kontrolör bir test aracına uyarlanarak test pistinde ve araç test düzeneğinde testler yapılmıştır. Yapılan çeşitli testler sonucunda model tarafından hesaplanan değerlerle ölçülen partikül madde emisyonları arasında oldukça iyi korelasyon gözlemlenmiştir. Model nitel anlamda ve bazı bölgelerde nicel olarak iyi sonuçlar göstermiş ve farklı çalışma koşulları arasındaki emisyon gradyanlarını başarıyla ortaya koymuştur. İlave bir optimizasyon yapılmamasına rağmen ham emisyon kontrol sistemi partikül madde ve azot oksit emisyonlarını egzoz gazı çevrim oranı ve ön enjeksiyon miktarını ayarlayarak kontrol etmede başarılı olmuştur. Kazanç ayarlama yöntemi sayesinde motorun bir invers modeline ihtiyaç duyulmamıştır. Egzoz gazı çevrim ve enjeksiyon sistemlerinin referans değerleri ardışık yapıda yapıda oransal integral kontrol kullanılarak ayarlanmıştır. Böylelikle motorda halihazırda var olan kontrol sistemlerinden faydalanılmıştır.

Anahtar sözcükleri: Partikül madde, is, azot oksit, emisyon kontrolü, silindir içi basınç, empirik modelleme, kazanç ayarlama, dizel motor.

CONTENTS

	Page
PH.D. THESIS EXAMINATION RESULT FORM	ii
ACKNOWLEDGEMENTS	iii
ABSTRACT	iv
ÖZ	v
CHAPTER ONE – INTRODUCTION	1
1.1 State of the Art and Motivation.....	1
1.2 Objectives.....	8
1.3 Outline.....	9
CHAPTER TWO – FUNDAMENTALS.....	11
2.1 HSDI Diesel Engine – System Overview	11
2.2 Combustion in Diesel Engines.....	13
2.3 Pollutants.....	19
2.3.1 NO _x Emissions	21
2.3.2 PM Emissions	22
2.3.3 Soot - NO _x Tradeoff.....	27
2.3.4 Effect of Engine Parameters on NO _x and PM.....	27
2.3.4.1 Exhaust Gas Recirculation	28
2.3.4.2 Boost Pressure.....	29
2.3.4.3 Inlet-Port Shutoff	30
2.3.4.4 Injection Timing.....	31
2.3.4.5 Rail Pressure	32
2.3.4.6 Pilot Injection.....	33
2.3.4.7 Post Injection.....	34
2.3.4.8 Glow Plug Activation.....	34
2.4 Emission Modeling Approaches	35
2.4.1 Empirical Models.....	35

2.4.2	Phenomenological Models	36
2.4.3	Complex Multidimensional Models.....	36
CHAPTER THREE – DATA ACQUISITION & PROCESSING		38
3.1	Calibration & Validation Datasets	38
3.2	Measured Data and Derivations	40
3.2.1	In-Cylinder Pressure	40
3.2.1.1	Offset Correction.....	41
3.2.1.2	Heat Release Rate Calculation.....	42
3.2.2	Particulate Matter Mass.....	45
3.2.2.1	Cycle Based PM Mass	48
3.2.3	Fuel Injection Rate	49
3.2.4	ECU Signals.....	52
3.3	Emission Test Cycles	52
CHAPTER FOUR – PM EMISSIONS MODELING.....		55
4.1	Phenomenological Modeling Approach.....	55
4.2	Empirical Modeling Approaches	56
4.2.1	Variable Selection	58
4.2.1.1	Rail Pressure	59
4.2.1.2	Unburned Air Mass Concentration at IVC & EVO	59
4.2.1.3	Main and Diffusive Combustion Duration.....	61
4.2.1.4	Characteristic Time	63
4.2.1.5	Engine Speed.....	65
4.2.1.6	Other Variables	66
4.2.2	Engine Operating Regions	66
4.2.3	Polynomial Approach	67
4.2.3.1	Calibration.....	67
4.2.3.2	Results.....	68
4.2.4	Exponential Products Approach.....	70
4.2.4.1	Calibration.....	71

4.2.4.2	Results	73
4.2.5	Sensitivity Analysis of the Model Variables.....	81
4.2.5.1	Engine A	81
4.2.5.2	Engine B.....	83
4.2.6	Model Sensitivity to Pressure Signal Deviations.....	86
CHAPTER FIVE – IN-CYLINDER EMISSIONS CONTROL		89
5.1	Actuating Variables Selection.....	91
5.2	Emissions Controller Design	92
5.2.1	Gain Scheduling.....	94
5.2.2	Calibration.....	95
5.2.3	Implementation & Tests.....	99
5.2.4	Results	102
5.3	Discussion on overall performance.....	107
CHAPTER SIX – CONCLUSIONS & OUTLOOK.....		111
REFERENCES.....		115
APPENDICES		131
A.1	Specifications of In-Cylinder Pressure Sensors	131
A.2	Specifications of PM Measurement Instrumentation.....	132
B.1	Nomenclature	133
B.2	List of Figures	136
B.3	List of Tables	141

CHAPTER ONE

INTRODUCTION

Diesel fuel powered vehicles have been quite popular in the last decades and diesel engines have been a great benefit to the society. They were used mainly for transportation of goods, people and for heavy duty applications. Later on they became increasingly popular in the passenger car sector, especially in Europe and continuing to be the power source behind commercial transportation worldwide as mentioned by Walker (2004) and many others.

The main reason for the diesel engine's popularity has been the superior fuel economy. It has been the foundation of the competitiveness of the diesel engine. Fuel efficiency is followed by other factors such as better drivability due to high low-end torque at lower engine speeds, excellent durability owing to more robust engine construction and lower engine speeds during operation etc.

On the other hand it has some well known weaknesses that have hindered it to become more popular. The well known black smoke coming out of the exhaust pipe of a diesel powered vehicle and the high noise levels compared to a gasoline powered counterpart have been the greatest disadvantages in the past (Majewski & Khair, 2006).

1.1 State of the Art and Motivation

There have been certain advances in the diesel engine technologies that have helped diesel engines make their way into light duty vehicles and small passenger cars by eliminating the two main problems, black smoke, i.e. PM (Particulate Matter), and high noise levels. However due to the progressive drastic decrease in legislative emission limits especially for PM and NO_x (Nitrogen Oxides) as seen in Table 1.1, producing diesel engines in conformity with these limits has become a challenge whilst keeping the costs at an economically feasible level.

Research evidence suggests that the diesel engine combustion product, PM, is

injurious to human health and environment (Birmili & Hoffmann, 2006; Kagawa, 2002; Majewski & Khair, 2006; McEntee & Ogneva-Himmelberger, 2008). Besides the carcinogenic effects of these particles, PM also contributes to the carbon footprint of diesel vehicles, which is referred to as the amount of carbon produced by any process in the industry. Johnson (2010) stresses that up to one fourth of the carbon footprint of an unfiltered diesel vehicle comes from black carbon, i.e. soot. Furthermore as seen in Figure 1.1 diesel on-road vehicles accounted for already 5% of fine particles produced overall in the industry and over 20% produced by mobile sources in 1997. The reduction of PM together with NO_x has been a crucial subject faced by the automotive industry. It is becoming harder to keep up with the ever decreasing emission limits (Table 1.1) without sacrificing overall engine efficiency.

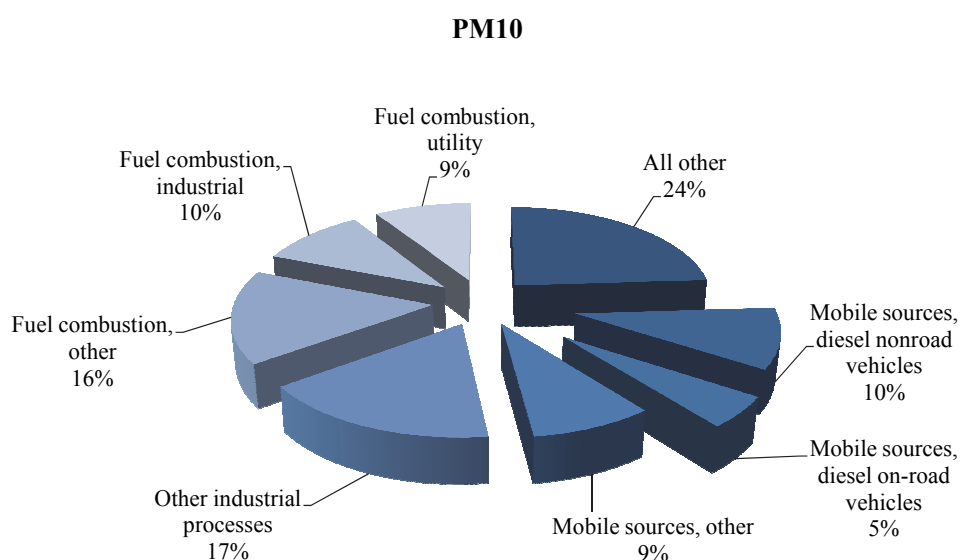


Figure 1.1 U.S. PM₁₀ emission inventory in 1997. PM₁₀ data include exhaust, brake, and tire wear emissions. “Mobile sources, diesel nonroad vehicles” includes railway locomotives, marine vessels and aircraft (Majewski & Khair, 2006). With PM₁₀ it is referred to the particles with less than 10 μ m in diameter.

Exhaust gas leaving the combustion chamber during the exhaust stroke contains the combustion products including pollutants that are harmful to the environment. The emissions at the exhaust manifold, as seen in Figure 1.2, upstream of the exhaust gas aftertreatment system are called raw emissions or engine-out emissions. Main focus of this work is on these raw emissions. Exhaust gas aftertreatment and end-of-

pipe emissions are not the subject of this work.

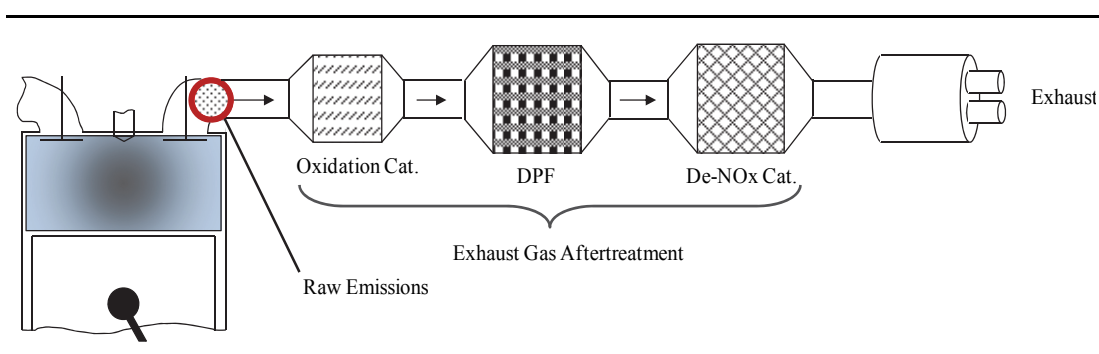


Figure 1.2 Exhaust manifold and the exhaust gas aftertreatment elements on an exemplary state of the art passenger car diesel engine designed to conform to the latest emission norms.

Calibration of engines is namely a three way optimization problem between emissions, fuel consumption and performance. For that purpose, nowadays the raw emissions are estimated in a statistical way with the help of lookup tables that need intensive measurements and the engine parameters are adjusted in such a way that the emissions are kept within certain limits before the exhaust gas aftertreatment system. Also taking fuel consumption and performance into account, an initial calibration of engine parameters is done.

Table 1.1 EU emission standards for passenger cars with compression ignition (diesel) engines. Taken from DieselNet (2012).

Stage	Date	CO	HC	HC+NO _x	NO _x	PM	PN
		g/km					#/km
Euro 1	07.1992	2.72	-	0.97	-	0.14	-
Euro 2, IDI	01.1996	1.0	-	0.7	-	0.08	-
Euro 2, DI	01.1996	1.0	-	0.9	-	0.10	-
Euro 3	01.2000	0.64	-	0.56	0.50	0.05	-
Euro 4	01.2005	0.50	-	0.30	0.25	0.025	-
Euro 5a	09.2009	0.50	-	0.23	0.18	0.005	-
Euro 5b	09.2011	0.50	-	0.23	0.18	0.005	6.0x10 ¹¹
Euro 6	09.2014	0.50	-	0.17	0.08	0.005	6.0x10 ¹¹

Besides this initial calibration, an onboard adaptation of the parameters over the engine's lifetime is desired. However since there is no emissions information available onboard, onboard adaptation can't be realized. There are some sensors that provide feedback and the input values of the actuators are known on the ECU (Engine Control Unit) but these are not enough for especially PM emissions modeling. The reasons will be discussed in the following chapters.

Exhaust gas aftertreatment systems are capable of reducing the emissions to below the legislative limits without too much attention on the raw emission concentrations. However that is possible at the cost of fuel consumption and initial engine part costs. For example a modern DPF (Diesel Particle Filter) for reduction of PM has a considerable effect on fuel economy and initial costs (Richards, Jouaneh, & Bradley, 2003). The same is true for LNT (Lean NO_x Trap) or SCR (Selective Catalytic Reduction) systems for reduction of NO_x emissions. Particles trapped in the DPF cannot be regenerated, i.e. oxidized, passively in cases where the exhaust gas temperatures are too low. In such cases the method called active DPF regeneration is used to warm up the DPF (Walker, 2004). Active regeneration is usually realized by utilizing a post fuel injection by the end of the combustion in the cylinder. Therefore, if the DPF needs to regenerate actively more often due to high raw PM emissions, fuel consumption increases. Respectively, if the raw NO_x emissions are too high a larger LNT might be required. There are different strategies and configurations present that are being or planned to be applied as presented by Leonhard (2009). Depending upon the chosen catalysis strategy; initial cost of the engine could increase (MacLean & Lave, 2003).

Moreover, adaptation of the engines with respect to emissions is only done through initial calibration. If the emissions were to be measured onboard this could change and adaptation of the system parameters could be carried out throughout the complete lifespan of the engine. Thus, it would allow corrections against aging, operational deviations (e.g. fuel quality) and dispersion due to serial production tolerances.

Therefore there is a need for new technologies in order to reduce the operational

tolerances and allow for improved operational flexibility. Improvements can result from modifications to propulsion systems, aftertreatment systems, or fuel types (MacLean & Lave, 2003). These modifications to optimize emissions or combustion in general can be constructional or operational. Constructional means could be through engine or exhaust gas aftertreatment system design as in Majewski & Khair (2006) and Heywood (1988). On the other hand, operational means could be for example taking in-cylinder measures during operation to keep the engine running under certain optimal conditions (Husted, Kruger, Fatic, Ripley, & Kelly, 2007; Bobba, Genzale, & Musculus, 2009). So far the conventional methods of emissions reduction have mainly focused on exhaust gas after-treatment systems as in Johnson (2008 & 2010). As a result, there is a loss in fuel efficiency due to the energy required to power the emission control systems as mentioned earlier. Although these systems are also being tried to be optimally controlled and prove to be effective as in Willems, et al. (2007) the problem originates from the combustion within the cylinder

One way to cope with the problem would be the onboard measurement of engine-out emissions to control the combustion process and the exhaust gas after-treatment system with respect to pollutant emissions. If the engine out PM emissions were to be known with sufficient accuracy, new powertrain control strategies could be developed. For example; during an active DPF regeneration phase, the combustion parameters could be adjusted in a way so that lower NO_x and higher PM could be emitted out of the engine. The decrease in NO_x emissions could be made possible according to the well known soot- NO_x tradeoff (to be discussed in chapter two). As a result, the fuel consumption could be decreased. Even that since the overall NO_x emissions would decrease, a lower performance LNT/SCR system could be realized in the engine package making the system more feasible from an economical point of view.

Regarding PM emissions control, the difficulties associated to onboard PM measurement makes it further complicated. Research is being carried out in order to develop a practical PM sensor as it is also becoming relevant for OBD (On Board

Diagnosis) applications besides closed loop control possibilities (Ochs, Schittenhelm, Genssle, & Kamp, 2010; Hall, Diller, & Matthews, 2008; Stewart, Kolavennu, Borrelli, Hampson, Shahed, & Rhodes, 2006; Warey, Hendrix, Hall, & Nevius, 2004). However a feasible solution for onboard PM measurement does not exist so far that could be mounted on serial production engines. Furthermore, as in Krijnsen, van Leeuwen, Bakker, Calis, & van den Bleek (2001) emission sensors introduce a certain dead-time to the system which is undesirable for control and catalysis purposes. Overall, this motivated the development of an onboard PM estimator, a cost saving software solution compared to a sensor mounting.

PM emissions modeling is a great challenge mainly due to the fact that a great portion of PM, which is formed during the diesel combustion, is oxidized simultaneously, leaving out only a smaller portion emitted out of the engine (see Figure 2.7). Therefore it is seen essential to acquire information about the combustion process in the cylinder. Today's technologies allow acquiring this information from in-cylinder pressure data.

In-cylinder pressure sensors have a long history in engine research and such research sensors for serial production engines with adequate lifetime have been under development for many years (Anastasia & Pestana, 1987; Herden & Küsell, 1994). They have become more durable over the years and series application examples are to be seen. Besides, there is a trend towards closed loop combustion control, which has been made possible with these sensors and other advances in hardware technology. Today, manufacturing of in-cylinder pressure sensors that can withstand the high pressures and shock waves in the combustion chamber has become economically feasible. These in-cylinder pressure sensors are mounted onto the engines as standalone sensors or it is also a common approach that they are integrated into the glow plug. Based on mounting position and structural properties, water cooling can be utilized. Furthermore the processing of crank angle resolved in-cylinder pressure data needs high computational effort which has been impossible for serial production ECUs to handle. Newer ECUs with higher processing power and multiple processing cores would enable the processing of such data (Beasley, et al.,

2006; DaimlerChrysler AG, 2006; Hadler, Rudolph, Dorenkamp, Kösters, Mannigel, & Veldten, 2008; Huang, Yang, Ouyang, Chen, & Yang, 2011; Husted, Kruger, Fattic, Ripley, & Kelly, 2007; Sellnau, Matekunas, Battiston, Chang, & Lancaster, 2000; Schten, Ripley, Punater, & Erickson, 2007; Schiefer, Maennel, & Nardoni, 2003; Schnorbus, Pischinger, Körfer, Lamping, Tomazic, & Tatur, 2008; Steuer, et al., 2009).

This whole trend supports the idea of utilizing in-cylinder pressure in raw emissions modeling since the required hardware components are likely to already exist in the engines. Such emission models in literature vary in complexity and calculation effort to a high extent and are discussed at the end of Chapter 2.

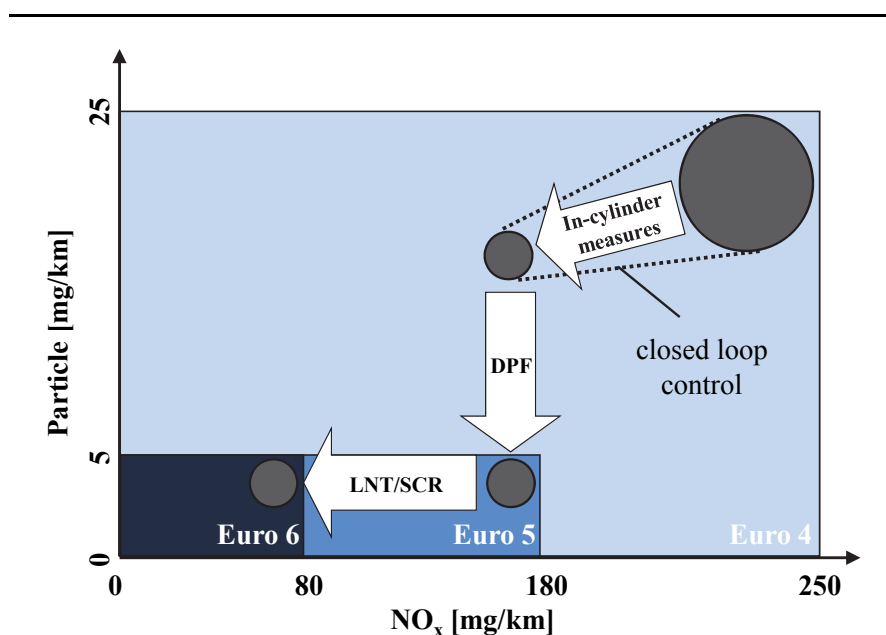


Figure 1.3 Methods of decreasing diesel engine emission levels according to the legislative emission limits

Research concerning the reduction of PM using in-cylinder methods has been carried out for a long time as in Kamimoto & Bae (1988) and Kuo, Henningsen, & Wu (1988). With the utilization of an accurate raw emissions estimator, closed loop control of the combustion would be possible. This would allow economical solutions to be developed in order to keep the emissions under the legislative limits. The aim of closed loop emissions control is not only an overall decrease of the emissions, but

to decrease overall costs. Combustion process and exhaust gas aftertreatment system include significant safety tolerances due to operational uncertainty and aging of the components. Primary objective here is the reduction of system tolerances and increased reproducibility of the system output as depicted in Figure 1.3.

Thanks to the advances in technology and new methods that have been financially cultivated, development times of passenger cars and also powertrains have been drastically reduced. Nevertheless the deadlines to be held during the development for a punctual start of serial production are getting consequently more and more important. Besides, with each model line there is also an increase in the variety of engine configurations. Apart from these the manufacturers are trying to produce more efficient engines with higher performance. Therefore new technologies are being utilized each year. This creates a greater calibration demand with each new technology, not only at the end of the development but also in the early phases (Pasternak, Mauss, Janiga, & Thévenin, 2012). Number of parameters to be calibrated initially for each engine is increasing. Atkinson & Mott (2005) mention that since 1998, the calibration effort required has been drastically increasing for diesel engines. With each new parameter to be calibrated the effort will continue to increase exponentially due to the so called curse of dimensionality. Therefore it is important to have models that can be calibrated easily. This introduces a further challenge into PM emissions modeling.

1.2 Objectives

Below is a list of the objectives that had been set. These can be allocated in two main groups; modeling of PM emissions and controller development.

- I. Development of an emission model for estimating the raw PM emissions of a passenger car diesel engine (refer to Table 3.1 for the engines used in this work). Further desired attributes can be listed as follows:
 - Real time capability and ECU compatibility
 - Based on in-cylinder pressure information

- Preferably, physically motivated
- II. Design of a raw emissions controller utilizing the developed PM emission model. Further, desired attributes can be listed as follows:
- Utilization of common engine actuators
 - Combination with a NO_x emissions controller using a readily available NO_x model or on-board sensor.
 - Implementation and operation of the aforementioned model and controller in the research vehicle.

Main focus of the work has been on the first part. It has been the main challenge, since PM emissions modeling is a difficult task. Furthermore, development of the emissions model was a prerequisite for the second part, the controller.

1.3 Outline

In the following, an outline is given to guide the reader through the different chapters of the thesis. Subject of the chapter and the main points covered are given briefly:

- Chapter 1

This chapter has focused on the initial situation and the motivation behind this work has been briefly discussed. Moreover the main objectives have been defined with the involved boundary conditions.

- Chapter 2

Second chapter will give an insight into the fundamentals involved. An introduction is given to the modern diesel engines for passenger cars that fall into the scope of this work. Diesel combustion process and the emission relevant aspects are covered. Information regarding the relevant emissions and the involved mechanisms are presented. Finally the conventional modeling and control approaches are discussed that have shed light upon this work.

- Chapter 3

Chapter three focuses on the data acquisition and processing as a prerequisite for further work. Equipment and setup used for the measurements along with the measured data and range are presented. Another point covered briefly is the heat release rate calculation from the in-cylinder pressure. Lastly, used standard emission test cycles are mentioned.

- Chapter 4

Fourth chapter marks the main body of the work done and presents the subject raw emissions modeling. Various modeling approaches that have been considered or tried out, the final approach chosen and the reasons for this choice are discussed. Finally the validation results of the developed model are presented along with sensitivity analysis of the model.

- Chapter 5

Fifth chapter unveils the raw emissions controller that is based on the developed model in chapter four. Controller structure and preliminary results are laid out and discussed. Furthermore the implementation of the model on a test vehicle and the hardware configuration is presented.

- Chapter 6

Finally chapter six sums up the work, discuss the strengths and weaknesses of the emissions model and controller. Also some future prospects are presented that should support further research in this field.

CHAPTER TWO

FUNDAMENTALS

In this chapter, diesel engines and the related conventional combustion processes are generally overviewed. After giving an insight to the essential diesel combustion phenomena, diesel engine pollutants are presented followed by a more detailed explanation of the emission mechanisms that are related to this work. Subsequently the relationship between the emissions and several common engine operation variables is discussed. Finally, background information on emission modeling in internal combustion engines with a classification of different approaches is presented.

2.1 HSDI Diesel Engine – System Overview

The first HSDI (High Speed Direct Injection) diesel engine was introduced for light duty vehicles back in 1984 and the first passenger car with DI diesel engine made its way to serial production in 1988. For many years, the diesel engines continued to have a bad reputation worldwide because of their poor performance and black smoke they produced. However certain advances in the engine technologies have made it difficult to distinguish diesel engines from their gasoline counterparts nowadays. Today the HSDI diesel engines can be seen in a large portion of the passenger cars. Out of all the known internal combustion engines, it is the one with the highest efficiency in practice. Its superior fuel efficiency continues to attract many customers especially those who travel or commute long distances (Hawley, Brace, Wallace, & Horrocks, 1998).

Today's HSDI diesel engines incorporate technologies such as flexible high pressure common rail injection systems with piezo-actuators, single or multi-stage turbocharging with VTG (Variable Turbine Geometry), EGR (exhaust gas recirculation) with cooling, intake swirl valve, etc. As discussed in the first chapter diesel engines have many advantages compared to their gasoline counterparts, yet also some disadvantages.

Figure 2.1 is a symbolic layout of a typical HSDI diesel engine system without the exhaust gas aftertreatment. It is taken as reference for the forthcoming parts of the work. Air path and fuel path can be seen clearly on the figure with the respective colors. Also some of the important auxiliary actuators are shown which are controlled by the ECU. This configuration is engine dependent so it usually shows differences from engine to engine.

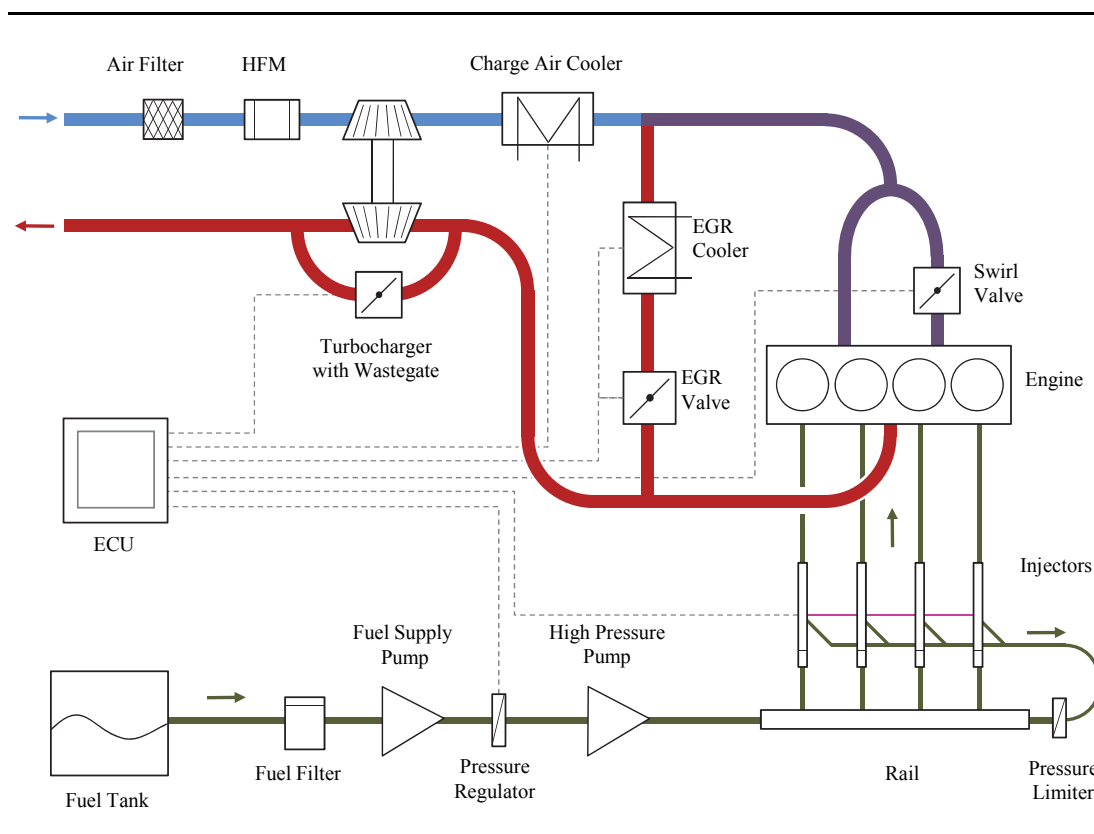


Figure 2.1 HSDI engine system layout without the exhaust gas aftertreatment. Extended from Schmidt (2007).

Common diesel engines – as well as the ones used in this work – (Table 3.1) are equipped with common rail high pressure injection technology with piezo actuators, which enable precise injection with flexible timing. Common rail technology allows high injection pressures even at low engine speeds by keeping the rail pressure at a high level. Furthermore constant injection pressures can be maintained throughout multiple injections in a cycle.

Engines utilized in this work (Table 3.1) are both equipped with high pressure EGR systems with closed loop controlled EGR valves. Recirculated exhaust acts as inert gas during the next combustion cycle and used for reducing the pollutants. This effect will be discussed in section 2.3. An EGR cooler with or without a bypass valve decreases the temperature of the hot exhaust gas amplifying the effect. Some engines are also equipped with an EGR cooler bypass channel with a valve

Higher boost pressures induced by the turbocharger increase the volumetric efficiency of the engine by increasing the charge air density. Boost pressure is regulated via a wastegate valve and/or a VTG depending on the engine configuration. Pressure at the compressor side is usually limited by a pressure limitation valve.

A swirl valve (Elsäßer, Braun, & Jensen, 2000) controls the air passing through the swirl inlet pipe. Usually the opposite valve to the one equipped with the actuator has swirl inducing properties and once the actuator closes one port, air is forced to flow through this inlet pipe with higher speeds creating more swirl inside the cylinder.

ECU controls the whole process chain from the fuel tank, leading to the combustion and power output to the transmission. It analyzes signals received from various sensors (temperature, pressure, mass flow etc.) and sends signals to the actuators to control the engine. Many of the processes are controlled based on lookup tables and some are model based. Although the engine is regarded as a closed loop system as a whole, many processes and their outputs cannot be measured or modeled directly and need better understanding. Especially, there is little feedback on the combustion itself and combustion is still an open loop controlled system based on lookup tables.

2.2 Combustion in Diesel Engines

High boost pressures, high injection pressures and high EGR rates are employed by today's diesel engines. However this hasn't changed the fundamental diesel combustion processes which are still governed by mixture formation, auto-ignition

and turbulent diffusion.

A combustion cycle starts with air induction as in any internal combustion engine. Air consisting of fresh air and recirculated exhaust gas is inducted during the expansion stroke and the inlet valve is closed shortly after the BDC (Bottom Dead Center). Towards the end of the compression stroke, before TDC (Before Top Dead Center), liquid fuel is injected into the compressed air. The fuel-air mixture is prepared physically and chemically for combustion immediately after the penetration of the fuel droplets into the air (Sauter diameter 2-10 μm). Mixture formation is followed by a self ignition of air-fuel mixture in the cylinder under high temperature and pressure, starting the combustion. Self-ignition is characteristic of diesel engine combustion process.

The processes mentioned in the preceding paragraph, namely fuel evaporation, mixture formation, self-ignition and the subsequent combustion occur in parallel sequence. This complicates the detailed analysis of the combustion inside the cylinder.

Mixture formation in the cylinder, preferably prior to combustion start, causes a rather rapid combustion and favors the complete and efficient utilization of the injected fuel. However, it is hard to realize such a favorable case since the time available for the mixture formation is quite short, especially in higher speed passenger car DI diesel engines. Even though the primary injected part of the fuel may conveniently be mixed with the surrounding air, as the mixture ignites after the very short ignition delay time, the rest of the fuel that has still not evaporated or that is yet being injected is forced to burn under inhomogeneous conditions. Mixture formation and combustion are occurring in parallel in this phase. The mixture formation process is accelerated by the increased temperature, pressure and turbulence in the cylinder, but usually there is still not enough time to realize an almost homogeneous mixture (Tschöke & Hieber, 2010).

In Figure 2.2 Renner & Maly (1998) have identified the effects of the several injection and charge air related variables on the combustion output. It could be

interpreted from the diagram that mixture formation is the number one key point in the combustion followed by flow and turbulence.

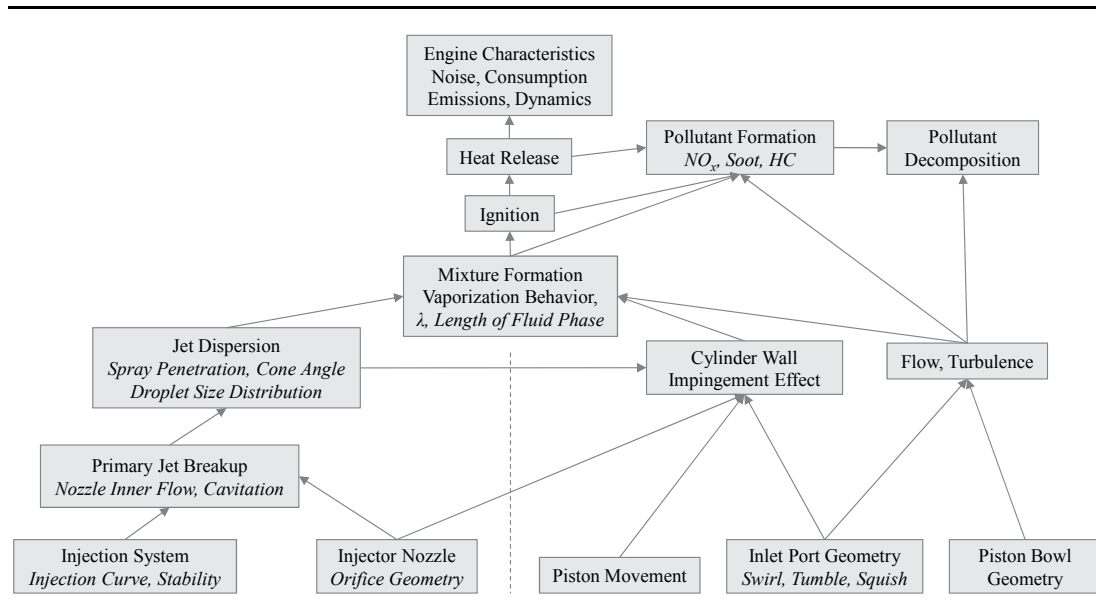


Figure 2.2 Effect chain of fuel injection (lower left) and charge movement parameters in the diesel engine combustion process and pollutant formation (Renner & Maly, 1998).

Mixture formation has a tremendous effect on quality of the combustion. Combustion efficiency and pollutant formation strongly rely on it. Chmela & Orthaber (1999) considers the injection process, coupled strongly with the mixture formation, the most important aspect in controlling the heat release rate. Mixture formation depends on rather constructional factors such as injector geometry, injection system stability and inlet port, cylinder chamber and cylinder bowl geometries. However some operationally adjustable parameters also come into play that could have a significant influence such as injection pressure, swirl valve position and injection timing.

Second key player in the diesel combustion processes is the flow and turbulence. They are discussed together in the following as flow turbulence. An increase in the flow turbulence and the coupled kinetic energy increase favor better mixture formation and usually have desirable effects on the pollutant formation and decomposition processes. Flow turbulence is increased by the following factors (also

taking Figure 2.2 into account):

- High pressure injection of the fuel
- Cylinder charge movement with the help of a swirl valve
- Tumble movement due to the cylinder bowl geometry
- Squish effect of the piston towards the end of the compression stroke
- Combustion itself

High injection pressure induces direct turbulence on the cylinder charge and is mainly effective around TDC. Inlet air turbulence decreases almost linearly towards the end of the cycle. Therefore the injection timing shouldn't be too late to be able to make use of the turbulence induced at IVC. Squish induced turbulence is intense before and after TDC. Turbulence due to cylinder bowl shape is high at TDC and diminishes during expansion (Schubiger, 2001).

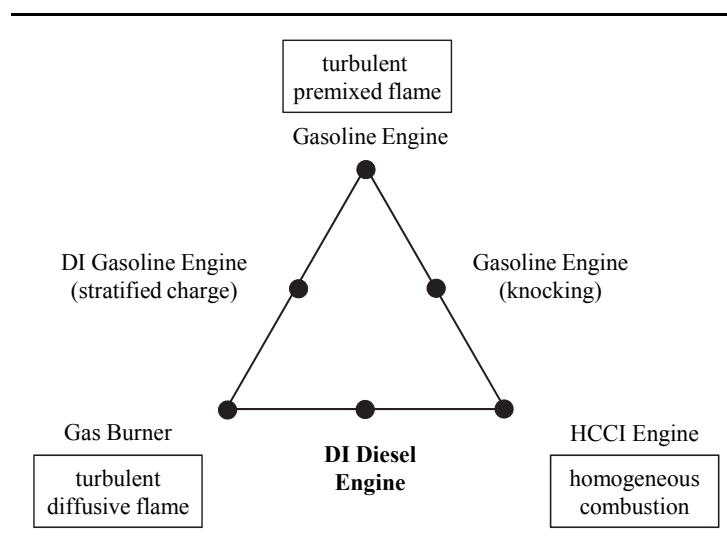


Figure 2.3 Types of combustion in internal combustion engines and their allocation to engine types (Otto F.).

Yet, a homogeneous mixture formation in diesel combustion is not possible as mentioned earlier. Local lambda values within the cylinder vary from zero to infinity in the combustion chamber with the inhomogeneous mixture. This prevents a complete and therefore efficient combustion of the fuel and results in unwanted incomplete combustion products to form. These are referred to as pollutants

(Tschöke & Hieber, 2010).

Regarding diesel combustion, there are two main flame types during combustion. That is premixed and non-premixed - in other words diffusive - flames (see Figure 2.3). In case of premixed flames, fuel and oxidizers are mixed homogeneously prior to the start of combustion and the speed of the combustion is governed by the chemical reaction. Whereas in case of non-premixed flames, combustion and mixture formation take place at the same time, causing physical mixing – molecular diffusion rate of the fuel and the oxidizer – the deciding factor on the speed of the combustion.

Another phenomenon is homogeneous combustion which has partly desirable outcomes in terms of efficiency and pollutant emissions. It is realized in HCCI (Homogeneous Charge Compression Ignition) engines which use gasoline or diesel as fuel depending on the case. However this subject is still under research.

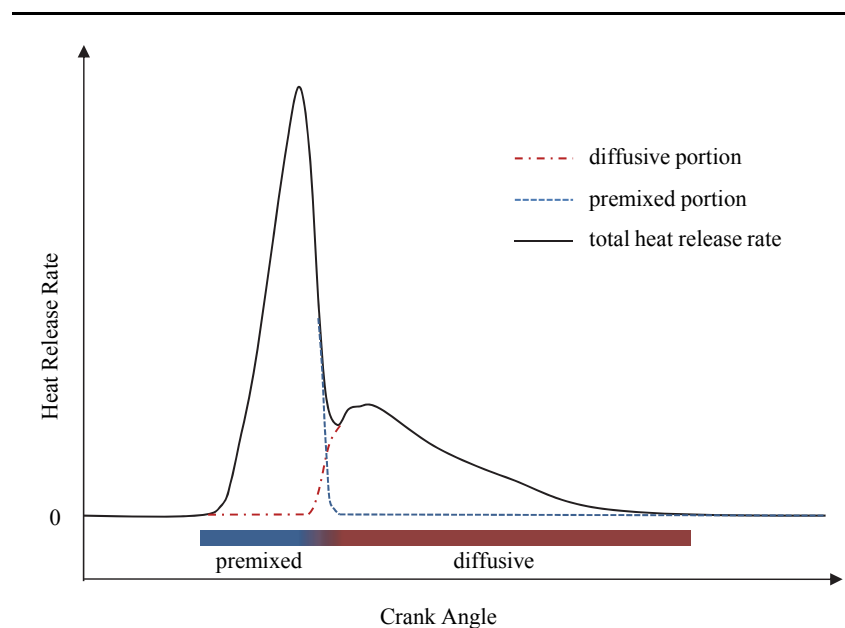


Figure 2.4 Diffusive and premixed portions of the heat release rate approximated by Schubiger (2001) on a heat release rate curve for a single injection. Heat release rate of combustion can be calculated using in-cylinder pressure as described in section 3.2.1.

Schubiger (2001) discusses that it is a challenge to determine the premixed and

diffusive portions of the heat release rate by deriving this from in-cylinder pressure curve. Premixed and diffusive combustion phases occurring not exactly in an order but simultaneously makes the analysis even more difficult. Figure 2.4 roughly depicts how the heat release rate curves look during these two phases of combustion and their sum gives the total heat release rate curve.

For combustion processes with pilot injections, the premixed portion becomes even smaller and the peak heat release rate during the diffusive combustion phase becomes higher. Diffusive combustion is still the predominant portion for conventional diesel combustion. In cooperation with Lay (2009), the diffusive portions of the combustion for individual cycles have been approximated (Figure 2.5) by comparing the temporal curves of fuel injection energy and heat release rate, that are presented later in Figure 4.4 (top). Although the analysis is rather simple and does not necessarily represent accurate data, it has been qualitatively shown for a measured data set on Engine A (Table 3.1) that the combustion is dominated by the diffusive portion. This is an expected behavior of a common HSDI diesel engine.

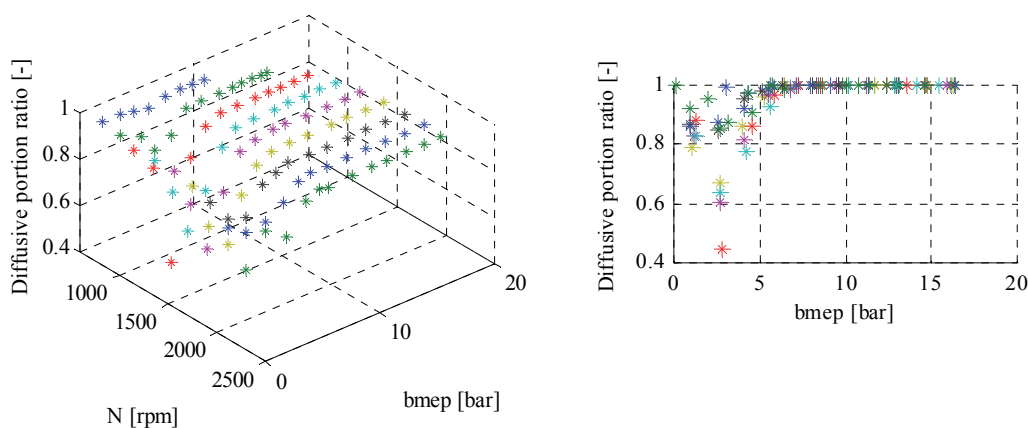


Figure 2.5 Approximated diffusive to total combustion ratio in terms of burned fuel mass fractions (Lay, 2009). Isometric view (left), diffusive portion ratio vs. bmep view (right).

During the more intense premixed combustion peak temperatures are higher than in diffusive combustion which is undesirable in terms of combustion efficiency and mechanical stress on the engine. In case of an ideal diesel cycle, efficiency of the cycle decreases with increasing peak temperature for a given state before

compression and a given compression ratio (Sonntag, Borgnakke, & Van Wylen, 1998). On the other hand, diffusive combustion is easier to be controlled and does not have these effects. But sooting characteristics of diffusion controlled flame type remains to be great problem in concerning PM emissions.

2.3 Pollutants

During the combustion of hydrocarbon based fuel and oxygen present in the air an exothermic reaction occurs. Under ideal conditions, at stoichiometric air/fuel ratios ($\lambda=1$), the combustion products are only nitrogen, water and carbon dioxide. These ideal conditions can be achieved only in average in the cylinder. Diesel engines operate at globally high lambda values of usually higher than one. However, as mentioned earlier, due to the diffusive nature of the combustion relatively lower lambda values are encountered locally. Thus, resulting in incomplete combustion and leading to the formation of pollutants or their precursors.

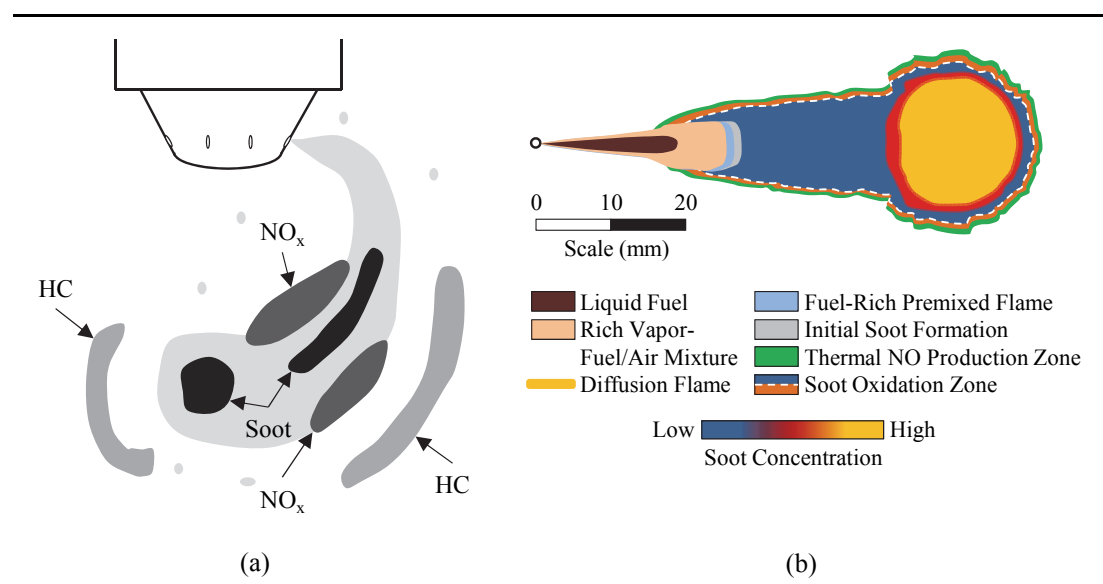


Figure 2.6 (a) Qualitative representation of diesel engine combustion and pollutant formation regions (Merker & Stiesch, 1999). (b) Quasi steady diesel combustion plume displaying the NO production and soot concentration distribution (Dec, 1997).

Main harmful products of internal combustion engines nowadays are NO_x (nitrogen oxides), HC (hydrocarbons), CO (carbon monoxide) and soot/PM

(particulate matter). Exhaust emissions of HC and CO are lower in diesel engines compared to gasoline engines. NO_x exhaust concentrations are comparable to that of gasoline engines and the PM emissions are relatively high compared to gasoline engines. HC emissions become important during the cold start and warm-up phases of engine operation. Specific aromatic compounds of hydrocarbons are responsible for the source of diesel odor and also act as precursors during soot formation. CO emissions are more or less inversely proportional to air/fuel ratio as CO is oxidized during the combustion to form CO_2 (carbon dioxide). CO_2 is typically not mentioned as a pollutant but it has become important owing to its greenhouse gas effect in the atmosphere. As a natural product of combustion CO_2 emissions are directly coupled to the fuel consumption.

Merker & Stiesch (1999) roughly depict the diesel pollutant formation regions as presented in Figure 2.6a. HC is formed in the regions where the flame is unable to reach, such as piston ring cavities or also where the temperatures are relatively low for combustion; along the cylinder walls where flame quenching occurs. Soot is formed in the rich regions of the fuel jet under high temperature and pressure. NO_x is formed in the regions where air entrainment occurs with high turbulence under high temperatures. Another source of pollutants is the foreign substances present in the fuel due to impurities. Sulfur present in the fuel accounts for the SO_2 (sulfur dioxide) and SO_3 (sulfur trioxide) emissions (Heywood, 1988)

In the following subsections, the relevant pollutants NO_x and PM are explained in more detail. Primary focus as expected is on the PM emission mechanisms. Although the final model developed within this work (Chapter 4) does not constitute the detailed emission mechanism, it has been important to understand the processes to be able to select the appropriate approach and the adequate variables.

Next two sections present the theory behind the NO_x and PM formation chemistry. Afterwards, the dependency between these emissions and diesel engine operation is presented. Relationship between emissions and engine operation is regarded to be an important aspect within this work.

2.3.1 *NO_x Emissions*

Nitrogen oxides involve mainly NO and smaller amounts of NO₂ in internal combustion engines. There are two main NO_x formation mechanisms.

- Fuel NO
- Thermal NO (Zeldovich mechanism)

There is a third mechanism called Prompt NO or Fenimore NO where NO is formed as a by-product during some chemical reactions in rich premixed flames. Nonetheless, the contribution of this to the total NO formation is considered negligible (Stebler, 1998).

Fuel NO originates through bonding of the molecular O₂ (oxygen) and N₂ (nitrogen) present in the air under high temperatures and thermal NO mechanism is the reaction of the O₂ with the N₂ present in the fuel. Diesel fuels contain more N₂ than gasoline which would mean higher amounts of fuel NO. Nevertheless the amounts are still considered negligible according to Heywood (1988) at the time but Stebler (1998) denotes that with the emission limits getting stringer the NO that originates from the fuel will become more important. Nevertheless thermal NO in the combustion air is still the most popular mechanism for NO_x formation. Thermal NO formation rates are usually approximated using the Arrhenius reaction rate constant in various models available in literature.

Furthermore, NO_x formation mechanisms result mainly in NO formation, even though NO₂ is thermodynamically favored at lower temperatures. This is due to the short residence times in internal combustion engines (Hawley, Brace, Wallace, & Horrocks, 1998). On the other hand, Majewski & Khair (2006) report that the fraction of NO₂ emissions has increased from 5% in older technology engines up to 15% in the newer turbocharged ones. In spite of this increase, NO still continues to be the precursor and the subject of investigation for internal combustion engine applications.

NO₂, as mentioned earlier, can be formed under low temperature conditions. The

importance of this aspect is that, NO that is discharged into the atmosphere within the exhaust gases can react with the atmospheric O₂ and O₃ (ozone) to form NO₂. NO is an odorless and colorless gas yet toxic gas. Moreover, NO₂ is a major air pollutant as a highly toxic gas with a red-brown color and an unpleasant odor.

Formation of NO occurs in the lean flame region mainly during the premixed combustion where O₂ concentrations are high. Higher peak pressures due to premixed combustion result in higher peak temperatures. Since the NO formation mechanisms are governed by rather fast chemical reactions, such short high temperature time frames are sufficient for high NO formation rates. Likewise thermal NO is produced in the high temperature diffusion flame surrounding the fuel jet according to Dec (1997) as seen in Figure 2.6b.

The biggest difference of in cylinder NO_x mechanisms compared to soot mechanisms is that NO is mainly formed during the combustion and a breakup does not occur. As a result the net NO_x formation rate during the combustion is always positive. Challenges in determining PM emissions will be discussed further in the next section.

At this point no more details about the NO_x formation mechanisms will be given since the subject extends beyond the scope of this work. Only the simple conceptual relations have been enough to understand and implement the measures in the emissions controller which will be discussed in chapter five. For further info in corresponding mechanisms and modeling, refer to Egnell (2001), Gärtner (2001) and Majewski & Khair (2006).

2.3.2 *PM Emissions*

Diesel PM, seen as black smoke coming out of the tailpipe is considered to be one of the most important diesel emissions. The definition of PM extends to all solid and liquid material emitted out of the engine. As a matter of fact, the greater portion of PM is combustion generated elemental carbon, i.e. soot and other compounds adsorbed onto it (condensed HC/SO₄, metallic ash etc.) (Heywood, 1988; Kirchen &

Boulouchos, 2009; Maricq, 2007; Majewski & Khair, 2006; Merker & Stiesch, 1999). This composition of PM depends on engine type and operating point (Abbass, Andrews, Ishaq, Williams, & Bartle, 1991). Net PM formed and emitted out of the engine is a result of soot formation and oxidation processes (see Figure 2.7).

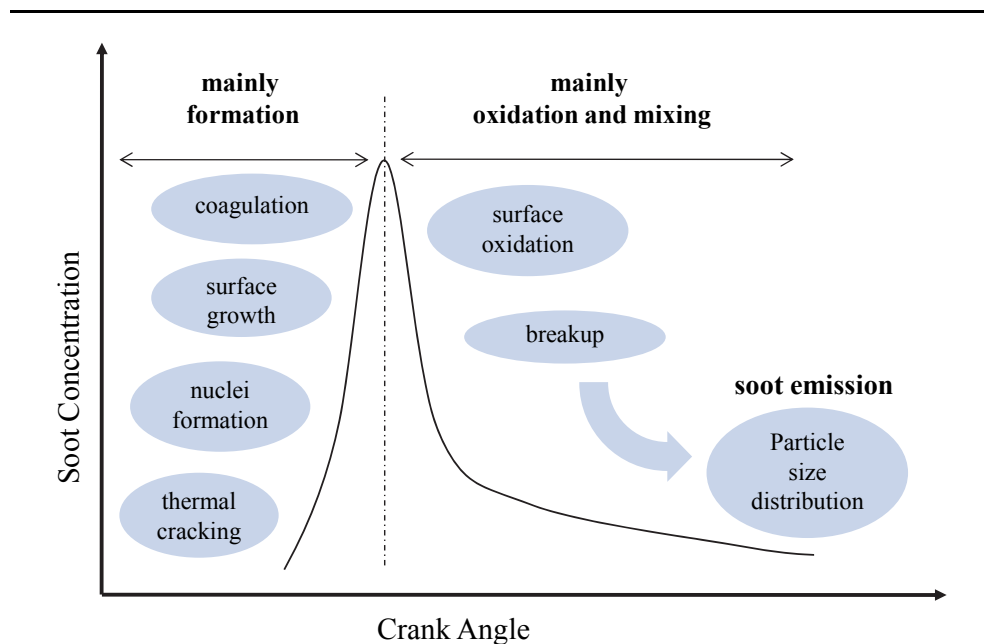


Figure 2.7 Phases of soot formation and oxidation in diesel engine combustion, depicted over crank angle. Adapted from Hopp (2001).

Hopp (2001) mentions two different soot formation mechanisms:

- Ion Formation
- Acetylene Pyrolysis

In spite of many uncertainties in the soot processes, out of the two mechanisms, the formation mechanism through the pyrolysis of acetylene is the widely accepted hypothesis today (Böhm, Bönig, Feldermann, Jander, Rudolph, & Wagner, 1994; Frenklach, 2002; Sung, Lee, Kim, & Kim, 2003; Hopp, 2001). According to this, the key steps in soot formation have been listed as follows:

- Chemical break-up (pyrolysis) of fuel molecules into acetylene and production of simple aromatic compounds) in the partial absence of oxygen.

- Polymerization and formation of PAH's (Polycyclic Aromatic Hydrocarbons) followed by formation of carbon (C) atoms.
- Condensation and formation of radical soot nuclei, formation of the first lattice structures.
- Surface growth of the primary soot particles through adsorption of various substances on the surface. The number of particles stays constant in this phase, whereas the mass concentration increases through surface growth.
- Agglomeration of the primary soot particles to form the longer chain formed structures.
- Coagulation, i.e. the combination of the soot nuclei to form soot particles. Mass concentration stays constant but the number of particles decreases in this phase.
- Finally the particles are oxidized and broken up into elementary carbon. Hopp & Pungs (1998) claim that a partial oxidation of the particles is not possible, they can either be oxidized or stay unoxidized.

In Figure 2.8 these processes described are depicted in a schematic way.

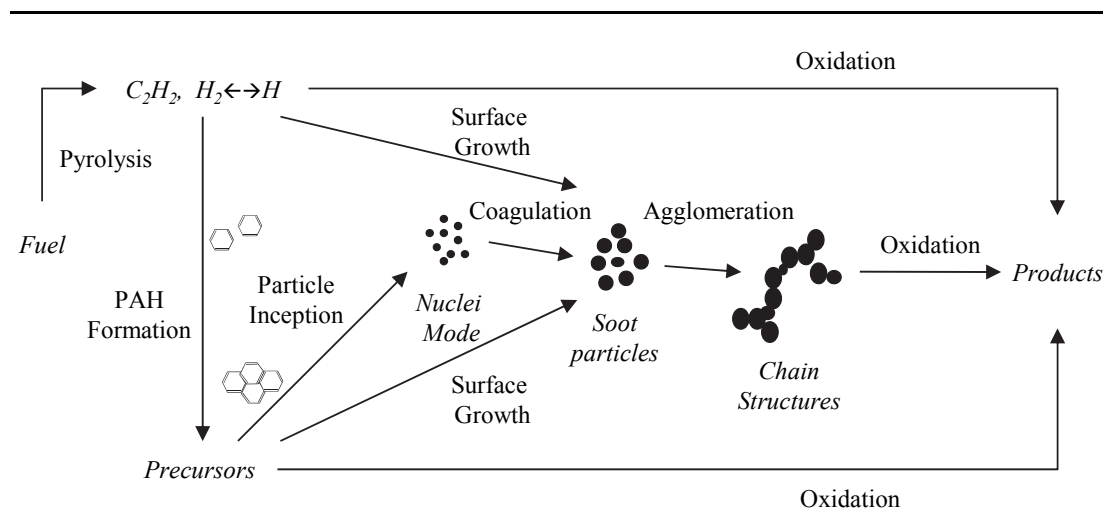


Figure 2.8 A general look into soot formation and oxidation mechanisms. Adapted from Martinot, Beard, & Roesler (2001).

As already mentioned, the composition of PM varies depending on various conditions. According to Vander Wal & Tomasek (2004) there is a dependence of

the soot particle nanostructure upon conditions such as temperature, formation time and fuel type having an effect on the average reactivity of the particles formed. Furthermore the oxidation rates of soot derived from acetylene and benzene differed by nearly five-fold in their work.

Soot is formed as a result of complex physical and chemical processes. The six commonly identified processes involved in soot formation are pyrolysis, nucleation, coalescence, surface growth and agglomeration. Oxidation of soot takes place simultaneously during the formation and continues until the late phases of diesel combustion (Tree & Svensson, 2007). Soot is formed similarly from fuel molecules primarily in under-stoichiometric (λ values around 0.65) and high temperature conditions around 1500 - 1900K (Warth, 2005; Wenzel, 2006). In Figure 2.6b, Dec (1997) describes a model in which the PM formation and growth occur in the fuel rich regions inside the fuel jet and oxidation process takes place at the outer edge of the jet in the diffusive mixing region. Soot is formed in these generally fuel rich regions with λ values around 0.62-0.72 according to Schubiger, Boulouchos, & Eberle (2002). Recalling from the preceding sections, the most significant factor effecting the PM formation is the diffusive combustion ratio. Mohr, Jaeger, & Boulouchos (2001) has carried out investigations on a modern common rail diesel engine. They have varied the premixed/nonpremixed ratio of the combustion systematically using a flexible injection system. At relatively high premixed ratios they have observed a significant decrease in PM emissions in terms of total mass and particle number and a change in the particle size distribution.

Oxidation and breakup of soot particles occur at high temperature regions with sufficient oxygen concentrations. With conventional diesel combustion strategy, where the mixture inside the cylinder is rather heterogeneous, soot formation is inevitable. The amount of PM formed during combustion is relatively high compared to the amount present in the exhaust gas. The reason is that the formed soot is oxidized to a great extent at the later stages of combustion under sufficient temperature and O_2 availability. Therefore oxidation is considered to be decisive on the net soot formed (Kozuch, 2004). Schubiger, Boulouchos, & Eberle (2002) have

also stated that lambda value has a great influence on the oxidation and oxidation is the deciding factor on the PM emissions.

According to Li & Wallace (1995) soot oxidation freezes at temperatures around 1800 K which is higher than the formation temperatures. Schubiger, Boulouchos, & Eberle (2002) argues whether if this is a true approach in modeling since possible reactions of soot in the exhaust and during the late phases of combustion are not taken into account. Hopp & Pungs (1998) have concentrated their work on merely on soot oxidation tried to develop a model for determining the temporal variations of soot during oxidization. They have determined 1300 K as a minimum temperature for soot oxidation in diesel engine conditions, and added that oxidation rates of over 60% are attained at temperatures higher than 1500 K. At peak temperatures of 1700 K, 80-90% of the soot was oxidized.

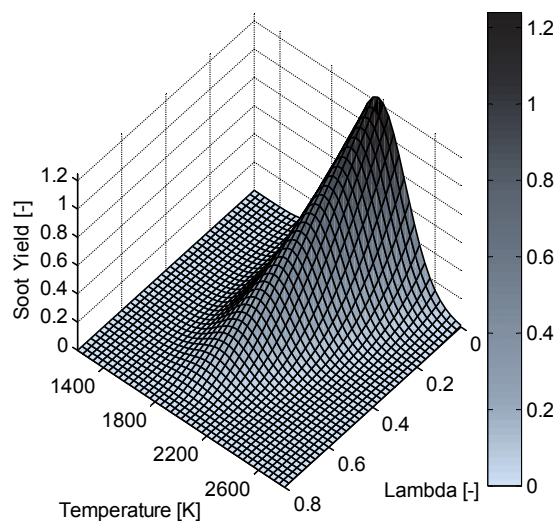


Figure 2.9 Soot yield map adapted from Warth, Koch, & Boulouchos (2003).

Figure 2.9 depicts the dependency of soot yield on temperature and lambda. It is a nowadays commonly used map introduced by Akihama, Takatori, Inagaki, Sasaki, & Dean (2001) and mathematically approximated by Warth, Koch, & Boulouchos (2003).

Temperature may have a great effect on the oxidation of soot, however it is not the only factor. It has been determined that lambda values below 1.1 have an adverse effect on the oxidation. Furthermore, there is a temporal variation of O₂ concentration in the cylinder due to other factors. It has been discovered that the O₂ concentration is determined by the oxidation of CO and HC during the combustion which take place earlier than soot oxidation. They have developed a phenomenological model based on partial pressure of O₂, temperature and initial soot concentration. However there are still some uncertainties left that were left for further research.

2.3.3 Soot - NO_x Tradeoff

The so called Soot - NO_x tradeoff is a known phenomenon. Increasing the EGR rate is one of the most common ways of decreasing in-cylinder NO_x levels. Mainly due to the decrease of the overall temperature in the cylinder, less NO_x is formed at high EGR levels. However this has an adverse effect on the soot, therefore PM emissions. Soot emissions stay at a more or less constant level before they start to increase abruptly above a certain EGR rate. Vice versa, increased oxygen concentrations with high temperatures would reduce the PM emissions but these are the exact same conditions that would increase the NO_x formation in the diesel engine.

In order to achieve a simultaneous decrease of both pollutants the combustion process has to be altered completely which is not possible with the usual actuators and the boundary conditions in the engine (Beasley, et al., 2006; Gao & Schreiber, 2001; Fischer, 2011; Poorghasemi, Ommi, Yaghmaei, & Namaki, 2012).

2.3.4 Effect of Engine Parameters on NO_x and PM

There are various parameters that can be adjusted in the ECU for manipulating the combustion process. It is considered important to discuss the effects of these engine parameters on emissions. In this section only these parameters are discussed that can be altered without any changes on the engines. Also, parameters such as fuel quality

that define the boundary conditions are not discussed. Furthermore, the parameters presented here are seen as potential candidates as actuating variables for in-cylinder emissions control.

Adjustable engine parameters can be grouped in three categories. First group contains the following air path parameters.

- EGR
- Boost Pressure
- Inlet Port Shutoff

Second group consists of fuel path parameters, in this case limited to the injection system:

- Injection Timing
- Injection Pressure
- Pilot Injection
- Post Injection

Finally, one last parameter that has effect on the self ignition properties of the mixture is:

- Glow Plug Activation

In the following subsections, these parameters and their effect on NO_x and PM emissions are briefly discussed whilst giving a review from the literature.

2.3.4.1 Exhaust Gas Recirculation

EGR rate is one of the main parameters used in controlling in-cylinder emissions. There are two different types of EGR systems; high pressure EGR and the low pressure EGR systems. The used engines in this work are only equipped with high pressure EGR with cooling (Figure 2.1). Part of the exhaust gas is recirculated at a desired rate via an EGR valve. The actual value is usually modelled within the ECU and regulated with a model based feedback controller.

Increasing the EGR rate leads to a decrease of the lambda value in the cylinder due to the increased burned gas portion. The two are inversely proportional. Burned combustion products act as inert and the combustion temperature sinks due to lower combustion intensity. As a result of the drop in oxygen concentration oxidation of PM is badly affected. Due to high temperatures and lacking oxygen NO formation rate decreases. Aronsson et al. (2009) also points out to a substantial decrease in PM emissions and an increase of NO_x emissions with increasing oxygen concentration in the cylinder in their work on a heavy duty diesel engine. A 4% increase in the inlet O₂ concentration has lead to a PM concentration decrease of over 90% in their measurements.

This effect is also confirmed by Schubiger, Boulouchos, & Eberle (2002). They have observed in their experiments that increasing the EGR rate did not result in a sudden increase in soot levels. In the beginning as the EGR rate is increased the global O₂ concentrations decrease but have little effect on the local conditions as there is usually an excess in O₂ in diesel combustion. However, as the concentrations decrease further beyond a critical point, turbulent mixing rates become insufficient leading to a drastic increase of PM emissions.

2.3.4.2 Boost Pressure

Higher air pressure at the inlet means higher cylinder charge densities which allow higher injection rates leading to more intense combustion with higher outputs. Increasing boost pressure at constant charge air temperature increases the mass of air entering the combustion chamber. This causes an increase in the NO_x emissions at first due to higher peak temperatures and better O₂ availability. On the other hand a decrease in PM emissions is experienced. NO_x and PM reach their maximum and minimum and start to decrease and increase respectively with further increasing boost pressures. The reason for this is that with further increasing the boost pressure, temperature inside the cylinder drops due increased air mass and the lower temperatures slow down NO_x formation. Higher cylinder charge densities result in shorter spray penetration and smaller diffusion mixing area on the fuel jet. This

means a higher portion of the fuel is burned under low local lambda conditions causing an increase in the soot formation (Chmela, Werlberger, & Cartellieri, 1992; Herzog, Bürgler, Winklhofer, Zelenka, & Cartellieri, 1992; Stebler, 1998). It is possible that this point of turnaround in emission gradients depends on engine type and operating conditions. As Ehleskog, Gjirja, & Denbratt (2009) observed in their experiments on a heavy duty diesel engine, that the same increase in boost pressure caused NO_x emissions to decrease without EGR and to increase with EGR. Furthermore they have observed no change in net soot emissions.

Effect of boost pressure on PM emissions is seen as the most important in transient operating modes. At the beginning of an acceleration injection system can react faster to increased torque requests from the ECU. But for the build-up of boost pressure there is a certain turbo lag. Turbo lag is defined as the time required for a turbocharger build up the desired boost pressure at the intake manifold. Within this turbo lag time lambda values in the cylinder drop causing higher PM outputs. This undesirable outcome is prevented to some extent by increasing the responsiveness using VTG and/or multi-stage turbochargers with smaller inertia elements to handle the acceleration conditions. This transient increase in PM emissions is especially observed during accelerations from low load, low engine speed conditions and it is less obvious in accelerations from middle load and middle speed. Hence mixing conditions in cylinder are better in the cylinder at higher speeds and loads (Stumpf, Velji, Spicher, Jungfleisch, Suntz, & Bockhorn, 2005).

2.3.4.3 Inlet-Port Shutoff

One of the inlet ports of the engine A (Table 3.1) can be shut off to direct more air to the other inlet port which induces swirl during the charge air intake. As in Bergin, Reitz, Oh, Miles, Hildingsson, & Hultqvist (2007) it can be seen that this swirl primarily affects the initial soot formation and has little influence on soot oxidation rates. Soot formation is decreased by increasing swirl which also increases the mixing rate, thus eliminating rich local zones. Another effect is the deflection of fuel jet which would otherwise impinge upon the cylinder wall and cause an increase in the soot formation. One negative aspect of swirl is that it reduces the thermal

efficiency of the engine.

Koyanagi, Öing, Renner, & Maly (1999) have observed a reducing effect of swirl on soot and have seen that swirl may increase NO_x in later phases during combustion. Similarly, Ishikawa, Uekusa, Nakada, & Hariyoshi (2004) report a decrease in soot with increased swirl. Effect of swirl on combustion is best realized at lower injection pressures as the relative turbulence induced by swirl is the higher (Kim, Cho, & Lee, 2008).

2.3.4.4 Injection Timing

A common method to manipulate the combustion is to alter the injection timing. Advancing the injection timing increases the ignition delay creating more time for mixture formation and therefore increases the premixed to diffusive combustion ratio. Since fuel burned during diffusive combustion is mainly responsible for soot emissions, advancing the ignition timing results in a decrease of PM emissions. Furthermore, for retarded injection timing, combustion efficiency drops. In order to be able to get the same output more fuel needs to be injected causing even a larger diffusive portion and higher soot formation.

Kweon, et al. (2003) have determined in their work that advanced injection timing led to a more intense premixed combustion especially at higher loads. This results in higher pressures and Schubiger (2001) has noted that higher pressures during premixed combustion cause higher soot formation rates. However this effect through the higher pressure seems to be counterbalanced since Kweon, et al. (2003) reported that the more intense premixed combustion promoted better mixture formation and had a good influence on the diffusive combustion intensity. Furthermore, Sung, Lee, Kim, & Kim (2003) observed that retarded injection timing reduced the soot formation and oxidation, but the net soot mass at the exhaust increased due to the greater decrease in soot oxidation.

In the case of NO_x , as expected there is an increase in the emission levels with advanced ignition timing primarily due to the higher peak temperatures during the

more intense premixed combustion. Additionally advancing the ignition timing has a positive effect on fuel consumption (Stebler, 1998; Wenzel, 2006).

2.3.4.5 Rail Pressure

An increase in injection pressure has mainly a positive effect on the atomization of fuel particles resulting in a better mixture formation and higher local lambda values. There may be a momentary increase in the soot formation at high injection pressures. This is caused by the increased injection rate per time causing fuel richer zones. Nonetheless, the increased kinetic energy of the mixture and the high turbulence induced favor faster oxidation of the formed soot particles. Besides, at higher injection pressures the end of the combustion is earlier, leaving more time for later oxidation. In general it has been concluded by many that PM emissions decrease with increasing injection pressures. Especially higher injection pressures at higher loads have a more significant effect on PM reduction. On the other hand, NO_x emissions increase again due to the more intense combustion in a shorter time interval leading to higher peak pressures. (Aronsson, et al., 2009; Meyer-Salfeld, 2004; Mollenhauer & Tschöke, 2007; Schubiger, Boulouchos, & Eberle, 2002; Stebler, 1998). High injection pressures are beneficial in combustion regarding the better atomization of the fuel spray leading to higher combustion efficiencies and there is a trend towards injection systems capable of higher pressures in the automotive industry.

Fischer & Stein (2009) have observed a critical injection pressure, after which there was no effect observed on NO_x and soot emissions. The limiting factors through NO_x emissions are usually compensated through other means, such as advancing the injection timing or using higher EGR rates. At the PM side, the main limiting factor is to have too high injection pressures under light load which may cause wall impingement of the fuel jet and lead to substantially higher HC and PM emissions and also lower combustion efficiency.

2.3.4.6 Pilot Injection

There are two pilot injection parameters that can be altered; timing and injection quantity. Pilot injection is used for conditioning the cylinder charge before the main combustion. In case of a pilot injection and a corresponding combustion taking place before the main injection, the temperature levels rise at the time of the main injection. Therefore the boundary conditions for the fuel atomization and mixture formation rates change causing a shorter ignition delay. Even if no pre-combustion occurs because the pilot injection amount is too small or the timing is too close to the main injection, it still causes an earlier start of the main combustion. Thus, it makes a difference in terms of emissions.

Stebler (1998) proposes that a decrease in NO_x emissions can be realized with increasing the pilot injection amount, at rather low amounts without any PM penalty, as also pointed out by Ishida, Chen, Luo, & Ueki (1994) and Stegemann, Meyer, Rölle, & Merker (2004). However if a pre-combustion occurs prior to the main injection event, a sharp increase in PM emissions is to be seen. The reason is the fuel jet coming into direct contact with the flame at high temperatures and low local lambda values, preparing the perfect conditions for sooting combustion. Advancing the pilot injection too far early might also cause the same effect mentioned with PM. Yet there needs to be a certain minimum interval between the pilot and the main injection for the above mentioned advantages to be realized with NO_x emissions.

Hence, the contrary effect has been observed by Chen (2000) and de Ojeda, Zoldak, Espinosa, & Kumar (2009) under different circumstances, as reduced pilot injection quantities have resulted in lower NO_x emissions. Carlucci, Ficarella, & Laforgia (2003) and Minami, Takeuchi, & Shimazaki (1995) report that pilot injection quantity has a decreasing effect especially at low loads. It is also mentioned that several researchers have observed first a decrease, then an increase in NO_x with increased pilot injection quantity. That might be due to the increased cylinder temperatures with the more intense pre-combustion at higher quantities.

Rajkumar, Pramod, & Bakshi (2011) have observed an increase in peak pressures with increasing pilot injection quantities. Furthermore the occurrence of the peak cylinder pressure has been retarded. This can cause lower NO_x emissions since the peak pressures and the resulting peak temperatures in the cylinder are reached at later stages of combustion with lower O₂ concentrations. Later peak pressures could then promote the oxidation of soot at later stages.

A decrease in soot with increased quantities has been observed by de Ojeda, Zoldak, Espinosa, & Kumar (2009) and Kim, Cho, & Lee (2008). Analogical to the relationships discussed so far regarding PM emissions, Mohr, Jaeger, & Boulouchos (2001) have also observed similar effects and were able to decrease the PM emissions by varying the engine parameters correspondingly in their research. They have also determined that the decrease in PM was mainly associated to a decrease in soot. Soluble fraction has stayed the same unless extreme premixed ratios were reached.

2.3.4.7 Post Injection

Post injection in the later phases of combustion is an alternative way to decrease PM emissions. Badami, Mallamo, Millo, & Rossi (2003) propose that a pilot-main-post injection strategy can be very effective in reducing soot emissions. Exhaust temperature is increased leading to better soot oxidation rates. However it can be realized naturally at the cost of consumption as the later injected fuel does not burn with high efficiency. Post injection method has not been further investigated within this work.

2.3.4.8 Glow Plug Activation

Glow plug normally exists for cold start conditions in diesel engines. Yet, glow plug activation during normal operation has been a subject of investigation with respect to combustion and emissions control.

Arregle, Bermúdez, Serrano, & Fuentes (2006) have shown in their experiments

that an active glow plug caused higher PM emissions during emission test cycles, especially in idling conditions, which make up a large portion of these cycles. This is due to the higher temperatures reached at the fuel rich zone around the glow plug causing higher soot formation rates. The resulting excess soot needs to be oxidized under higher temperatures to reach the same emission level. Nonetheless, the higher temperatures reached around the glow plug did not have any effect on the overall soot oxidation relevant temperature in the cylinder and excess soot was unable to be oxidized.

2.4 Emission Modeling Approaches

There are various approaches when it comes to emissions modeling methods that are used in engine research and development. As described by Warth (2005) and Barba (2001), the model classification is usually dimensional or complexity level based. Dimensional classification describes the models as zero, quasi and multi-dimensional, whereas based on the complexity level these models can be described as empirical, phenomenological and complex. Various approaches can also differ in parameterization techniques (Xiaobei, Hongling, & Zhaowen, 2008).

2.4.1 Empirical Models

Empirical models are based on experimental data. A certain model structure is defined based on the scatter of data available. Afterwards that data set is used to calibrate the model. This is similar to curve fitting, or it may also be called model fitting. Empirical approaches usually don't make use of any physical relations and chemical reactions. These models are rather fast and are suitable for real-time control applications.

Some examples to these models are seen in literature. Gärtner (2001) has developed a NO_x emission model based on a quadratic polynomial structure and Wenzel (2006) has also developed a NO_x model based on an exponential products approach. Both models are zero dimensional and however statistical they may be, the authors tried to make use of physical variables for having partly physically motivated

models rather than pure statistical models.

2.4.2 Phenomenological Models

Phenomenological approaches are seen as solutions between the rather simple empirical models and the complex multidimensional models. They aim to describe physical, chemical and thermodynamic processes in quasi to multi-dimensional approaches and try to find a balance between computational effort and accuracy. Local conditions are usually taken into account more seriously than with simple models and physical methods are described in a more detailed way. As stated by Gao & Schreiber (2001), phenomenological multi-zone models are suitable for parameter studies and they help in acquiring a better understanding of the processes within the cylinder.

Complexity of phenomenological models varies greatly. Some handle numerous steps of detailed chemical reactions and take a greater effort whereas some only utilize two zones for the pollutant formation and break-up. Besides it is common that such models compute the temporal variations of the combustion variables within one cycle using simplified approaches.

Egnell (2001) and Ericson, Westerberg, Andersson, & Egnell (2006) developed multi-zone and two-zone NO_x models. Schubiger, Boulouchos, & Eberle (2002) have developed a real time capable soot model handling soot formation and oxidation processes separately. Tao & Chomiak (2004) came up with a phenomenological soot emissions model coupled to a complex chemistry mechanism. Moreover, Sung, Lee, Kim, & Kim (2003) and Gao & Schreiber (2001) have listed various complex phenomenological models for soot formation and oxidation in their work.

2.4.3 Complex Multidimensional Models

These models are generally based on fluid mechanics. They aim to reproduce the physical and chemical processes with emphasis on relatively high accuracy and detail. Partial differential equations are involved in calculating conservation of mass,

energy, momentum and species concentrations are utilized.

Andersson, Johansson, Hultqvist, & Nöhre (2006) have proposed a multizone model supported by many lookup tables. Barths, Pitsch, & Peters (1999) have developed a model based on 3D simulation of the processes within the cylinder.

Complex multidimensional models have not been further investigated within this work since the focus here is on faster models that require little computational effort. This makes empirical simple models most desirable with the possibility of utilizing rather simple phenomenological models for better possible results.

CHAPTER THREE

DATA ACQUISITION & PROCESSING

This chapter focuses on data acquisition techniques and data processing methods used for determining variables for use in modeling in this work.

3.1 Calibration & Validation Datasets

Within this work two engines have been used for emissions model and controller development (see Table 3.1). Both are common rail DI diesel engines with piezo injectors and they are both equipped with single stage turbocharging and high pressure EGR.

Table 3.1 Specifications of the engines that are used for the model development (Werner, Schommers, Breitbach, & Spengel, 2011; Schommers, et al., 2008).

	Engine A	Engine B
Type	Daimler OM 642 LS	Daimler OM 651
Number of cylinders	6	4
Swept volume	2987 cm ³	2143 cm ³
Stroke	92 mm	99 mm
Bore	83 mm	83 mm
Compression ratio	15.5:1	16.2:1
Number of valves	4 (2/2)	4 (2/2)
EGR System	High Pressure	High Pressure
Aspiration	Turbocharged	Turbocharged
Max. injection pressure	1800 bar	2000 bar
Max. power	195 kW @ 3800 rpm	125 kW @ 3000-4200rpm
Max. torque	530 N·m	400 N·m

The operating point of an internal combustion engine is usually specified through its speed and load in terms of engine torque and mean effective pressure. Calibration

and validation of the PM model presented in the next chapter have been done with the datasets shown in Figure 3.1. For each engine a calibration measurement data set has been used for determining the constant coefficients, and a second data set for model validation. It is worth mentioning that, for both engines the calibration and validation sets come from two different engines of the same type.

In the case of engine A both the calibration and validation sets consist of steady state test bench measurements. The calibration data set was selected such that it covered a large region on the standard engine map with additional EGR rate and SOI variations. Data selected for model validation consist of EGR rate variations at several points on the engine map.

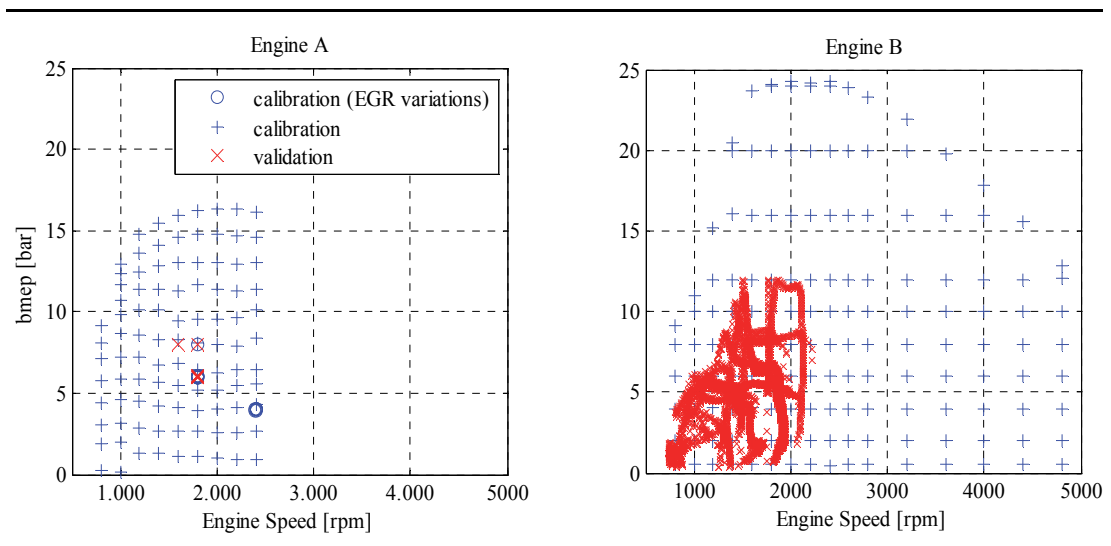


Figure 3.1 Operating points of calibration and validation datasets for the two engines.

On engine B, the calibration data was more convenient in the sense that, the available measurement set covered the whole standard engine map, and there were less number of data points. Contrary to the case in engine A, the model on engine B was validated using a transient measurement in NEDC (DieselNet). By this means, the capability of the PM estimator during transient operation has also been assessed.

Table 3.2 Further information on the calibration and validation datasets.

Engine	Dataset	# of pts.	Meas. type	EGR	PM measurement
A	calibration	326	stationary	0 - 44%	Filter Smoke Number
	validation	69	stationary	0 - 35%	Filter Smoke Number
B	calibration	147	stationary	0 - 40%	Filter Smoke Number
	validation	13000	transient	0 - 50%	Opacity

3.2 Measured Data and Derivations

In the following, measured data are briefly discussed that were used in the model development. Moreover, data processing in terms of cylinder pressure correction, heat release calculation and determination of PM mass emissions based on FSN (Filter Smoke Number) and opacity values are discussed.

3.2.1 *In-Cylinder Pressure*

Crank angle resolved in-cylinder pressure is an important variable in analyzing combustion in diesel engines. It is common that sensors are used to measure the pressure on research engines. Yet, in-cylinder pressure information is not available in series production engines as they are not equipped with such sensors. These sensors are costly and hard to integrate into the cylinder heads of engines as stand-alone sensors in a non-intrusive way. Some are glow-plug integrated eliminating the space problem, however such sensors have to cope with thermal shock problems that would otherwise prevent them from meeting road vehicle reliability standards.

Nevertheless, the automotive industry sees such sensors as beneficial and research and development is continuously being carried out cooperatively between the automobile manufacturers and their suppliers. Main use of such sensors would be as mentioned already, to enable the feedback control of the combustion and considerable research has been concentrated on this subject. There are even the first examples of engines in series production equipped with in-cylinder pressure sensors

such as in Hadler, Rudolph, Dorenkamp, Kösters, Mannigel, & Veldten (2008).

Piezoelectric cylinder pressure sensors screwed to a hole (bored on the cylinder head) without water-cooling, were used for cylinder pressure acquisition. The pressure curve was used to calculate the heat release rate in order to define new variables relating to PM emissions. Further details concerning the setup are explained in Steuer et. al. (2009).

It should be taken into account that the used cylinder pressure sensors from Kistler (see Table A.1) have a higher accuracy than the sensors that are likely to be available in serial production engines in the near future. Furthermore, the high cylinder pressure sampling rate of $10\text{ }^{\circ}\text{CA}^{-1}$, which was available on test bench measurements, is somewhat higher than the feasible sampling rates that would be available in a series production engine application today. Thus, the higher accuracy of the cylinder pressure data acquisition on the experimental engines is expected to provide better results. This subject is briefly analyzed in section 4.2.6 based on in-cylinder pressure deviation.

Measurements are taken on the engine test bench over hundred cycles at a stable operating point. Basis of a used cylinder pressure curve is an average of cylinder pressure curves over these hundred cycles and averaged over all the cylinders. That gives one cylinder pressure curve for one operating point that has been used in further calculations and derivations.

3.2.1.1 Offset Correction

Cylinder pressure curve has to be corrected for offset errors due to the differential measurement principle of the piezoelectric sensor element. This is done by assuming the early compression from crank angles -90° to -65° before TDC as isentropic that is by assuming:

$$p \cdot V^n = \text{const} \quad (3.1)$$

where p is cylinder pressure and V is cylinder volume the polytropic exponent n can be taken constant as 1.37 for diesel compression phase. Using this approach for two points in the interval aforementioned:

$$p_1 \cdot V_1^n = p_2 \cdot V_2^n \quad (3.2)$$

By also taking the offset pressure p_{offset} constant throughout the curve, it can be calculated as:

$$p_{offset} = p_1 - \frac{p_2 - p_1}{\left(\frac{V_1}{V_2}\right)^n - 1} \quad (3.3)$$

Taking the constant polytropic exponent n instead of the physically correct isentropic exponent would lead to a maximum error of <0.25 % in the cylinder pressure, which is considered to be negligible.

Cylinder pressure curve can have inaccuracies. Therefore it is advisable to determine the offset using more than one pressure value couple. This approach is used in practice, since it provides high accuracy despite the small calculation effort (Wimmer & Glaser, 2002):

3.2.1.2 Heat Release Rate Calculation

There are several approaches for determining the heat release rate curve from the cylinder pressure curve as in Mladek (2003). However, based on experience it has been concluded that there isn't a significant deviation in the output of these approaches (Jippa, 2002). Hohenberg's approach (1982) as also used by Heywood (1988) has been chosen as the calculation method for the heat release rate, not only because of the small deviation mentioned above but also it was the commonly used method where this work has been carried out. Therefore no further research effort

has been made in this subject.

From the first law of thermodynamics using a crank angle φ resolved approach:

$$\frac{dU}{d\varphi} = \frac{dQ}{d\varphi} - \frac{dW}{d\varphi} \quad (3.4)$$

Reordering the equation to get the heat transfer, in other words heat release rate in this case:

$$\frac{dQ}{d\varphi} = \frac{dU}{d\varphi} + \frac{dW}{d\varphi} \quad (3.5)$$

The thermodynamic process can be divided into two parts. Change in internal energy can be assumed as an isochoric process:

$$\frac{dU}{d\varphi} = c_v \cdot m \cdot \frac{dT}{d\varphi} \quad (3.6)$$

And the work part can be considered as an isothermal process:

$$\frac{dW}{d\varphi} = p \cdot \frac{dV}{d\varphi} \quad (3.7)$$

Substituting into equation 3.5 gives:

$$\frac{dQ}{d\varphi} = c_v \cdot m \cdot \frac{dT}{d\varphi} + p \cdot \frac{dV}{d\varphi} \quad (3.8)$$

The ideal gas law for mass m and the gas constant R gives:

$$p \cdot V = m \cdot R \cdot T$$

$$p \cdot \frac{dV}{d\varphi} + V \cdot \frac{dp}{d\varphi} = m \cdot R \cdot \frac{dT}{d\varphi} \quad (3.9)$$

Substituting (3.9) into (3.8) gives:

$$\frac{dQ}{d\phi} = \frac{c_v}{R} \cdot \left(p \cdot \frac{dV}{d\phi} + V \cdot \frac{dp}{d\phi} \right) + p \cdot \frac{dV}{d\phi} \quad (3.10)$$

Next point would be determination of the specific heat c_v . There are different approaches such as assuming a constant specific heat or taking a temperature dependant approach or the physically most correct one that is dependent on the temperature and lambda value in the cylinder. For this work the second approach has been used. That is a temperature dependant solution with an estimated constant temperature for each combustion cycle, which has been determined empirically already.

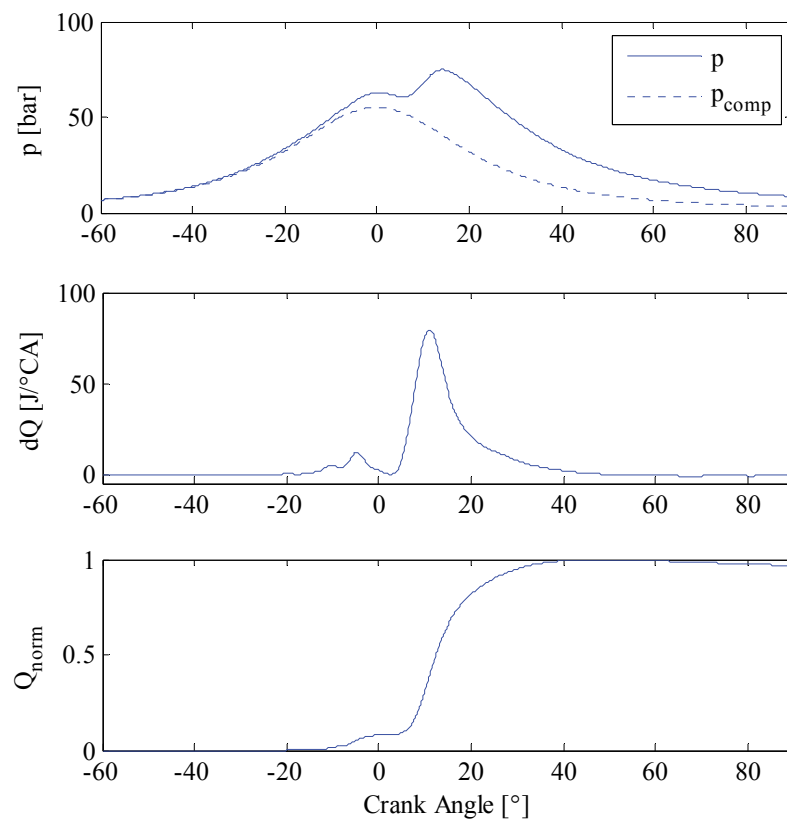


Figure 3.2 Heat release calculation..

It should be taken into account that the heat release rate derived so far also

includes the heat lost through the cylinder walls. Hence it can be called the net heat release. This net heat release rate has been used throughout this work as an improvement in model accuracies (chapter 4) has not been seen through the use of a gross heat release rate.

3.2.2 *Particulate Matter Mass*

Despite the fact that the soot formation and oxidation are rather complex processes, only the engine-out values have been measured and used for modeling purposes. This measured value is the net soot yield after the combustion process. Therefore no information was available on the soot formation and oxidation processes within the cylinder. Indeed, this has been a limiting factor on the modeling of emissions, on one hand.

On the other hand, the PM estimator is desired to be as simple as possible and easily applicable. This favored the emission measurements with standard engine test bench equipment. Besides, this would also make the re-calibration of the model easier for other engines, since no special measurement techniques would be necessary, other than what is standard in the automotive industry. Common measurement methods for diesel particulate mass determination which are also used for research purposes have been summarized by Vouitsis, Ntziachristos, & Samaras (2003) in their review.

Table 3.3 Devices used for PM emissions measurement

Device Name	Measurement Principle	Measurement Environment	Operation Mode	Output
Smokemeter	filter paper blackening	engine test bench	stationary	cumulative
Opacimeter	optical	engine test bench	transient	real-time
Particulate Sampler	gravimetric filter	vehicle test bench	transient	cumulative
Micro Soot Sensor	photo-acoustic	vehicle test bench	transient	real-time

Devices used for PM measurement are listed in Table 3.3 and their specifications are presented in the Appendix.

The device used for measuring PM emissions during steady state operation was Smoke Meter (see Table A.2). A sample of the exhaust gas is channeled through a clean filter paper in the instrument where PM is trapped, causing a blackening on the paper. It is then detected by a photoelectric measuring head and converted into an FSN (Filter Smoke Number) value (AVL List GmbH, 2012d; Majewski & Khair, 2006). The paper blackening is determined over a predefined time duration where the engine is running at a steady state.

On the transient engine test bench, the Opacimeter (see Table A.3) has been used, which is capable of measuring opacity also during transient tests. The measurement principle is based on the loss of the intensity of light passing through a chamber filled homogeneously with exhaust gas (AVL List GmbH, 2012d; Majewski & Khair, 2006).

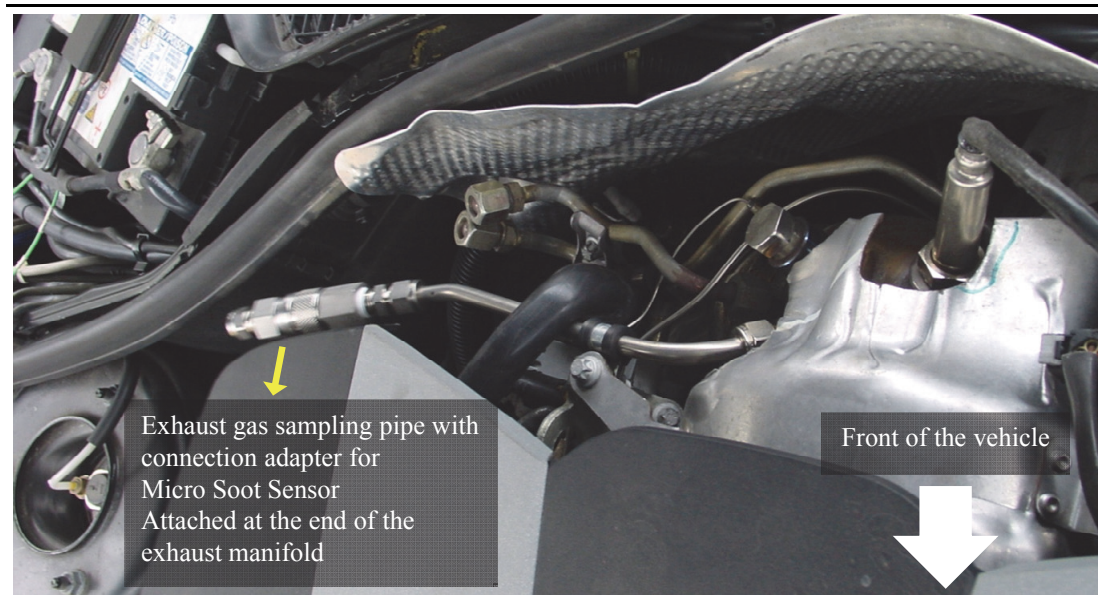


Figure 3.3 Installation of an exhaust gas sampling valve for measurements with MSS.

Vehicle test bench measurements were done with the help of Particulate Sampler and Micro Soot Sensor (MSS). The constant volume particulate sampler passes the

diluted exhaust gas through a filter throughout the test cycle and eventually mass of PM is determined with a gravimetric analysis on the filtered mass (AVL List GmbH, 2012c). MSS allows continuous measurement of soot concentration in the diluted exhaust. It utilizes a photo-acoustic measurement principle to determine soot concentration. Sampled gas with particulates is heated with a modulating light source. The expansion and contraction of the particles due to periodical warming and cooling produces a sound wave which is detected by microphones. By this means concentration of the PM in the sampled gas can be determined (AVL List GmbH, 2012a).

All the measurement devices except for MSS take exhaust samples from the exhaust pipe. Since the test vehicle did not have any DPF filter, this wasn't a problem. MSS on the other hand is connected directly to the exhaust manifold through a sampling valve for accurate measurements. This is important since the measurement output is time resolved and possible time delay is eliminated by taking samples close to the cylinder output.

Therefore, a sampling valve has been built on the test vehicle's engine as shown in Figure 3.3 for enabling measurements with MSS. The pipe needed to have the least possible amount of bends, since such bends would resist the air flow and facilitate soot accumulation at these spots.

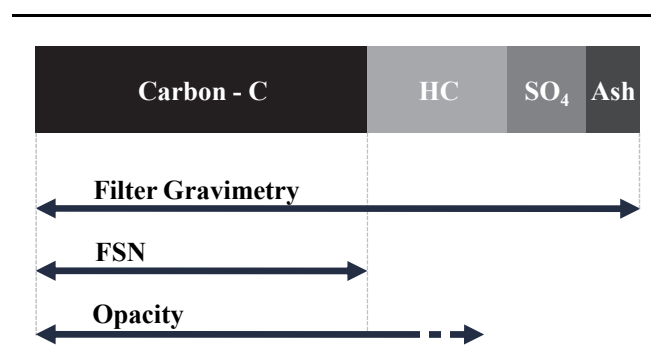


Figure 3.4 Particle emissions and their reference to different measuring principles. Adapted from AVL List GmbH (2005).

There is one important issue related to PM measurements. The different measurement levels yield different results as depicted on Figure 3.4. Based on the measurement technique, different substances are detected according to AVL List GmbH (2005). Filter gravimetry yields the highest emissions since the measured mass includes elemental carbon and other substances absorbed onto the particles. FSN measurements yield only elemental carbon and measurements based on opacity detect mostly elemental carbon and HCs.

3.2.2.1 Cycle Based PM Mass

Net PM mass per combustion cycle has been used as the measure for modeling and control of emissions as it is seen in the proceeding sections. Such values have been found physically correct, since as it will be presented in the following section, emissions have been calculated on a cycle basis.

Aforementioned measurement techniques produce PM emission results in different physical quantities such as mass concentration in the sampled exhaust gas, opacity or filter smoke number (FSN). In the following, determination of cycle based PM mass will be presented (AVL List GmbH, 2005).

PM mass density ρ_{PM} [g/m³] can be calculated from *FSN* measurement using the following correlation:

$$\rho_{PM} = \frac{1}{405} \cdot 5.32 \cdot FSN \cdot e^{0.31 \cdot FSN} \quad (3.11)$$

Using volumetric flow rate of exhaust gas flow rate \dot{V}_{exh} [m³/h], PM mass flow rate \dot{m}_{PM} [g/h] can be determined:

$$\dot{m}_{PM} = \rho_{PM} \cdot \dot{V}_{exh} \quad (3.12)$$

Using engine speed N and number of cylinders n_{cyl} cycle based PM mass m_{PM} in

[mg/cyc] can be calculated as:

$$m_{PM} = \dot{m}_{PM} \cdot \frac{1000}{n_{cyl} \cdot 30 \cdot N} \quad (3.13)$$

Moreover, if the measured PM is based on opacity *OPAC* it can first be converted into *FSN*. Correlation between *FSN* and *OPAC* is as follows:

$$OPAC = 0.12 \cdot FSN^3 + 0.62 \cdot FSN^2 + 3.96 \cdot FSN \quad (3.14)$$

It should be noted that, although there are certain conversion methods that are widely used, soot mass calculation from measured quantities is still a subject of discussion in the industry.

3.2.3 Fuel Injection Rate

Injection rate curve is used in determining certain variables in emissions modeling. There are different methods in estimating the injection rate. Kozuch (2004) has determined injection rate curve based on fuel volume, pressure difference, density and injector orifice diameter. Barba (2001) has used the approach that is presented in the following which is based on Vortmeier (1998). Figure 3.5 depicts the injection curve used for approximation.

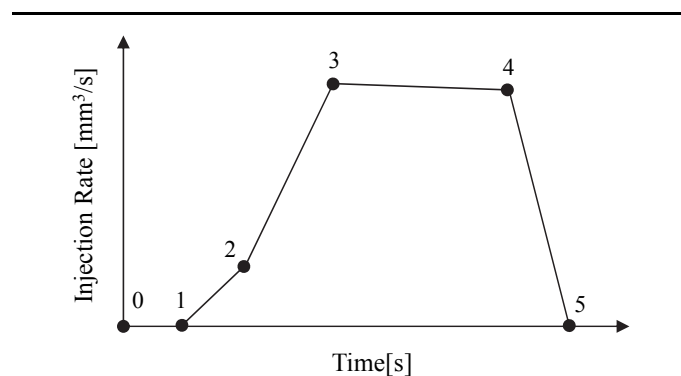


Figure 3.5 Fuel injection rate curve approximation (Barba, 2001).

Intervals on the figure between the numbered points represent the following:

- 0 Injector actuation
- 0 → 1 Injection delay
- 1 → 2 Needle opening, first part
- 2 → 3 Needle opening, second part
- 3 → 4 Maximum injection rate (falling based on system properties)
- 4 → 5 Needle closing

Injection delay is the time between injector actuation by the power stage and start of injection. It is dependent on injection pressure and is estimated as:

$$t_{0-1} = 0.26 - 5/p_{rail} \quad (3.15)$$

Needle opening duration, until maximum injection is reached, is divided into two intervals. The slopes of the injection curve in these intervals are respectively:

$$a_{1-2} = a_{1-2,ref} \cdot \left[\frac{p_{rail}}{p_{rail,ref}} \right]^{1.3} \quad (3.16)$$

$$a_{2-3} = a_{2-3,ref} \cdot \left[\frac{p_{rail}}{p_{rail,ref}} \right]^{1.3} \quad (3.17)$$

Duration of interval 1-2 is estimated as:

$$t_{1-2} = t_{1-2,ref} \cdot \left[\frac{p_{rail}}{p_{rail,ref}} \right]^{0.4} \quad (3.18)$$

Duration of interval 2-3 is based on the point where maximum injection rate is attained. This maximum injection rate is determined similarly in an empirical way:

$$\dot{V}_{max} = \dot{V}_{max,ref} \cdot \left[\frac{p_{rail}}{p_{rail,ref}} \right]^{0.6} \quad (3.19)$$

Slope of the needle closing curve is analogous to needle opening curves:

$$a_{4-5} = a_{4-5,ref} \cdot \left[\frac{p_{rail}}{p_{rail,ref}} \right]^{1.3} \quad (3.20)$$

Duration at maximum injection rate t_{1-2} is adjusted based on injected fuel quantity. For very small injection amounts the interval 3-4 or even 2-3 can be omitted. The curve is adjusted so that the area underneath is in agreement with the injected fuel quantity (desired value in ECU).

Reference values appearing in the preceding equations are determined based on injector measurements on hydraulic test bench. A reference rail pressure is selected and these reference values are adjusted accordingly on a sample measured injection curve.

Figure 3.6 shows an exemplary calculation of injection rate and the resulting theoretical energy Q_{fuel} that is delivered into the cylinder which is obtained from the thermodynamic equation:

$$Q_{fuel} = V_{fuel} \cdot \rho_{fuel} \cdot Q_{LHV,fuel} \quad (3.21)$$

Later on this term is used in deriving other variables for emissions modeling as presented in the next chapter.

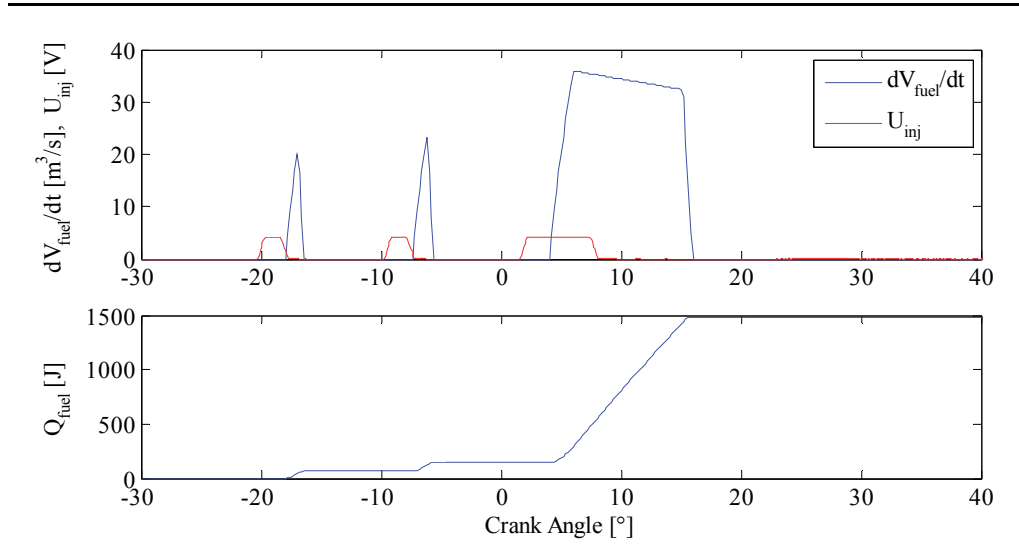


Figure 3.6 Fuel injection rate curve calculation. Injector actuator signal and injection and estimated curve (top). Cumulative theoretical injected fuel energy (bottom)

3.2.4 ECU Signals

Sensor data from the engine could be acquired from the engine ECU over the CAN (Controlled Area Network). Some signals have been directly used in the model, whereas others have been used to calculate other variables, which would have an effect on the emissions.

ECU signals are used in many derivations. For example, crank angle resolved cylinder volume is determined using crank angle together with engine geometry for heat release rate determination. Further, the injector actuator signal comes also from the ECU that is used in determining the injection rate curve.

3.3 Emission Test Cycles

Certain standard test cycles are used worldwide for measuring emissions and fuel consumption on either engine or vehicle test benches (dynamometer tests) (DieselNet). Two types of these test cycles have been used for testing developed emission model and controller in this work.

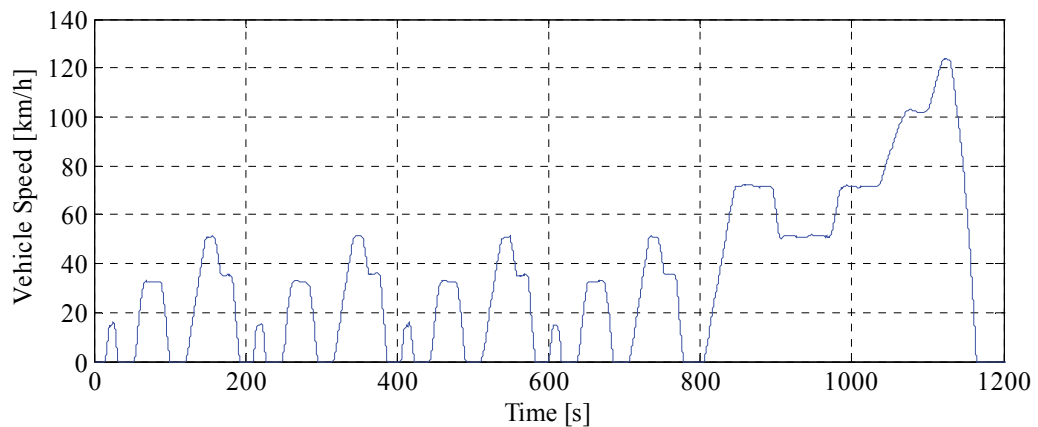


Figure 3.7 NEDC (New European Driving Cycle) used for emissions testing and certification in Europe.

First one is the NEDC (Figure 3.7) used in Europe. It consists of four ECE (also known as UDC – Urban Driving Cycle) and EUDC (Extra Urban Driving Cycle). Length of ECE's are 200s each and EUDC takes 400s. Through ECE and EUDC the cycle is divided into two phases as phase 1 and phase 2.

Figure 3.8 depicts the speed profile of US06 test cycle used in the USA. It is referred to as the Supplemental Federal Test Procedure. US06 is a rather aggressive cycle and it is developed to address the shortcomings associated to the steady state driving behavior in the standard FTP-75 test cycle.

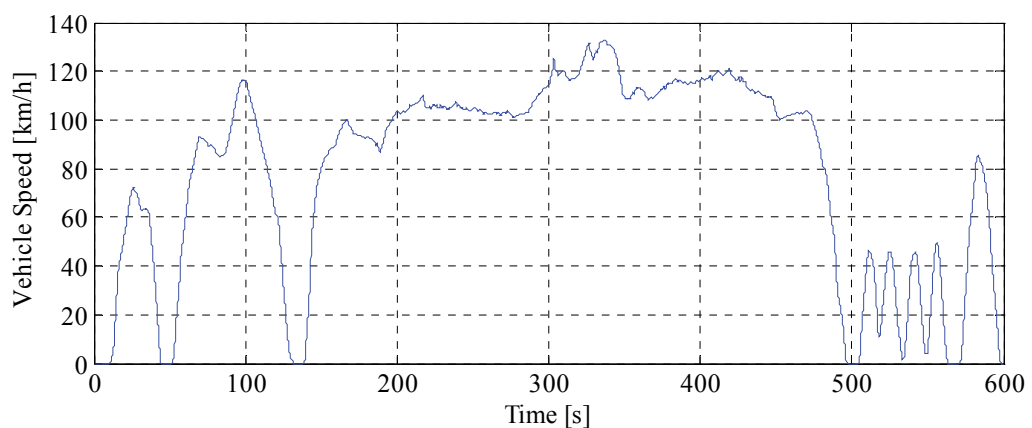


Figure 3.8 US06 driving cycle used for emissions testing and certification in USA.

It can be observed from the figures that US06 has a highly dynamic speed profile when compared to NEDC. Therefore it is able to address the particulate matter emissions problem due to transient conditions better.

CHAPTER FOUR

PM EMISSIONS MODELING

This chapter presents the developed PM estimator as in (Çebi, Rottenkolber, & Uyar, 2011). It is worth mentioning that throughout this work the focus was on high speed passenger car common rail direct injection diesel engines. The scope is limited to a maximum of two pilot injections and a main injection without any post injections or split main injection. Also no cold start conditions have been considered. All the measurements and development have been carried out for the so called normal operation mode.

4.1 Phenomenological Modeling Approach

A phenomenological model has been investigated a preliminary approach to assess the capabilities of such a model. The chosen approach originates from Hiroyasu & Kadota (1983) and has been modified by Schubiger, Boulouchos, & Eberle (2002) and Warth, Koch, & Boulouchos (2003) have used the model with some minor changes.

$$\frac{dm_{soot}}{d\varphi} = \frac{dm_{soot}}{d\varphi} \Big|_{form} - \frac{dm_{soot}}{d\varphi} \Big|_{ox} \quad (4.1)$$

$$\begin{aligned} & \frac{dm_{soot}}{d\varphi} \Big|_{form} \\ &= A_f \frac{dm_{fuel}}{d\varphi} \Big|_{diff} \left(\frac{p_{cyl}(\varphi)}{p_{ref}} \right)^{n_1} f(\lambda_{form}, T_{form}(\varphi)) \end{aligned} \quad (4.2)$$

$$\frac{dm_{soot}}{d\varphi} \Big|_{ox} = A_{ox} \frac{1}{\tau_{char}(\varphi)} m_{soot} \left(\frac{p_{O_2}(\varphi)}{p_{ref}} \right)^{n_2} f(T_{ox}) \quad (4.3)$$

This model shown throughout the Eqs. (4.1) to (4.3) is crank angle resolved. Therefore it requires much more computational effort than proceeding empirical models used in this work.

First part as seen in Eq. 4.2 considers the soot formation. It is based on the fuel

conversion rate during the diffusive part of the combustion, cylinder pressure and a soot yield term in the end. This term $f(\lambda_{form}, T_{form}(\varphi))$ in Eq. 4.2) comes from the soot maps presented in Figure 2.9.

This model did not yield quantitatively satisfying results on the Engine A calibration data set. Nevertheless the results on the validation data set and on Engine B datasets did not show deteriorating results pointing out the extrapolation capability of this model. It was an expected behavior since the phenomenological model takes physical processes partly into account.

One should be able to understand physical phenomena to be able to calibrate such phenomenological models. Additionally appropriate measurement techniques or data should be existent so that the variables representing local conditions within the cylinder can be correctly calibrated. The reason for this model's poor performance was due to the deficiency of measurement data that would enable correct estimation of partial oxygen pressure and local lambda in soot formation zones. Otherwise this model has proved high accuracy in other projects even in the modified form as a mean value model (Kirchen & Boulouchos, 2009). Furthermore, it was of interest to contribute a new model to literature for PM emissions estimation.

4.2 Empirical Modeling Approaches

In the modeling phase, one of the primary requirements has been minimal calculation effort, to allow for real-time capability and make the model compatible in use with an onboard emissions controller. Following model structures have been applied:

- Second order polynomial
- Exponential products

These are presented in the proceeding sections. As the results revealed the exponential products approach proved to be better over the polynomial model. There are two main reasons for that. Exponential products model has demonstrated better

extrapolation capabilities and it has less number of constants to be determined. Furthermore as it is presented later on, the results for PM emissions modeling with the exponential approach are rather promising compared to the polynomial approach.

In Figure 4.1, the path starting from the measured quantities to the generated variables and PM emissions model is presented. There are two paths where the variables originate from; either from ECU signals or from in-cylinder pressure data.

ECU signals are either measured quantities with the help of sensors or they are readily available modeled quantities that are used in other modules within the ECU. Some examples are inlet, outlet temperatures and pressures, exhaust gas lambda value, inlet mass flow rate, EGR, swirl valve positions, engine speeds, desired injection quantities and timings and the injector triggering signal etc.

In-cylinder pressure signal can be used to derive variables based on the pressure curve or it is useful for determining the heat release rate and the global temperature curve during combustion. Segment (cycle) synchronous variables can be derived from these curves that would relate to the emissions.

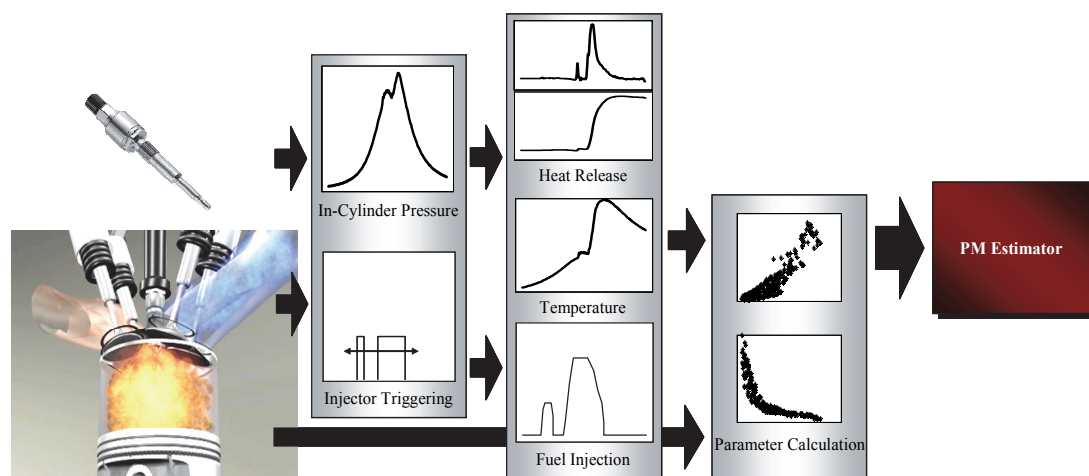


Figure 4.1 Empirical approach to PM raw emissions modeling.

Data originating from these mentioned paths have been used as standalone variables or new variables have been derived making use of several other. It should

be noted that the variables derived are all cycle based and no temporal variation has been taken into account. Hence a zero dimensional modeling approach has been applied.

Before moving on to the models, the selected variables for both approaches are presented in the following.

4.2.1 Variable Selection

Variables to be used in the PM estimator have been chosen such that they preferably had a direct physical relationship with the combustion and soot emission mechanism. Engine specific variables such as SOI have been avoided although they improved the model accuracy on one engine or the other, since the adaptability of the estimator to other engines is essential. The selected variables are listed in Table 4.1. Detailed explanations about the selected variables can be found in the proceeding sections.

Table 4.1 Empirical model inputs. Second column from the left shows the indices of the variables after scaling.

Variable	Scaled	Unit	Description
N	X_1	rpm	Engine speed
p_{rail}	X_2	bar	Rail pressure
x_{uIVC}	X_3	-	Unburned air mass concentration at IVC
x_{uEVO}	X_4	-	Unburned air mass concentration at EVO
$\Delta\varphi_{comb}$	X_5	°CA	Main combustion duration
$\Delta\varphi_{diff}$	X_6	°CA	Diffusive combustion duration
τ_{char}	X_7	°CA	Characteristic time

The first and last variables N and p_{rail} are acquired as ECU signals. Air mass concentrations at the inlet and exhaust; x_{uIVC} and x_{uEVO} are derived from other ECU variables. Last three variables $\Delta\varphi_{comb}$, $\Delta\varphi_{diff}$ and τ_{char} are derived using heat release rate and fuel injection curves (see Figure 4.3 and Figure 4.4).

Heat release rate curve, as mentioned earlier, is calculated using cylinder pressure curve according to Hohenberg's approach (1982) by assuming constant specific heat ratio. Inasmuch as the experience proves, heat release rate provides important information about the combustion related to soot emissions. For the time being, there is no real-time capable combustion model available for calculating the heat release curve with a high accuracy without in-cylinder pressure measurement. This makes again the cylinder pressure measurement indispensable.

Fuel injection curve is estimated based on Barba (2001). The fuel injection rate is also an important factor in calculating the soot emissions. It provides further information about the combustion characteristics, one of which is the characteristic time that has been found relevant.

In the proceeding sections selected variables that have been found PM emissions relevant are presented.

4.2.1.1 Rail Pressure

It has been observed that injection pressure has increased the model accuracies in both cases presented in the proceeding sections. Please refer to Section 2.3.4.5 for further explanation on this variable.

4.2.1.2 Unburned Air Mass Concentration at IVC & EVO

As mentioned earlier, soot emissions depend highly on local lambda values. The selected variables, unburned air concentration at IVC (Inlet Valve Closing) & EVO (Exhaust Valve Opening), do not directly relate to the local conditions in the combustion region. Nevertheless, these global variables have an indirect effect on the soot processes in the cylinder and therefore are influential variables in this empirical model. They support the model by introducing the effects of engine parameters; air mass flow rate, EGR and by making use of the exhaust gas lambda. Since the unburned air concentrations are global variables, the selection of these prevents the model from becoming engine specific. These variables are calculated according to

Heywood (1988). Further details regarding the calculation are presented in the following:

Figure 4.2 depicts an exemplary mass composition in the cylinder at IVC.

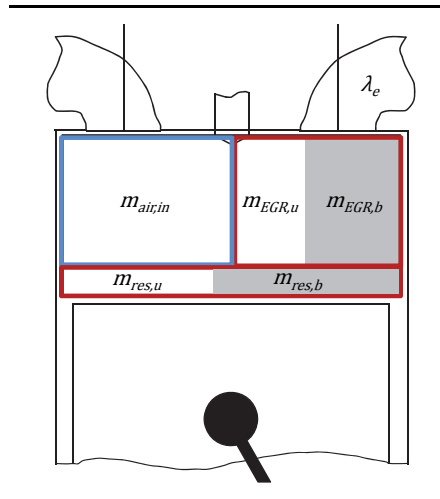


Figure 4.2 Mass composition in the cylinder at IVC

Inducted fresh air mass per cylinder can be calculated as follows:

$$m_{air,in} = \frac{\dot{m}_{air,HFM}}{30 \cdot n \cdot N} \cdot 10^3 \quad (4.4)$$

The recirculated exhaust gas mass is determined using the EGR rate (Eq. 4.5) and mass of the unburned portion is calculated using exhaust lambda sensor value (Eq. 4.6).

$$m_{EGR} = \frac{m_{air,in} \cdot x_{EGR}}{1 - x_{EGR}} \quad (4.5)$$

$$m_{EGR,u} = m_{EGR} \left(1 - \frac{1}{\lambda_e}\right) \quad (4.6)$$

Residual gas mass can be approximated using the ideal gas law with the temperature and pressure values at the exhaust (Eq. 4.7) and mass of the unburned

portion is calculated again using the exhaust lambda sensor value (Eq. 4.8).

$$m_{res} = \frac{p_3 \cdot V_c}{T_3 \cdot R_{air}} \cdot 10^6 \quad (4.7)$$

$$m_{res,u} = m_{res} \left(1 - \frac{1}{\lambda_e} \right) \quad (4.8)$$

Hence the unburned air mass and total mass in the cylinder at IVC is calculated respectively as:

$$m_{u_{IVC}} = m_{air,in} + m_{EGR,u} + m_{res,u} \quad (4.9)$$

$$m_{tot_{IVC}} = m_{air,in} + m_{EGR} + m_{res} \quad (4.10)$$

Finally, the unburned air mass concentration at IVC is calculated as:

$$x_{u_{IVC}} = \frac{m_{u_{IVC}}}{m_{tot_{IVC}}} \quad (4.11)$$

Furthermore, the unburned air mass concentration at EVO is calculated using only the exhaust lambda value:

$$x_{u_{EVO}} = 1 - \frac{1}{\lambda_e} \quad (4.12)$$

Further engine variables air mass flow rate, EGR rate or exhaust gas lambda were not used as direct inputs in the model because they are less relevant to the physical conditions within the cylinder.

4.2.1.3 Main and Diffusive Combustion Duration

Main combustion duration is defined as the duration in °CA from 5% to 95% heat release point (Figure 4.3) and it excludes the burnout from the main combustion. It can be calculated as:

$$\Delta\phi_{comb} = \phi_{Q_{95}} - \phi_{Q_{05}} \quad (4.13)$$

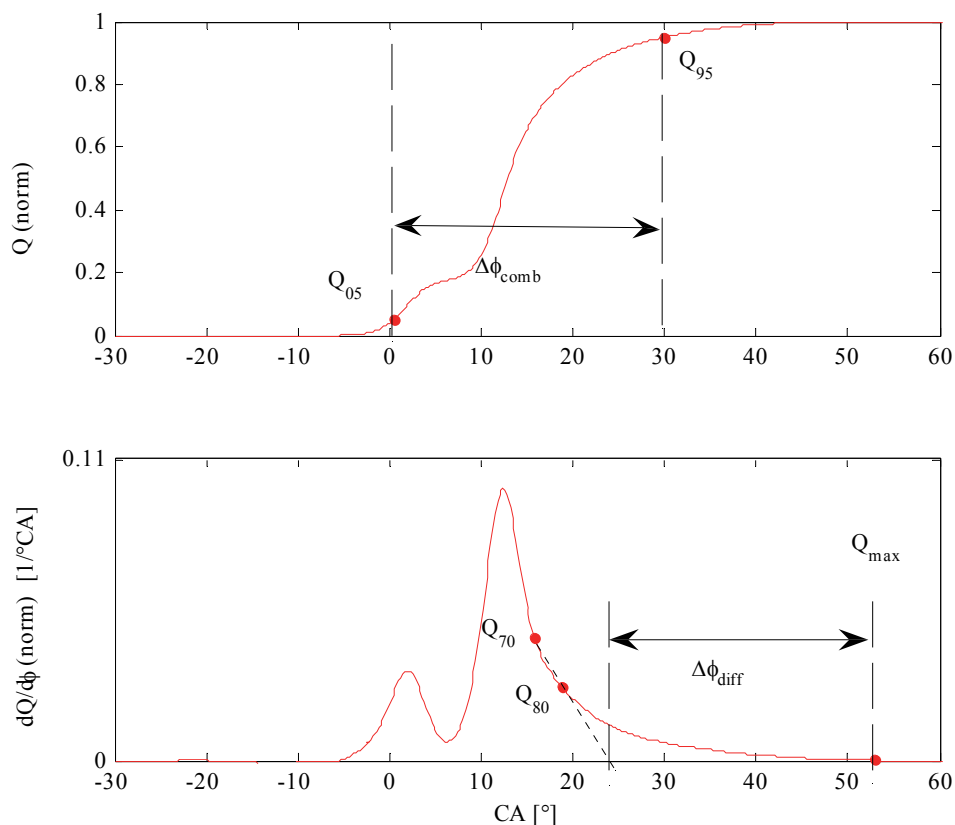


Figure 4.3 Determination of overall combustion duration (top) and diffusive combustion duration (bottom) variables.

Diffusive combustion duration on the other hand, contrary to its defined name should not be mistaken with the real duration of diffusive combustion. The variable defined as diffusive combustion duration here is merely a qualitative measure of the diffusive combustion, which is derived from Schubiger (2001).

During the ignition delay duration – the time it takes for fuel atomization, mixture formation and following ignition – injected fuel and air mixes to form a premixed state at the time of ignition. As discussed earlier, combustion of this mixture causes an abrupt increase in heat release rate followed by a steep descent after reaching the

maximum heat release rate. However the fuel is continued to be injected into the cylinder bowl during premix combustion leading to the typical diesel combustion process, diffusive, or in other words, non-premix combustion. Therefore it is assumed that a line drawn through 70% and 80% heat release points gives the end of the premix combustion at the zero intersection point ($\sim 24^\circ$ CA in Figure 4.3, bottom) and the combustion is only diffusive from this point on. In fact, diffusive combustion starts earlier than this point and the line drawn through 70% and 80% heat release points (see Figure 4.3, bottom) should be parallel to the heat release rate at its maximum declination point. In spite of that, the chosen points at Q_{70} and Q_{80} have been used since their onboard determination was easier and more stable than any other point on the steeper part of the heat release rate curve. Nevertheless, the chosen length is considered to be a good representation of the actual physical diffusive combustion duration.

Diffusive combustion duration is be calculated numerically as:

$$\Delta\varphi_{diff} = \varphi_{Q_{max}} - \left[\varphi_{Q_{70}} + \left(\frac{dQ}{d\varphi} \right)_{Q_{70}} \cdot \frac{\varphi_{Q_{80}} - \varphi_{Q_{70}}}{\left(\frac{dQ}{d\varphi} \right)_{Q_{70}} - \left(\frac{dQ}{d\varphi} \right)_{Q_{80}}} \right] \quad (4.14)$$

4.2.1.4 Characteristic Time

Rate of combustion, i.e. energy conversion rate, during the premixed phase of combustion depends mainly on the high chemical reaction rates, whereas it is governed by the lower physical diffusion rate during diffusive combustion. Considering that diffusive combustion is mainly responsible for soot formation it is meaningful to include a measure of the specific rate of combustion.

As introduced by Schubiger (2001), the energy conversion rate in the diesel engine can be defined as:

$$\frac{dQ(\varphi)}{d\varphi} = \frac{1}{\tau_{char}(\varphi)} \cdot Q_{avail}(\varphi) \quad (4.15)$$

It can be deduced from Equation 4.15 that the energy conversion rate depends on a characteristic time and available fuel energy.

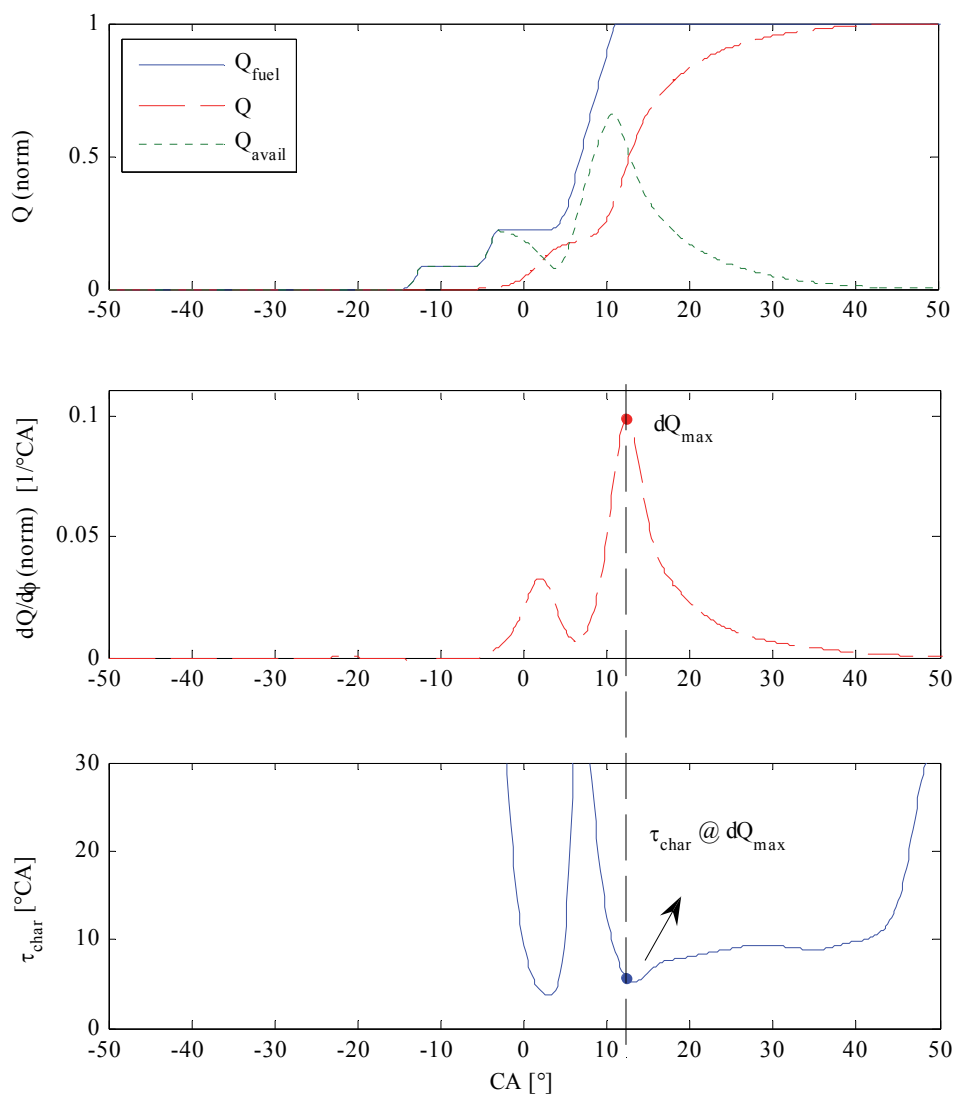


Figure 4.4 Determination of the characteristic time: Available fuel energy (top), heat release rate curve (middle), characteristic time curve (bottom).

The available energy of fuel in the cylinder Q_{avail} is a representative chemical energy of injected fuel in the combustion chamber that has not yet been converted to

heat through combustion. It is defined as the difference of chemical energy of injected fuel and net heat release (Equation 4.16).

$$Q_{avail}(\varphi) = Q_{fuel}(\varphi) - Q(\varphi) \quad (4.16)$$

where Q_{fuel} is calculated as presented in section 3.2.3.

Characteristic time curve is derived from Equation 4.15 and the variable to be used in the model has been chosen as the value at the maximum heat release rate instance (see Figure 4.4), which has shown a good correlation with the soot emissions. By choosing the value at one point, further calculation effort has been eliminated, since only the main injection has to be modeled and characteristic time is calculated at one point.

Reciprocal of characteristic time is considered as a measure of the specific rate of the kinetic reactions in premixed combustion and as a measure of specific mixing rate during the diffusive combustion. Hence, slow mixing, that is, lower values of the reciprocal should promote soot formation during combustion. Because the mixing rates are then lower, preventing soot oxidation, which is as discussed earlier, more or less the decisive process in soot emissions.

4.2.1.5 Engine Speed

Engine speed has a direct effect on the dynamics of combustion, since it is directly proportional with the average piston speed and therefore affects the kinetic energy of the cylinder charge.

However that is not the only effect that is sought after. The last three variables that are explained, namely, main and diffusive combustion duration and characteristic time, are all determined in terms of ° CA. It is clear, that the actual physical and chemical processes in nature are governed by temporal relations. However, due to the better correlation at different engine speeds, those variables

haven't been represented with temporal units. For this reason engine speed has been included in the model as a variable which should take effect as a corrective factor.

4.2.1.6 Other Variables

Trials with other variables than those explained so far have been done. However they either did not improve the model accuracy or were rather physically not related variables to soot processes.

Some of these variables which have been found rather irrelevant or which have not increased the model accuracy are the quantities and/or ratios of pilot and main injections, heat release rate inclination/declination angles (Wenzel, 2006), maximum heat release rate, position of inlet port shutoff valve (used to increase swirl), average cylinder temperature, spray penetration and spray cone angle (based on empirical models).

4.2.2 Engine Operating Regions

It had been expected that the developed model would not be able to cover the whole engine map. Despite the fact that the variables selected are directly related to physical variables of combustion, the following models are empirical approaches and do not directly represent the individual mechanisms involved in soot emissions.

As good as the empirical models can be, it should be kept in mind that soot mechanisms are relatively complex as described by many in chapter two.

Table 4.2 Empirical models are calibrated for these four engine operating regions separately.

	EGR \leq 5	EGR $>$ 5%
N \leq 2000 rpm	Region 1	Region 3
N $>$ 2000 rpm	Region 2	Region 4

Hence, instead of calibrating a model for the whole engine map, four regions are defined as shown in Table 4.2, with respect to engine speed and EGR. The reason for

choosing such limits comes from previous experience and carried out work together with Demirer (2009).

4.2.3 Polynomial Approach

First empirical approach is utilizing a second degree polynomial. Gärtner's (2001) NO_x emissions model has been influential in choosing this model structure for PM emissions modeling. It is a fast and easy way of fitting a polynomial model to statistical data spreads.

Model structure can be seen in Equation 4.17:

$$Y = A + B \cdot X^T + X \cdot C \cdot X^T \quad (4.17)$$

where Y is the output, X is the input matrix, A is the polynomial constant, B is the constant matrix with the first degree coefficients and C is the constant matrix with the second degree coefficients.

4.2.3.1 Calibration

Calibration of the model is done through ordinary least squares regression. It's a simple and fast method. The scatter of data is fitted to the second order polynomial in with the least amount of error and the constants are determined accordingly.

Using ordinary least squares regression, the constants can be determined as follows:

$$\left[a \ b_1 \ \dots \ b_k \ c_1 \ \dots \ c_{(k^2+n)/2} \right]^T = (X^T \cdot X)^{-1} \cdot X^T \cdot Y \quad (4.18)$$

Where, the matrices in Equation 4.17 are denoted as follows:

$$\begin{aligned}
 X &= [X_1 \ X_2 \ \dots \ X_k] \\
 A &= a \\
 B &= [b_1 \ b_2 \ \dots \ b_k] \\
 C &= \begin{bmatrix} c_1 & \dots & c_k \\ \vdots & \ddots & \vdots \\ 0 & \dots & c_{(k^2+n)/2} \end{bmatrix}
 \end{aligned} \tag{4.19}$$

For the 7 variables (Table 4.1) chosen in the preceding section, B is a 1×7 single row matrix and C is a 7×7 upper triangular matrix. Therefore also including constant parameter A the model has 36 constant parameters to be determined for each region shown in Table 4.2.

4.2.3.2 Results

The polynomial model shows good results in the first two regions, where the PM emissions are rather low.

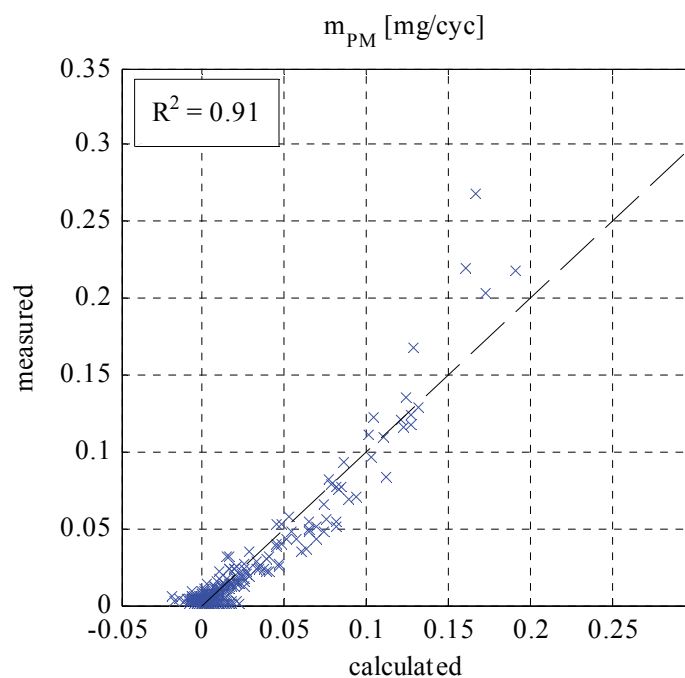


Figure 4.5 Measured vs. calculated PM mass per cycle for the steady state calibration data set from engine A. Polynomial model.

However it has problems in curve fitting in the third and fourth regions where there are more data points present and PM output is higher. It is likely that the soot mechanisms in this region change their behavior in a somewhat complex pattern with respect to the input variables. Hence, it could be the case that a second order polynomial is not sufficient to be able to represent this behavior.

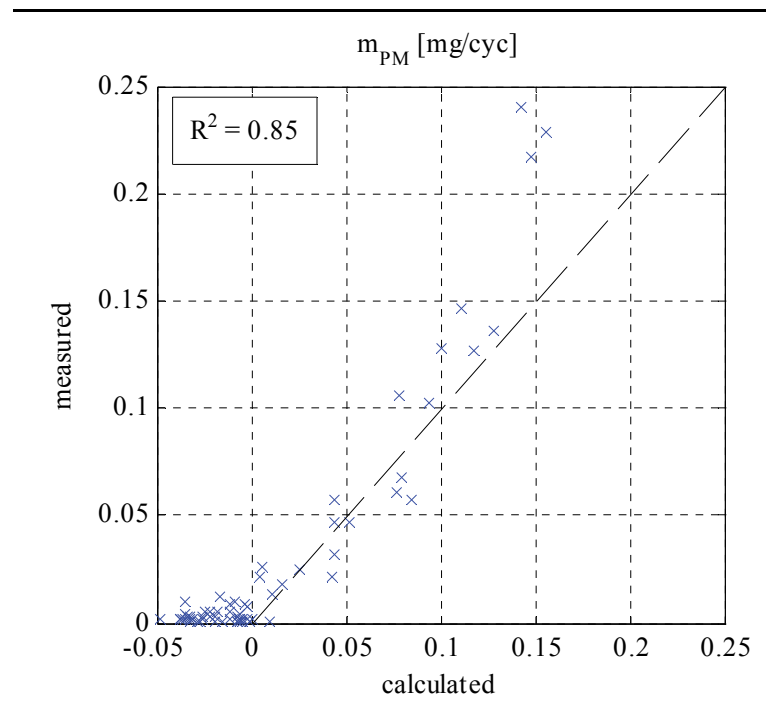


Figure 4.6 Measured vs. calculated PM mass per cycle for the steady state validation data set from engine A. Polynomial model.

Calculating the PM emissions for the validation data set using the constants already determined for the calibration data set, it is seen that the output is similar (Figure 4.6).

Largest deviations occur near the endpoints of the upper and lower intervals. This is expected for polynomial fitting. Besides, this effect points out the poor extrapolation ability of polynomial models.

It can be seen on Figure 4.7 that the tendencies of PM increasing with EGR rates can be replicated to some extent. Yet the negative values are unacceptable.

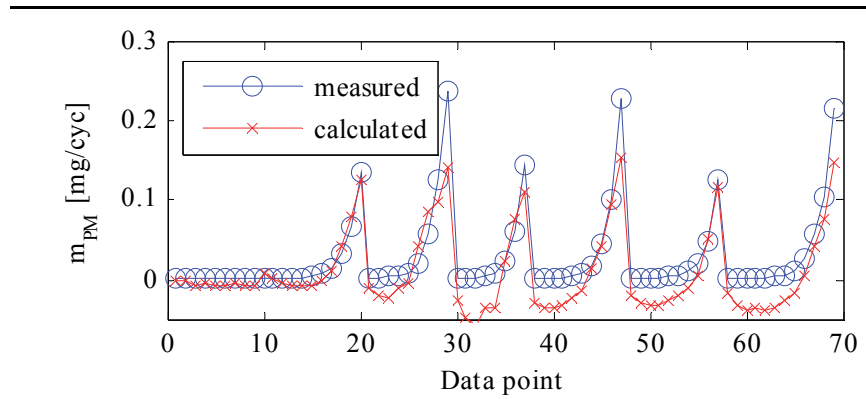


Figure 4.7 Measured and calculated PM mass per cycle for the steady state validation data set from engine A. Polynomial model.

4.2.4 Exponential Products Approach

PM estimator, the final model, has been developed in the form of an exponential products model similar to the approach used by Wenzel (2006). This model structure (see Equation 4.20) has proven itself to be better over polynomial models in terms of extrapolation ability.

$$Y = A \cdot X_1^{n_1} \cdot X_2^{n_2} \cdot X_3^{n_3} \dots X_k^{n_k} \quad (4.20)$$

Exponential terms in this equation are easy to calculate in the engine ECU using simple 1-D lookup tables. It saves calculation effort and makes the model easily applicable in practical conditions. Compared to the polynomial approach, this model has less number of configurable parameters. Therefore less memory space is allocated in the ECU for the used constants.

An overview of the PM estimator is depicted in Figure 5.11. Selected variables shown in the figure are the same variables used for the polynomial model and have already been presented in detail in the preceding sections. Firstly the variables are scaled then go into the corresponding lookup tables as input that are determined according to the constant exponents.

4.2.4.1 Calibration

Correction factor A and the exponents n_1 to n_7 have been determined separately for all four regions based on the minimization of the cost function f in Equation 4.21. This term is derived from the mean absolute error and the correlation factor.

The cost function used for model calibration is given as:

$$f = MAE \cdot (1 - R^2) \quad (4.21)$$

where MAE (Mean Absolute Error) is:

$$MAE = \frac{1}{n} \sum_{i=1}^n |X_i - Y_i| \quad (4.22)$$

and sample Pearson correlation coefficient is:

$$R = \frac{\sum_{i=1}^n (X_i - \bar{X})(Y_i - \bar{Y})}{\sqrt{\sum_{i=1}^n (X_i - \bar{X})^2} \sqrt{\sum_{i=1}^n (Y_i - \bar{Y})^2}} \quad (4.23)$$

Minimization of the term f has been done with the help of the common software *Matlab* using the function *fmincon*. The function tries to converge to a global minimum using quasi-Newton methods, starting off at initial given estimates of the exponents. Constraints have been set for the exponents so that a physically sound output is delivered at the end of the optimization. These constraints are presented in Table 4.3.

As seen in Table 4.3 all the exponents have been constrained to a value of ± 5 in general to prevent the model output from being too sensitive to respective variable changes.

Table 4.3 Model parameterization constraints used in calibration.

model variable	N	p_{rail}	x_{uIVC}	x_{uEVO}	$\Delta\varphi_{comb}$	$\Delta\varphi_{diff}$	τ_{char}
exponent	n_1	n_2	n_3	n_4	n_5	n_6	n_7
upper boundary	+5	0	0	0	+5	+5	+8
lower boundary	-5	-5/-8	-5/-8	-5	-5	0	0

The input n_7 has a higher constraint since an improvement on the model quality has been seen by raising the upper boundary. Moreover, n_2 and n_3 have different lower boundaries for the two different engines as it has been influential on the accuracy. Furthermore, n_2 , n_3 and n_4 are constrained to have negative values since the respective inputs need to reproduce the desired behavior of being inversely proportional with PM emissions. Vice versa holds for n_6 and n_7 since the PM emissions should ideally increase as the corresponding variables increase. However n_1 and n_5 could adapt positive or negative values as the corresponding inputs shouldn't have a straightforward defined relationship with PM.

Experience on setting these listed boundaries has also been gained through cross checking models of engine A and B on each other. For example the model that had been configured for Engine A was tested on Engine B data. If the results delivered by the model on engine B were found qualitatively ill conditioned, it had been concluded that model wasn't physically well founded, even if it fitted the engine A data accurately. In such a case the boundaries have been manually altered in search of a certain qualitatively acceptable behavior of the model on the other engine. After the constrained minimum has been found selected values of model constants for the two different engines are presented in Table 4.4 and Table 4.5. The effect of the inputs on the soot emissions can be deduced from the magnitude of the constants. Constants that are parameterized with zero showed little or no effect on the results.

Accuracy of the PM Estimator at different regions is highly dependent on the availability of calibration data, whereas the highest relative accuracies are achieved generally in region 2.

Table 4.4 Model parameterization, engine A.

Const.	Reg. 1	Reg. 2	Reg. 3	Reg. 4
A	0.0105	0.0032	0.0067	0.0003
n_1	1.081	1.713	-0.241	3.880
n_2	-0.738	-1.693	0	0
n_3	-5.000	-4.772	-1.192	-5.000
n_4	-2.850	-1.205	-2.047	-1.581
n_5	-0.048	0.706	-1.545	-4.943
n_6	0.239	0.607	3.537	2.447
n_7	3.269	0.308	2.173	0

Table 4.5 Model parameterization, engine B.

Const.	Reg. 1	Reg. 2	Reg. 3	Reg. 4
A	0.0012	0.0021	0.0019	0.0084
n_1	-0.096	0	0	0
n_2	-4.610	-3.910	-1.887	-1.884
n_3	-5.793	-6.388	-3.087	-3.868
n_4	-1.009	-0.964	-1.612	0
n_5	1.167	2.679	-0.005	1.323
n_6	1.162	0	1.236	0.315
n_7	5.424	0.535	2.244	1.786

4.2.4.2 Results

In the following, the results of the exponential products approach on the two engines are presented. Calibration and validation of the model are done based on the datasets presented in section 3.1.

Engine A

The fitness of the calibration can be seen on Figure 4.8.

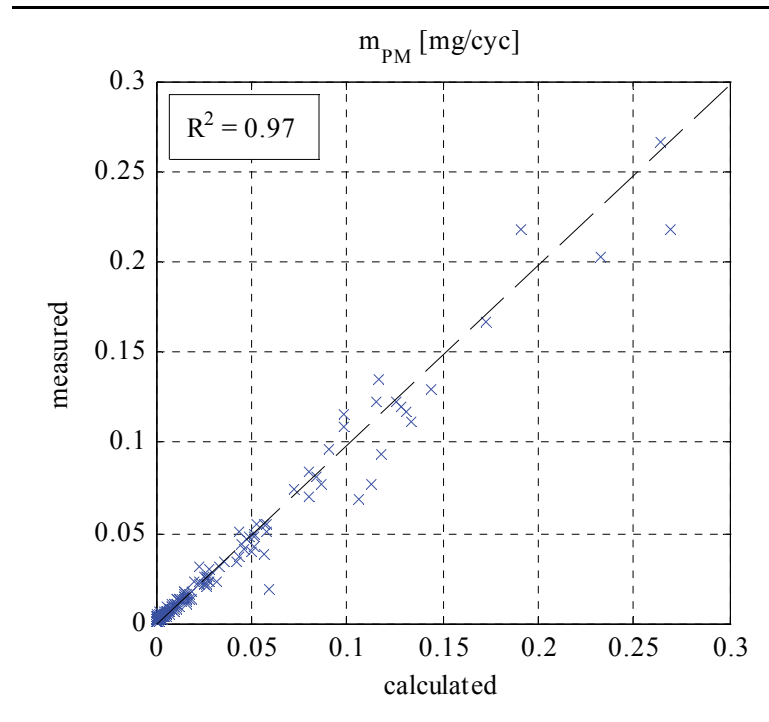


Figure 4.8 Measured vs. calculated PM mass per cycle for the steady state calibration data set from engine A.

High values of emissions result from the unusual application cases at some middle load operating points with EGR rate variations of up to 44%, which can be seen on Figure 4.9 starting around 100th data point. This was already an expected result with the calibration data set, since the model has a high degree of freedom. Unfortunately this wasn't the case on the polynomial model presented in the preceding section.

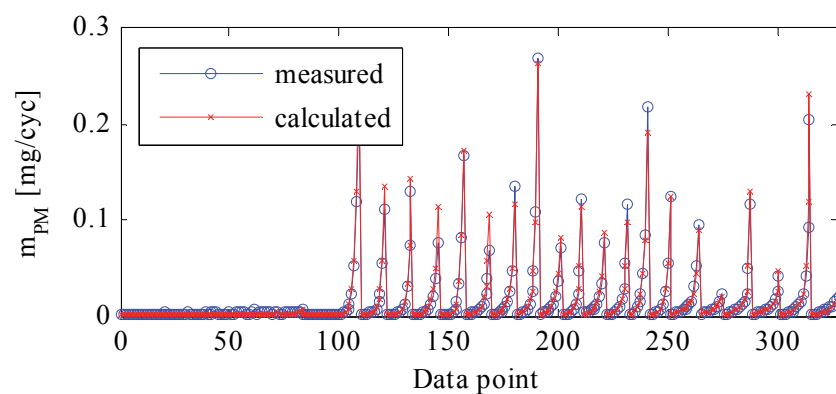


Figure 4.9 Measured and. calculated PM mass per cycle for the steady state validation data set from engine A.

The results with the validation data showed a constant drift (Figure 4.10) with increasing emissions. This may be related to the different test bench setup.

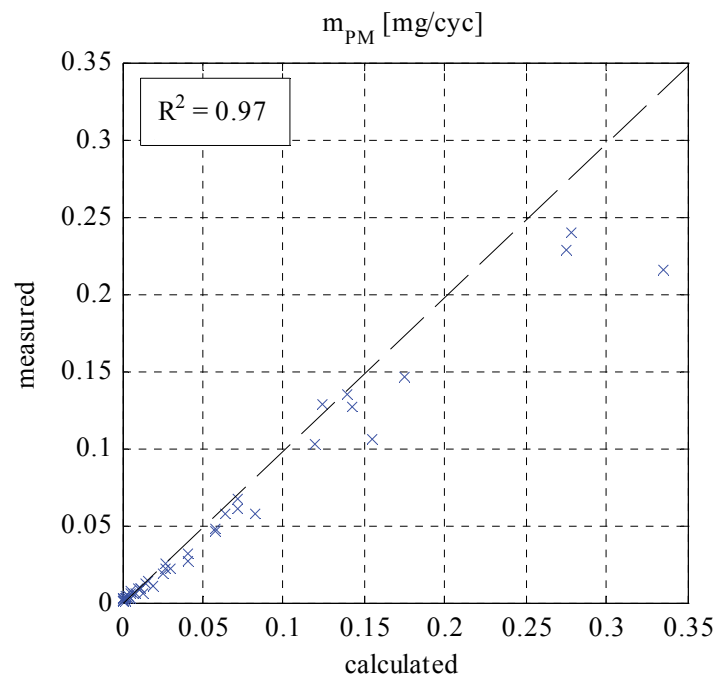


Figure 4.10 Measured vs. calculated PM mass per cycle for the steady state validation data set from engine A.

Thus, the accuracy of the model is acceptable, whereas there is still improvement potential through better distribution of measured data points on the engine map.

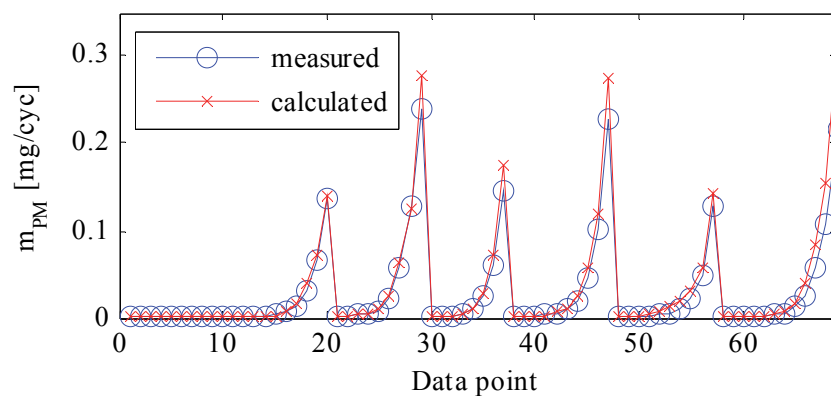


Figure 4.11 Measured and. calculated PM mass per cycle for the steady state validation data set from engine A.

On Figure 4.13, the effect of the EGR variations can be seen clearly on the model input variables. Characteristic time is seen to be increasing with increasing EGR rate. That is a sign that the combustion is getting slower as the EGR rate is increased.

However the correlation factor remained the same and it can also be seen from Figure 4.11 that the emission trends with varying EGR rates, at different SOI values and load conditions are successfully represented by the model (see Figure 4.12).

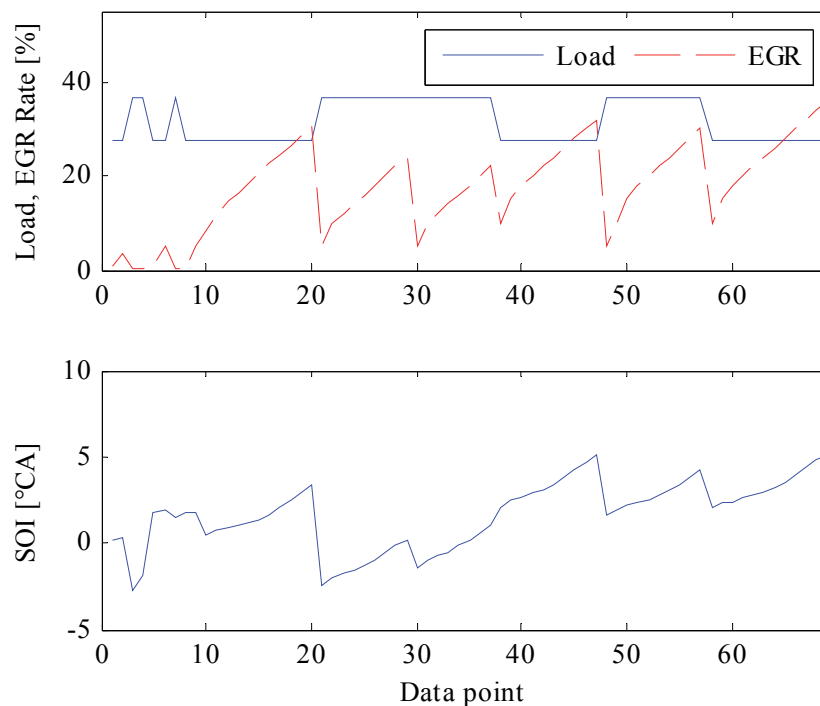


Figure 4.12 Load, EGR (top) and SOI (bottom) values for the steady state validation data set from engine A.

Moreover, if the data point intervals 20-30 and 30-40 are to be compared, it can be seen that SOI has been retarded at the interval 30-40 by about $+1^{\circ}\text{CA}$ (see Figure 4.12). Looking at Figure 4.13 in these intervals, it can be seen that the diffusive combustion duration $\Delta\varphi_{diff}$, as well as overall combustion duration $\Delta\varphi_{comb}$ are getting shorter with retarding the SOI. However, the ratio of diffusive combustion to the overall combustion duration is increasing, because with the later injection, a larger portion of the injected fuel is burned in non-premixed combustion.

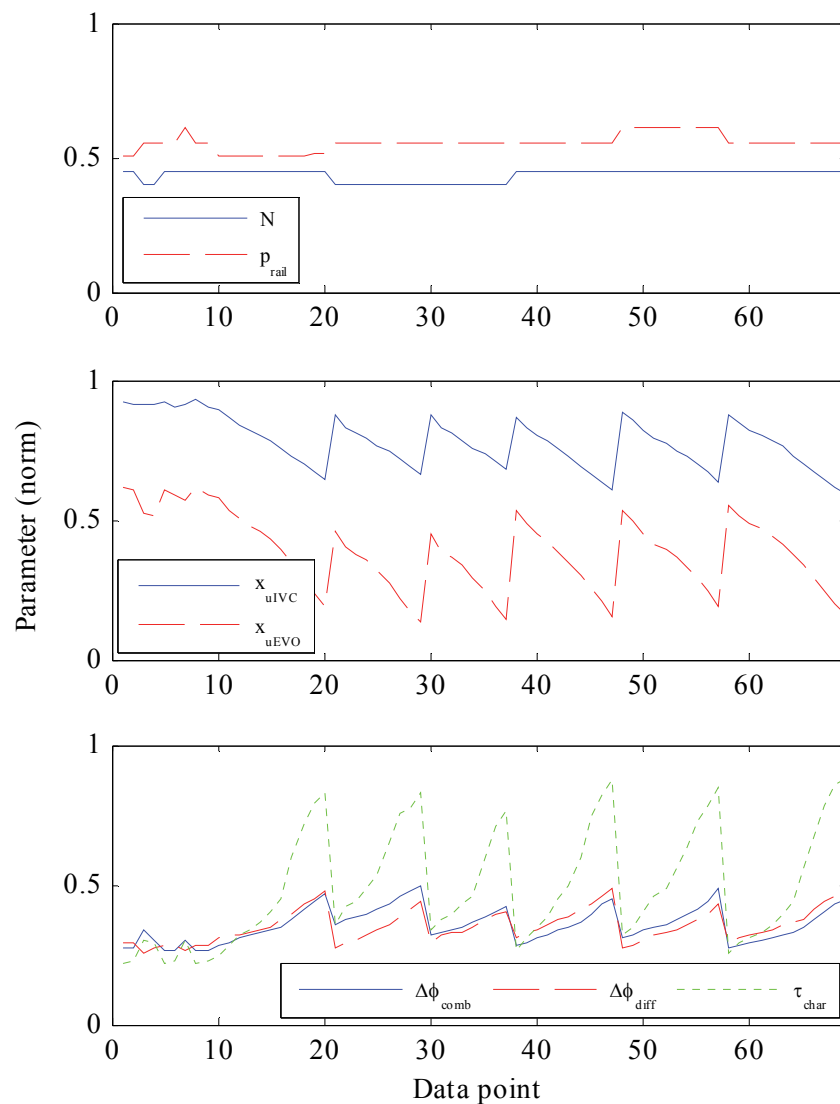


Figure 4.13 PM Estimator input values for the steady state validation data set from engine A.

This plausible change in the model variables with respect to changes in engine variables supports the reliability of the derived model input variables.

Engine B

Similar results with the calibration set from engine B have been obtained (see Figure 4.14). Please note that the number of data points in the calibration set is less than a half of the number of data points used for engine A.

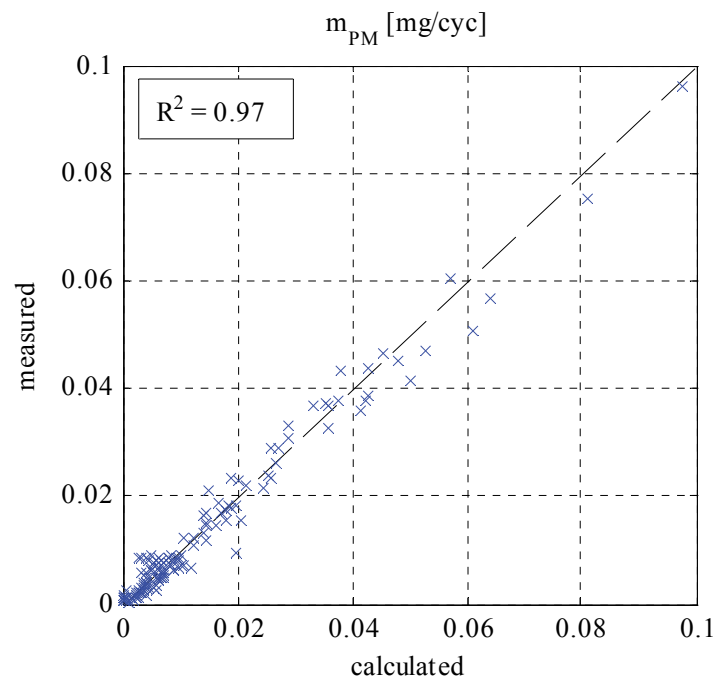


Figure 4.14 Measured vs. calculated PM mass per cycle for the steady state calibration data set from engine B.

However the data points are widely spread on the engine map covering a wide range of combustion characteristics and therefore allow a better calibration of the model (see Figure 3.1).

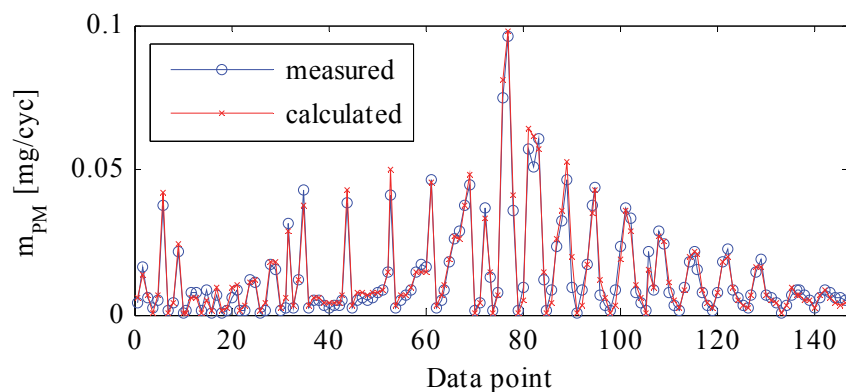


Figure 4.15 Measured and calculated PM mass per cycle for the steady state calibration data set from engine B.

For the validation of the model using transient measurements the model parameterization stayed unchanged, except for the correction factor A , which has

been multiplied by one constant for all four regions mentioned earlier. Measured and calculated emissions for the transient NEDC show good correlation and it is seen that the curves are even overlapping in some regions (see Figure 4.16). Even the emission peaks are estimated with a good accuracy, owing to the fast response of the cylinder pressure based model inputs.

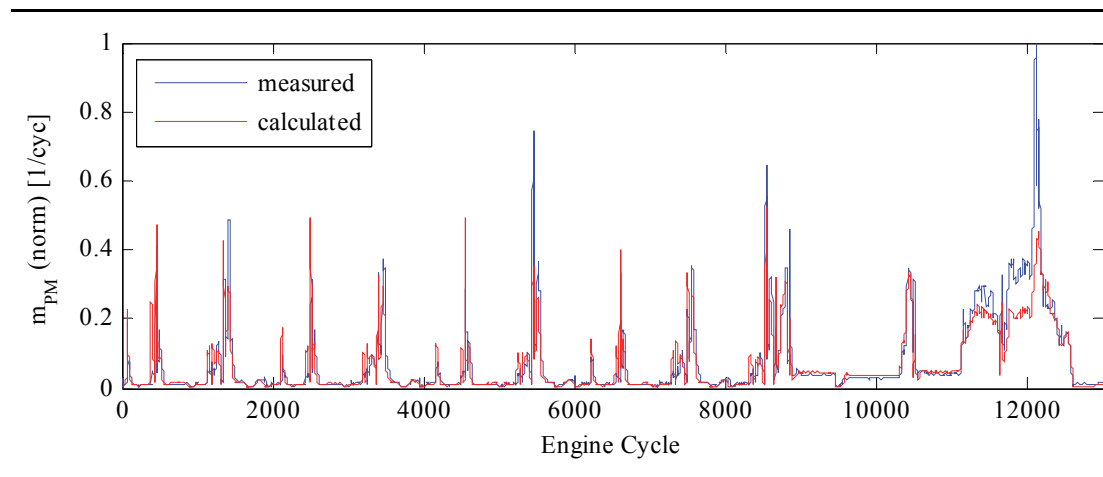


Figure 4.16 PM emission from engine B during NEDC for transient validation data set. Please note that the emission values are normalized.

Calculated cumulative curve shows good agreement with the measured emissions (see Figure 4.17).

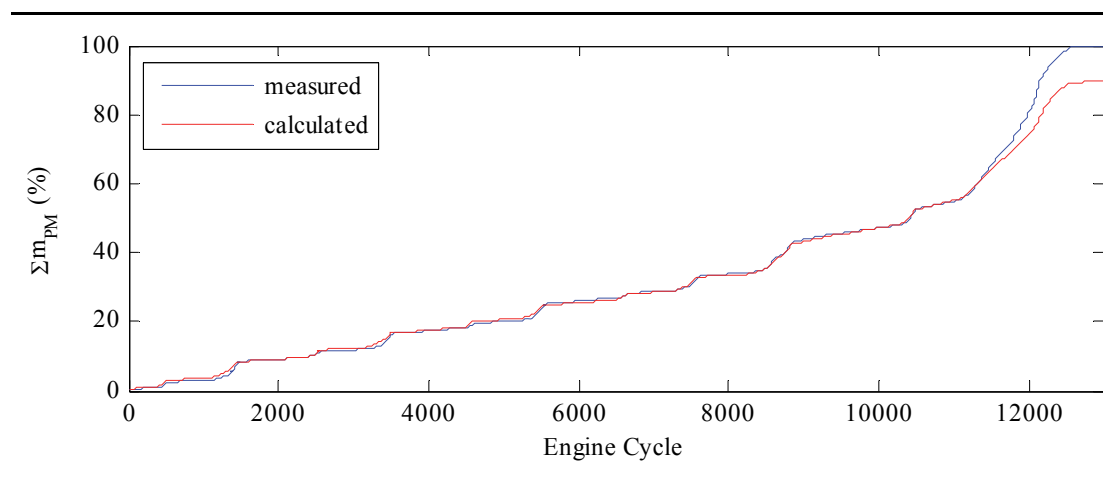


Figure 4.17 Cumulative PM emission from engine B during NEDC for transient validation data set..

It is presumed that the drift towards the end of the measurement cycle leading to a

cumulative error of approximately 10% is caused by a defective HFM measurement at higher rates of air mass flow. Considering the accuracy of the cumulative results, the model may even be suitable for estimating DPF loading.

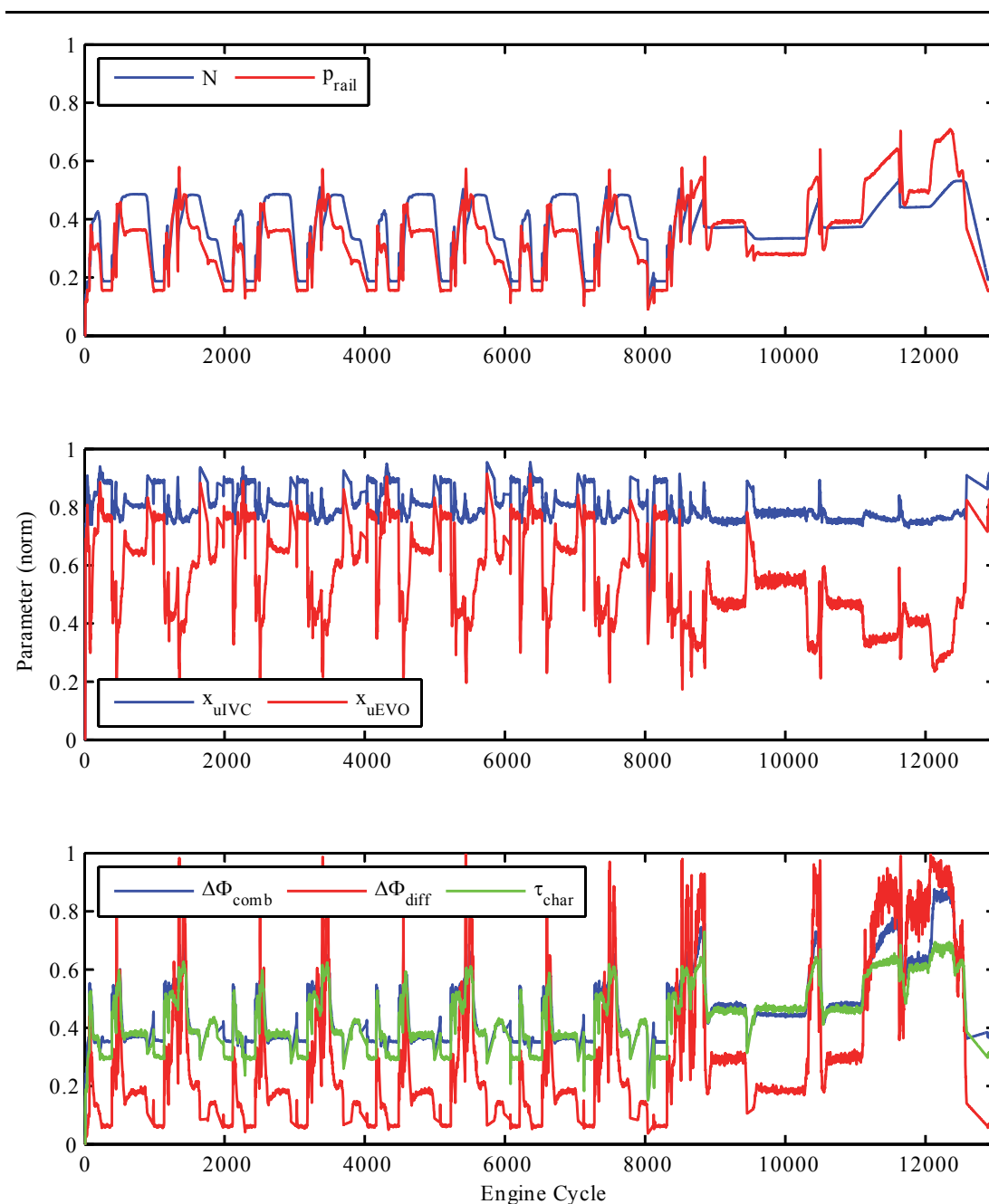


Figure 4.18 Model variables from engine B during NEDC for transient validation data set. Please note that the emission values are normalized.

Cylinder pressure signals from the transient test had a sampling rate of 1.0 °CA

instead of 0.5 °CA as in steady state measurements. Considering this, it can also be concluded that the high sampling rate of the experimental equipment is not necessary.

4.2.5 Sensitivity Analysis of the Model Variables

Following plots in this section depict the relationship of the chosen individual variables with PM emission values for each engine and operating region. Additionally, model approximation curves based on the exponential terms are shown on the figures. It should be taken into account that the plots have been scaled so that the area within the variables exist is shown in more detail. Further the vertical position of the approximation curve is aligned with the scatter of data points for better visualization. Vertical position of these model fitting curves are negligible since the model output is corrected by the factor A as seen in Equation 4.20.

4.2.5.1 Engine A

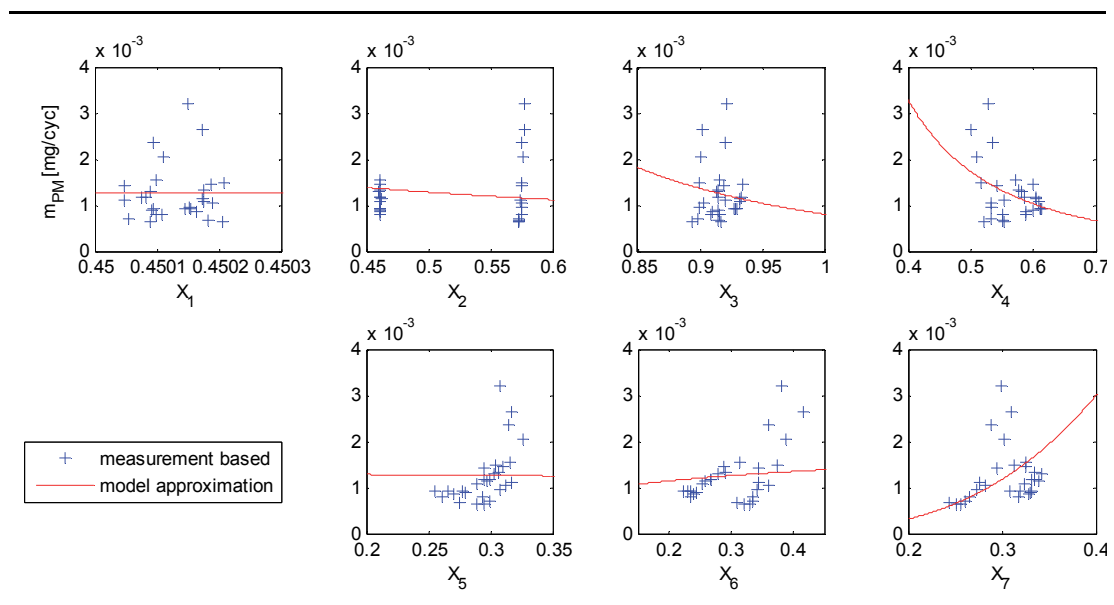


Figure 4.19 Variable sensitivities for Region 1 Engine A.

At regions 1 and 2 (Figure 4.19 & Figure 4.20) it is hard to find a good correlation of PM emissions with model variables. Emission values are relatively low in these regions and this makes PM values prone to measurement errors. Only correlation can

be seen for variables X_5 and X_6 on both regions which points out to the sensitivity of in-cylinder pressure based variables.

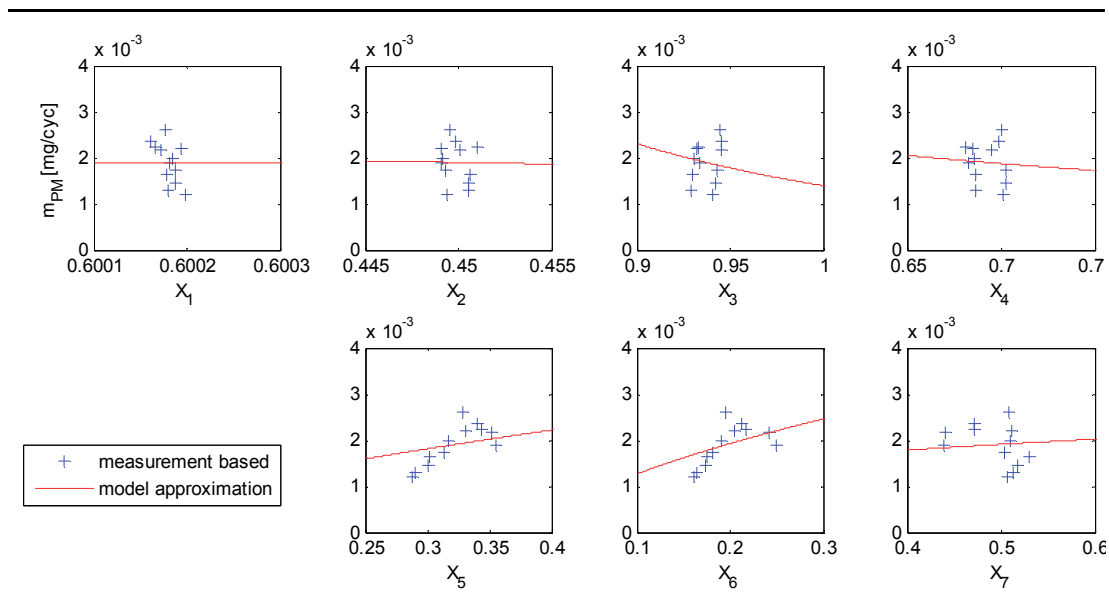


Figure 4.20 Variable sensitivities for Region 2 Engine A.

On the other hand, these plots also depict the irregular behavior of net PM emission values that are indirectly related to engine variables.

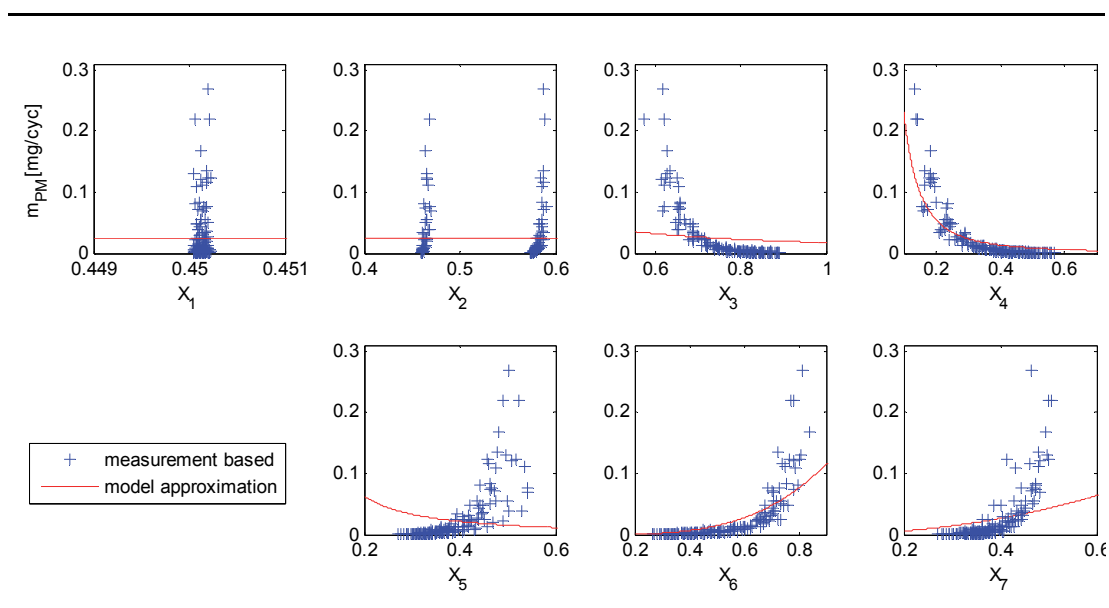


Figure 4.21 Variable sensitivities for Region 3 Engine A.

It is emphasized here that the exponents of the variables have not been determined individually because of the complex cross influences of the chosen model variables on PM emissions. As described in the preceding section these PM model exponents have been calibrated as a whole but separately for each region.

For region 3 and 4 (Figure 4.22 & Figure 4.23) on engine A correlation can be observed on variables X_3 , X_4 , X_5 , X_6 and X_7 .

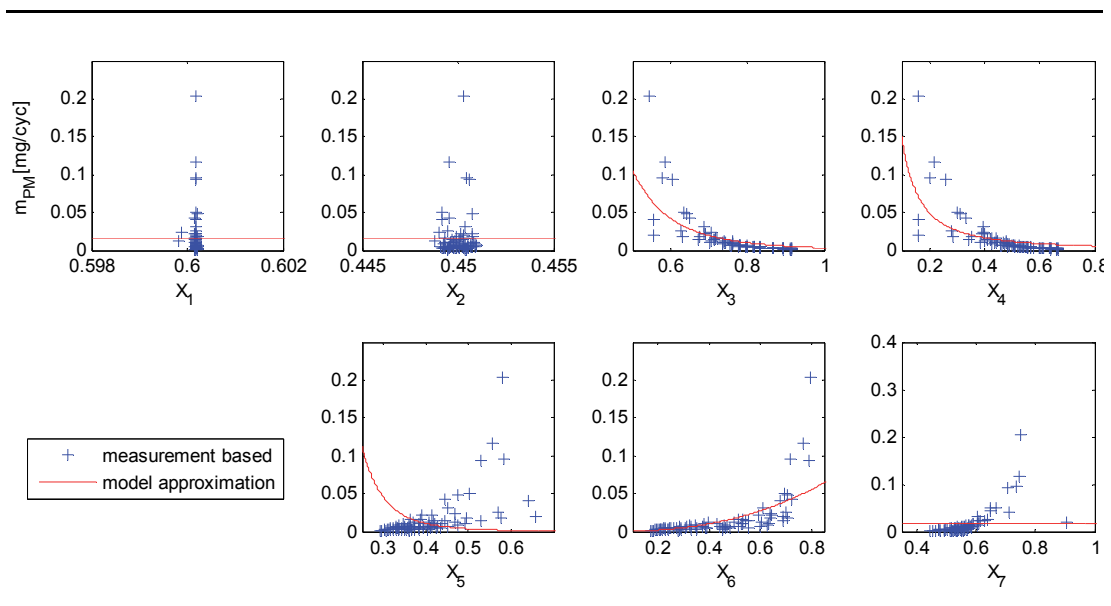


Figure 4.22 Variable sensitivities for Region 4 Engine A.

Although X_5 shows an opposite trend to the fitted curve, it has been observed that not constraining its exponent to have positive values during calibration (see Table 4.3) has produced better results for the complete model. Even if the curves were to be fitted on a variable individual basis, it hasn't led to an optimal solution as a whole.

4.2.5.2 Engine B

Calibration results for engine B in look better in the first two regions.

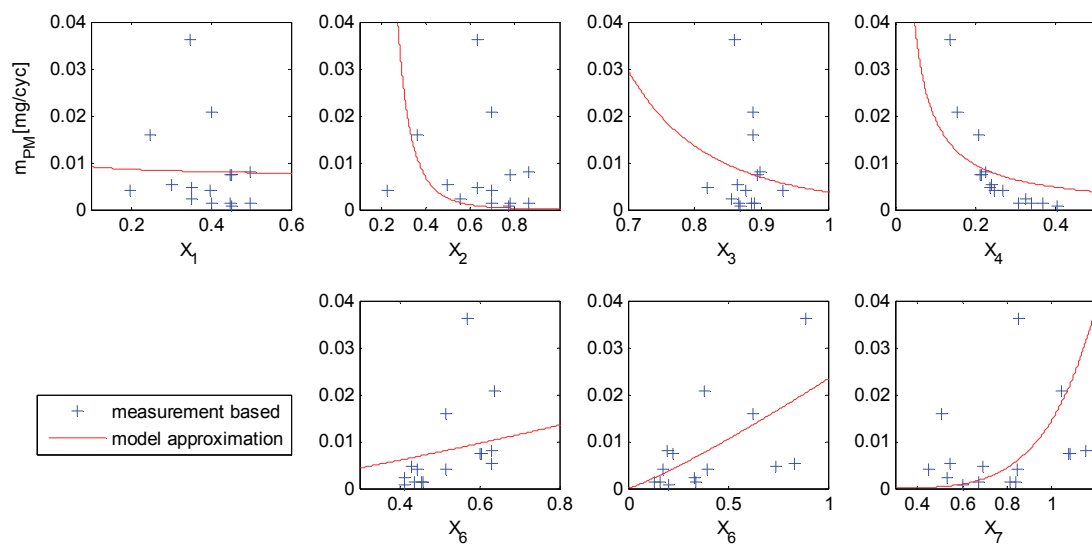


Figure 4.23 Variable sensitivities for Region 1 Engine B.

As it is shown on Figure 4.24 & Figure 4.25 PM emissions are higher for engine B compared to the engine A, mainly due to higher EGR rates realized at these operating conditions during measurements. Especially in region 2 some obvious correlation can be seen for variables X_3 , X_5 and X_7 .

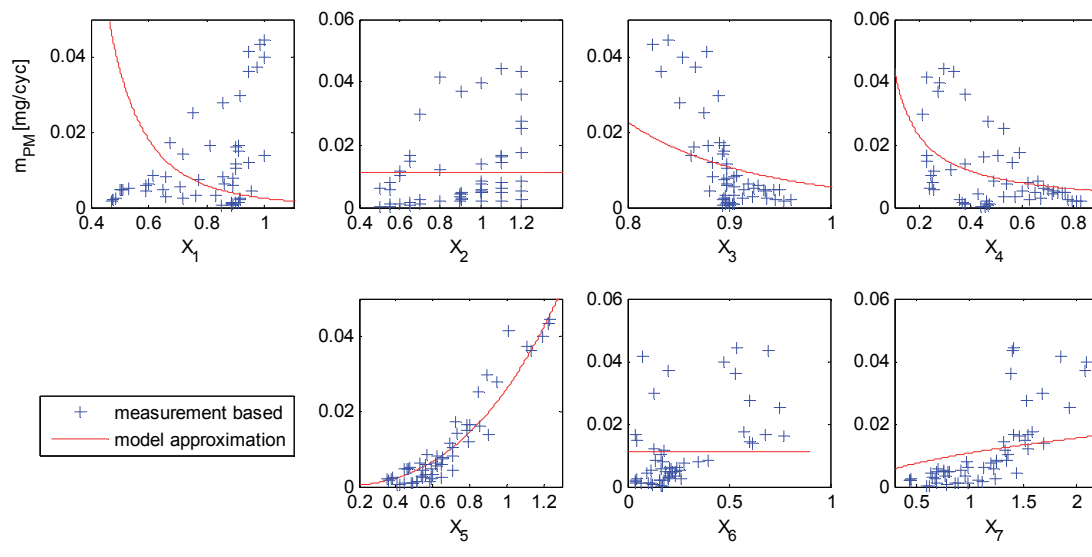


Figure 4.24 Variable sensitivities for Region 2 Engine B.

In Figure 4.25 & Figure 4.26, it can be seen that the correlation is not as obvious

as in engine A data.

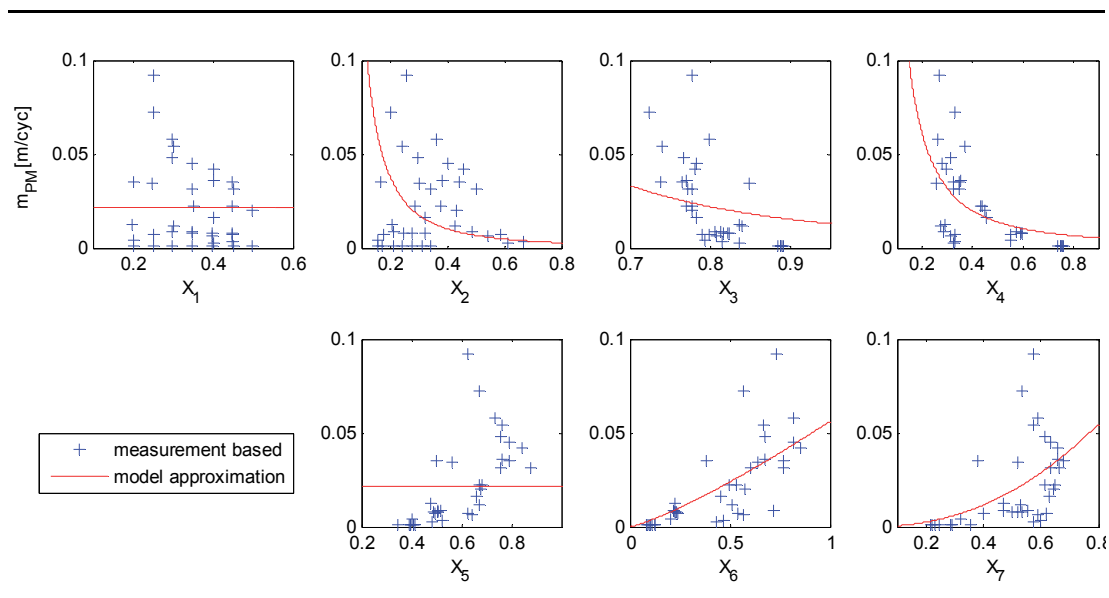


Figure 4.25 Variable sensitivities for Region 3 Engine B.

PM emissions in Figure 4.21 & Figure 4.22 are observed to change rather regularly with varying variables. This is due to the EGR variation measurements included in the calibration data set for engine A (Figure 3.1). These variations account mainly for the data points in the regions 3 and 4.

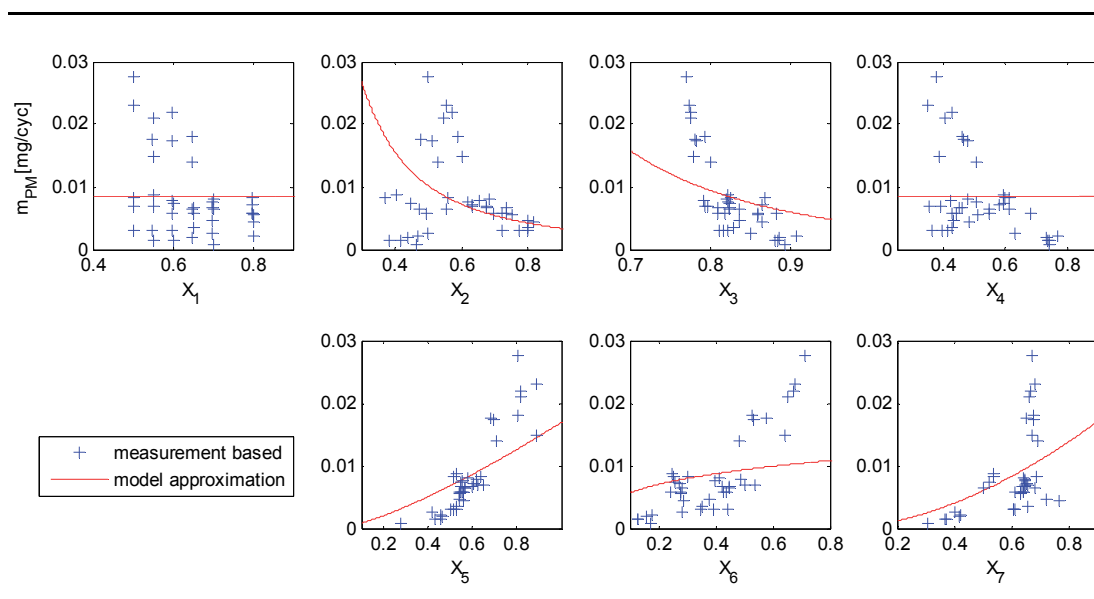


Figure 4.26 Variable sensitivities for Region 4 Engine B.

Since on engine B other variables are changing simultaneously with EGR rate, the data is rather scattered as seen in the last two figures.

4.2.6 Model Sensitivity to Pressure Signal Deviations

The effect of deviations in cylinder pressure on PM emission is investigated in this section. Figure 4.27 shows the value of pressure offset correction for transient test bench measurements on engine B. For this particular measurement it is observed that the cylinder pressure sensor offset error deviates roughly within ± 0.06 bar and the average error lies at approximately 0.02 bar. This offset error has been corrected as presented in section 3.2.1.1.

Based on this measurement the pressure offset error has been reproduced manually. At constant offset of $p \pm 0.03$ bar emissions have been calculated once again. Figure 4.28 depicts the variations of cylinder pressure based model variables. The highest impact is seen on X_6 (diffusive combustion duration) whereas X_5 (overall combustion duration) and X_7 (char. mixing time) are effected less from the offset error.

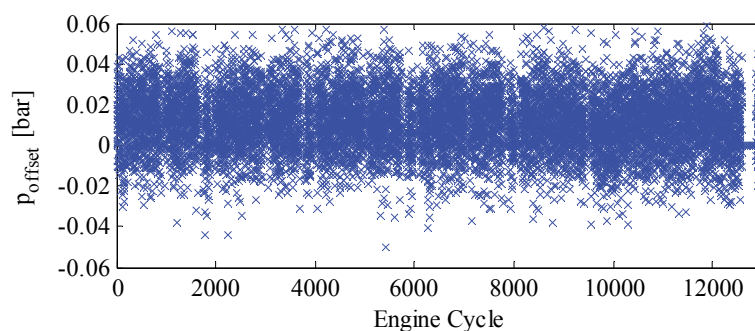


Figure 4.27 Effect of deviations of in-cylinder pressure signal on model outputs for engine B. Interval from transient validation dataset.

This deviation also affects the model output as shown in Figure 4.29. An error of ± 0.03 bar caused a deviation of $\pm 10\%$ in the cumulative PM emission for NEDC test.

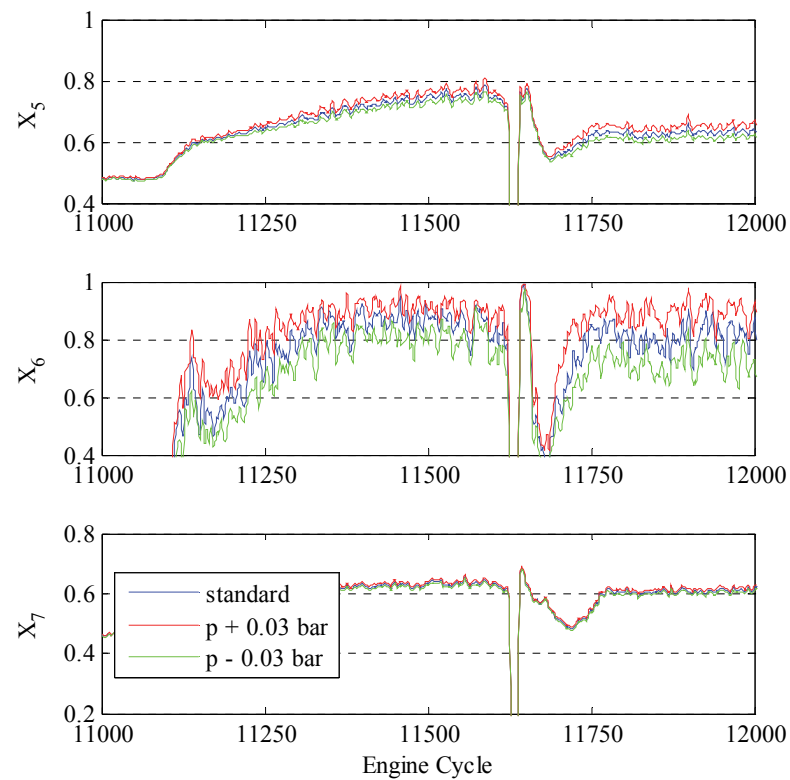


Figure 4.28 Effect of deviations of in-cylinder pressure signal on model outputs for engine B. Interval from transient validation dataset.

Since such small errors resulted in relatively high deviations in the model output, sensitivity of the PM estimator to cylinder pressure is considered significantly high based on the presented findings.

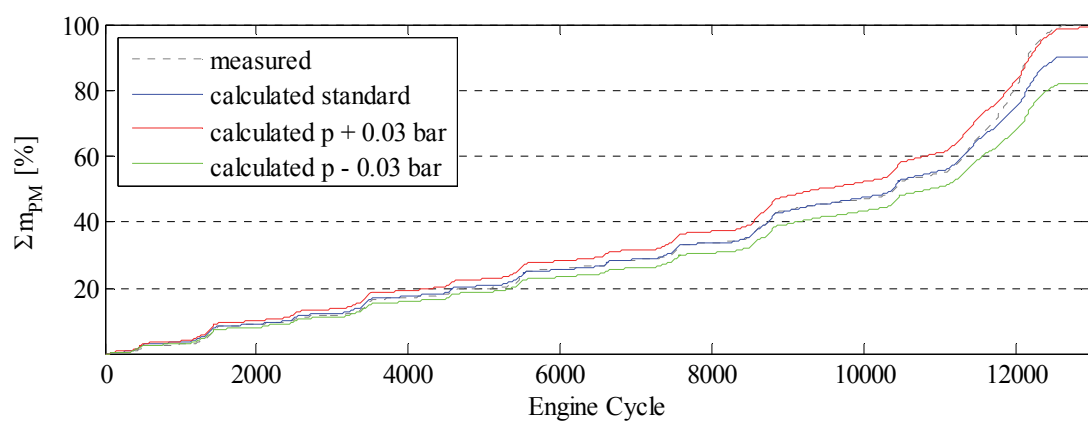


Figure 4.29 Effect of deviations of in-cylinder pressure signal on cumulative model output for engine B. Transient validation dataset.

This point should be further investigated in future studies based on the type of cylinder pressure sensor to be used. As discussed in the preceding sections, in-cylinder pressure acquisition systems to be used in series production engines would be rather economical solutions compared to the expensive research setup used for this model development with better pressure sensors and higher sampling rates. Therefore it should be ensured that the in-cylinder pressure signal is accurate enough to enable the PM estimator to produce sound results.

CHAPTER FIVE

IN-CYLINDER EMISSIONS CONTROL

Recalling from the first chapter, in-cylinder control of combustion is a rising trend. Back then, Leonhardt, Müller, & Isermann (1999) already discussed in-cylinder pressure based methods, engine supervision and control. They have highlighted many advantages of in-cylinder pressure based control strategies over conventional control as already mentioned:

- Improved engine supervision and driveability
- Better performance, consumption and emissions characteristics
- Reduced sensitivity to manufacturing tolerances and operational aging
- Less initial calibration effort

Once the in-cylinder pressure sensors go into serial production with sufficient reliability and a feasible price, automotive manufacturers would start utilizing them in their engines to be able to get the best out of their engines in terms of performance, consumption and emissions. In-cylinder pressure, heat release rate and temperature curve characteristics of an engine could be controlled in a closed loop by manipulating fuel and air path actuators to achieve these goals.

Controlling in-cylinder raw emissions is more difficult than combustion control as emissions are attached to the combustion processes through mechanisms that are relatively complex and partly unclear. Therefore, still being a subject of research, emissions control within the cylinder is becoming popular with the development of new raw emission sensors. Besides, there are also virtual emission sensors/models under development that would eliminate the need for these hardware sensors.

Stölting, Seeboda, Gratzke, & Behnk (2008) have developed a PM and NO_x emissions controller based on emission sensors on a heavy duty diesel engine. A so called dual split controller structure has been utilized where the PM and NO_x emissions are controlled using separate actuators for each. They stress that the series

application of such emission controllers depend on the development of suitable onboard sensors.

On the other hand there are also examples of in-cylinder pressure based emissions control utilizing virtual sensors. Willems, Doosje, Engels, & Seykens (2010) have developed such a controller firstly to control certain combustion parameters such as 50% heat release rate point and mean effective pressure. Afterwards they coupled their controller with NO_x and PM combustion models to take emissions into account. However as their NO_x prediction accuracy was comparable to a commercial sensor, PM model suffered under the complexity of soot emission mechanisms and was only able to deliver qualitatively acceptable results. Alfieri (2009) has developed an emissions model for controlling NO_x emissions and lambda simultaneously. Moreover, Barro & Tschanz (2010) presented an emissions controller based on air path and fuel path variables.

It is not an easy task to model a diesel engine and control its emissions. Zhijian, Ma, & Huang (2011) describes diesel engine control a typical constrained, nonlinear, coupled, MIMO, time varying optimal control problem. Therefore simplification and linearization of the system is required as well as decoupling of relationships between engine variables and emissions.

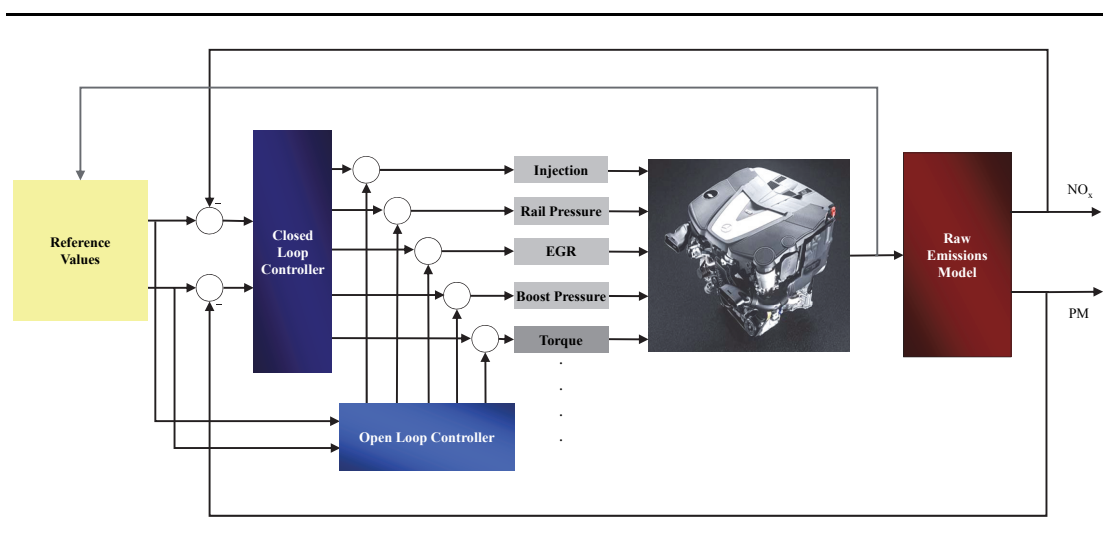


Figure 5.1 Schematic representation of a model based raw emissions controller.

In Figure 5.1 an initial controller design is depicted. Utilizing the developed PM estimator along with a readily available NO_x model with similar structure, a closed loop emissions controller has been developed and tested for DI diesel engines. In the following sections, actuating variable selection, controller structure, implementation and results will be discussed.

5.1 Actuating Variables Selection

Actuating variables are selected based on the engine parameters discussed in Section 2.3.4. Possible candidates are also shown on Figure 5.1.

Boost pressure has been the first variable to be eliminated. The effect of boost pressure on emissions is somewhat complicated (section 2.3.4.2). Besides, it would have a direct effect on the engine torque during operation.

Rail pressure (Section 2.3.4.5) has also been eliminated since it is usually calibrated to its limits, with respect to performance and emissions and generally higher pressures are already favored.

Out of the injection parameters, it has been decided that only the pilot injection amount (Section 2.3.4.6) would be used as an actuating variable. The decision has been made due to the presence of a readily available in-cylinder based closed loop combustion form controller. This controller keeps a desired value of a so called CFF (Combustion Form Factor) by controlling the pilot injection amount based on in-cylinder pressure feedback.

CFF describes a certain form based on the heat release curve (Otto, Pfaff, Liebscher, Bogachik, & Binder, 2006). It is almost proportional to the ratio of the pilot injection to the main injection quantity as seen in Figure 5.2.

It has been seen that this factor has a similar effect on the emissions as the pilot injection amount and even physically more correct to use since it directly represents a characteristic of the combustion itself.

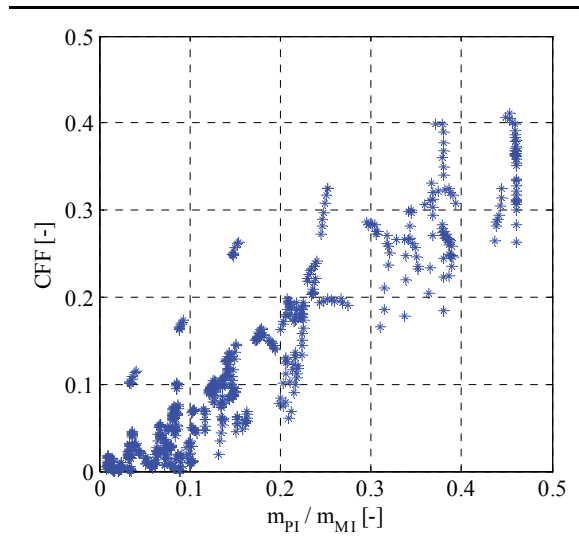


Figure 5.2 Relationship between CFF (Combustion Form Factor) and ratio of pilot injection to main injection amount.

Furthermore, EGR has been selected as the second actuating variable. It has vast effects on the emissions (section 2.3.4.1) without undesired effect on engine performance as long as the maximum EGR rate limits are not reached that would cause misfires in combustion.

5.2 Emissions Controller Design

Based on the chosen actuating variables a MIMO emissions controller with two inputs and two outputs has been designed.

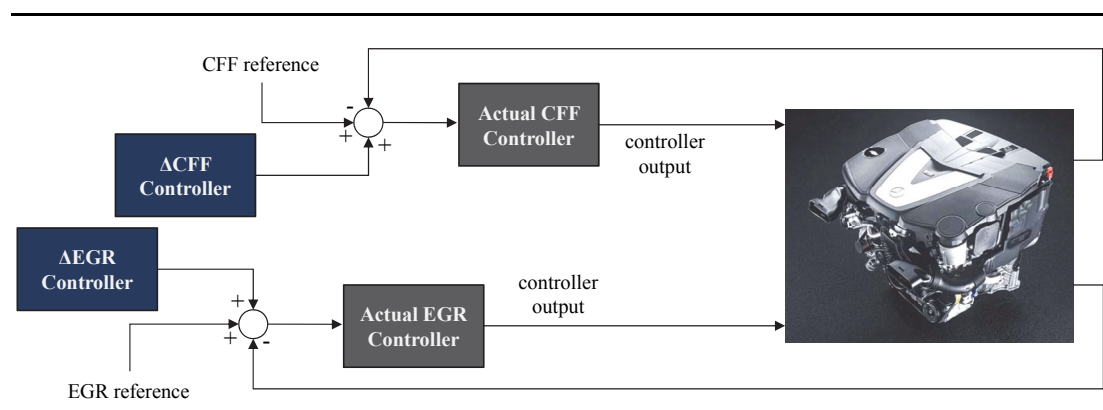


Figure 5.3 Cascaded controller structure.

A cascaded control structure has been chosen since the secondary process that is the EGR rate control and CFF control have causal effects on the NO_x and PM emissions that are to be controlled. Therefore existing (actual) controllers for the EGR rate and pilot injection amount have not been modified. As an analogy to management principle, the aim of the cascade controller is to manage these controllers in favor of emissions when desired. The two existing controllers have been regarded as black boxes and have not been further investigated.

Cascaded controllers are used to alter the reference values of these controllers by supplying them deviation values according to the desired and actual emission values. For this reason the two controllers are denoted with Δ 's as prefix ; namely ΔCFF and ΔEGR controllers (Figure 5.3).

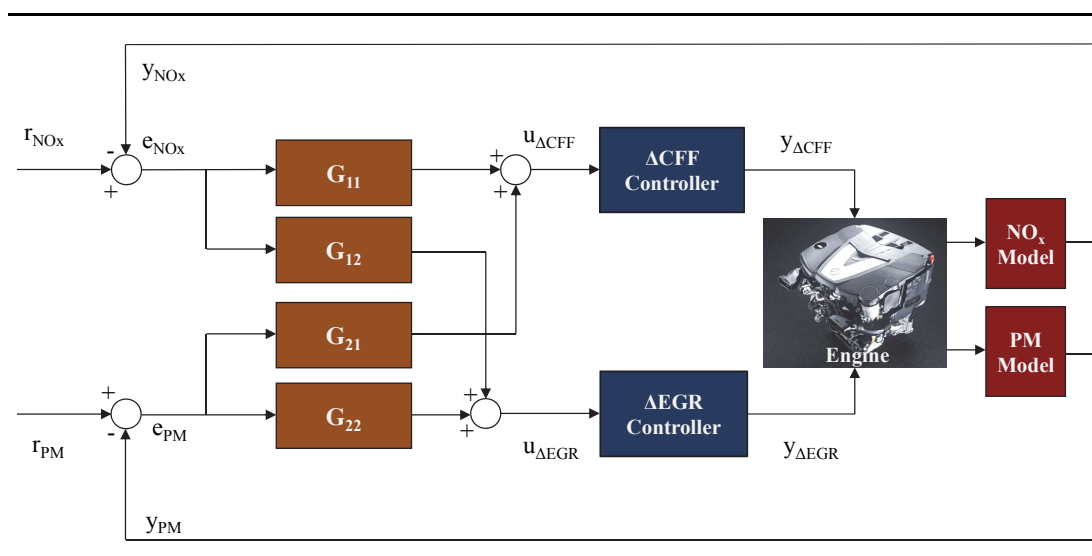


Figure 5.4 In-cylinder emissions controller.

Since CFF and EGR both have effects on PM and NO_x emissions; a MIMO structure has been used rather than splitting the system into two controllers. Furthermore, the structure has been decomposed for the sake of simplicity (Figure 5.4). Along with the P-canonical form presented, four feedforward couplings have been created so that the relationships between the actuating variables and emissions are represented in a simpler way. Therefore these system transfer functions (G_{11} , G_{12} ,

G_{21} , G_{22}), when configured accurately, should be able to provide the relevant information about the system to the controllers.

Outputs of the system transfer functions in Figure 5.4 are related to the inputs according to:

$$\begin{bmatrix} u_{\Delta CFF} \\ u_{\Delta EGR} \end{bmatrix} = \begin{bmatrix} G_{11} & G_{21} \\ G_{12} & G_{22} \end{bmatrix} \cdot \begin{bmatrix} e_{NOx} \\ e_{PM} \end{bmatrix} \quad (5.1)$$

Next section describes the determinations of these system transfer functions.

5.2.1 Gain Scheduling

Linear system models are hard to obtain for complex multivariable nonlinear systems. In case of the emissions controller a process model is needed that defines the relationship between emission values and actuating variables. This multivariable system needs to be therefore modeled. There are different approaches concerning this matter. The system can either be modeled analytically by using differential equations to describe the behavior of the emissions with respect to changes in the inputs or empirical models can be used. Regarding empirical models, black box modeling approaches are commonly used for modeling such systems when there is little information or understanding of the real system behavior.

Since creating a complex model was unfavorable in this case, the concept of gain scheduling has been adopted. Gain scheduling can be considered basically as a feedback control system in which feedforward compensation is used to adjust the system gains. It allows to change the gains and thereby the system behavior to adapt to changing system dynamics originating from system nonlinearities (Åström & Wittenmark, 1994).

In the case of the emissions controller, if the gains of G_{11} , G_{12} , G_{21} and G_{22} can be determined based on operating conditions, the system can be approximated in a discrete linear way. Hence, controlling the emissions would be possible.

5.2.2 Calibration

A series of measurement data has been obtained in which EGR and m_{pI} (pilot injection amount) have been varied in the operating map shown in Figure 5.5.

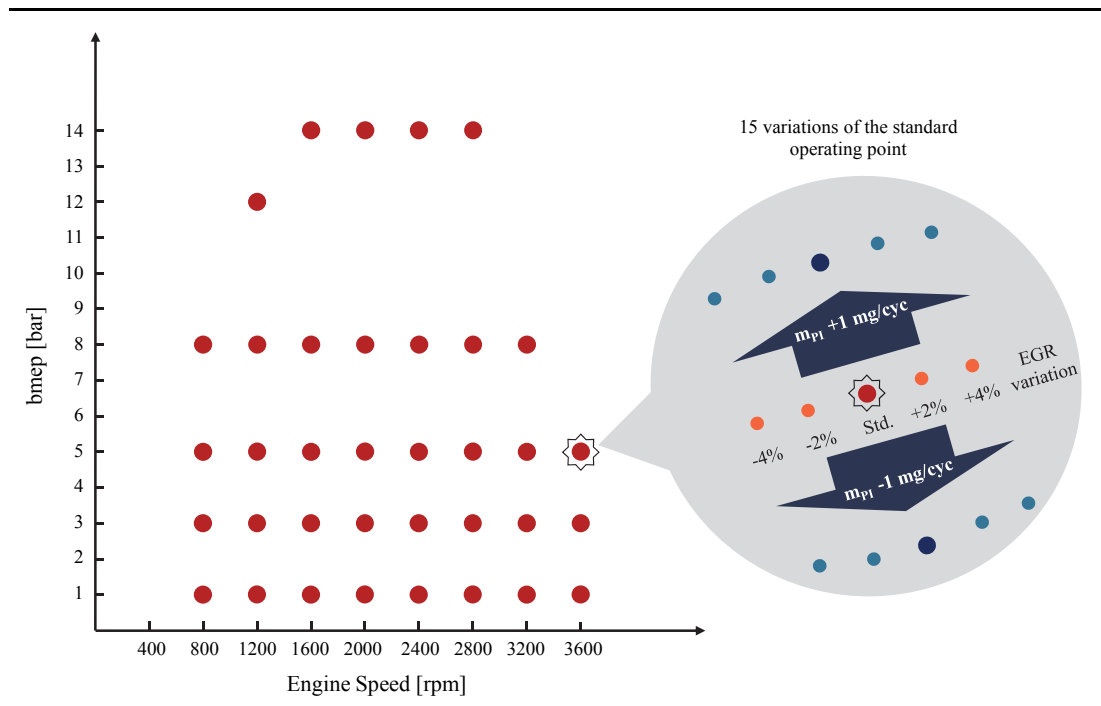


Figure 5.5 Operating points of engine B where the measurements were done for controller calibration.

At each operating point shown on the map, 5 EGR variations and 3 m_{pI} variations have been measured resulting in a total of 15 measurements each point on the operating map.

As seen on the plots in Figure 5.6 to Figure 5.9 output values of the system transfer functions have been plotted against the input values. Effect of the variable changes can be seen.

In each plot, linear fitting is done on the variation curves, a line is obtained and the slopes of these lines represent the gains at the corresponding operating point. Gains at these operating points are obtained by averaging the slopes of all lines in the plots.

On these plots, the effects of the EGR rate and m_{PI} variations on the emissions can be seen clearly. In Figure 5.6 it can be seen that increasing m_{PI} has a slight increasing effect on the NO_x emissions for both low and high load cases.

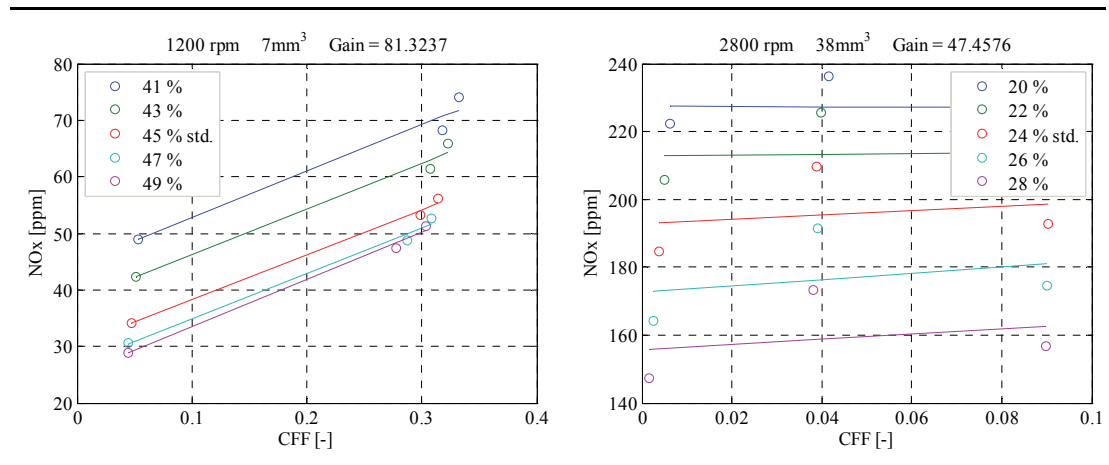


Figure 5.6 Variation of m_{PI} at five different EGR rates for determining the linear gain K_{11} value (NO_x/CFF) at two different operating points, low load (left), high load (right) on engine B.

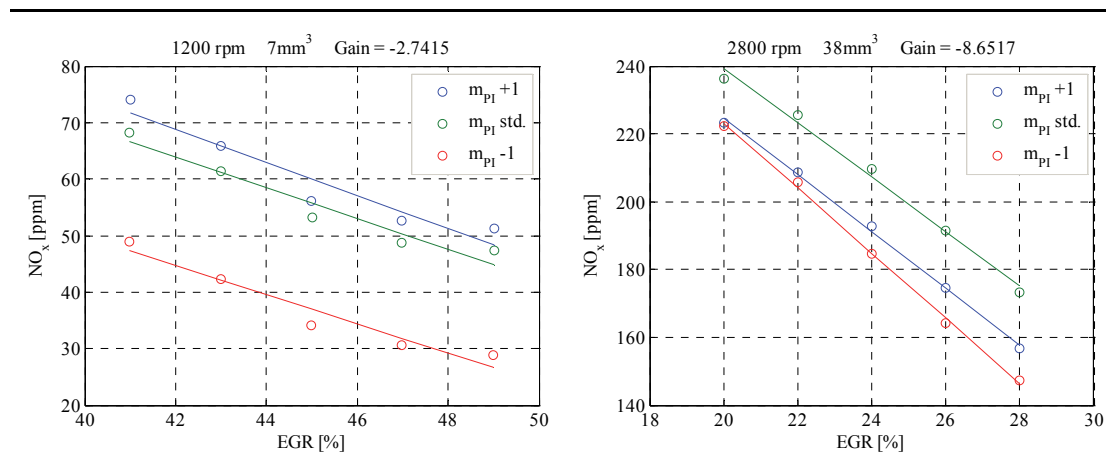


Figure 5.7 Variation of EGR at three different m_{PI} rates for determining the linear gain K_{12} value (NO_x/EGR) at two different operating points, low load (left), high load (right) on engine B.

It is already seen on PM plots that the relations between PM and engine variables are somewhat more complex. Varying EGR rate and m_{PI} values have affects on each other's relationship with PM. In Figure 5.8, it is seen that increasing m_{PI} has an increasing effect on PM.

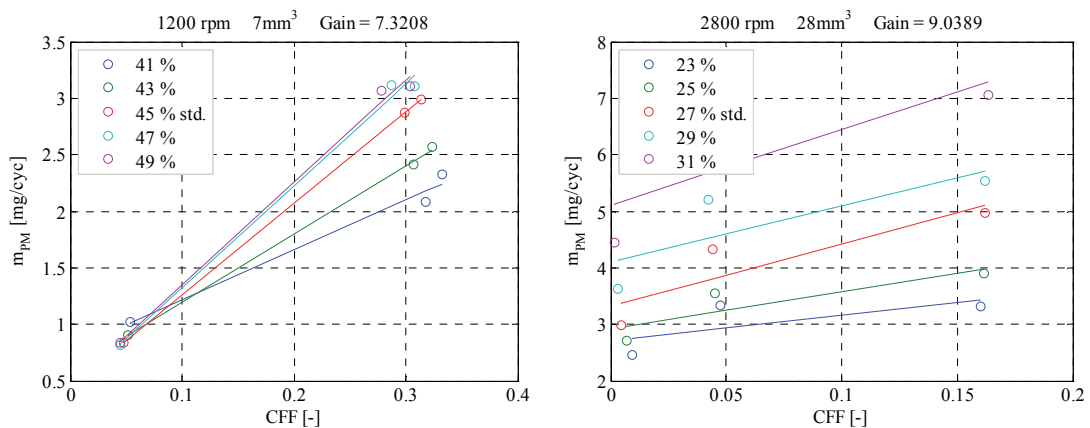


Figure 5.8 Variation of m_{PI} at five different EGR rates for determining the linear gain value K_{21} (m_{PM}/CFF) at two different operating points, low load (left), high load (right) on engine B.

In Figure 5.9 as expected, EGR has an increasing effect on PM. It is also seen that increasing m_{PI} magnifies the effect of EGR in general. In the low load case, the slope is even negative for low m_{PI} value. But the outcome is positive since the average of the slopes is taken as the gain.

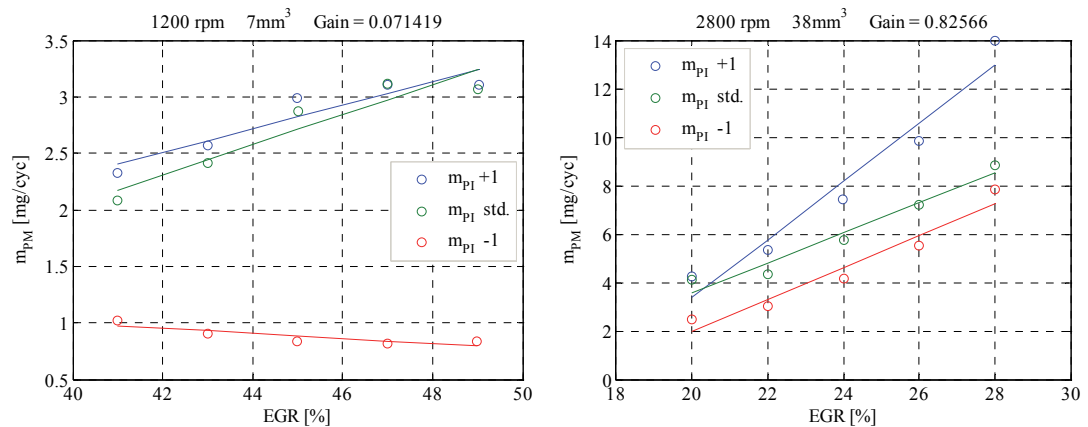


Figure 5.9 Variation of EGR at three different m_{PI} rates for determining the linear gain value K_{22} (m_{PM}/EGR) at two different operating points, low load (left), high load (right) on engine B.

Out of these system gains calculated for each operating point inverses of the gains are calculated so that they could be used in the controller.

As a result the gain maps in Figure 5.10 are obtained which are ready to be used as lookup tables in the controller. The operating point based linearization based on such auxiliary measurements of the system may naturally have inaccuracies. But the goal is to give direction to the controllers in a general sense, and the precision of the gains is not of great importance for the controller.

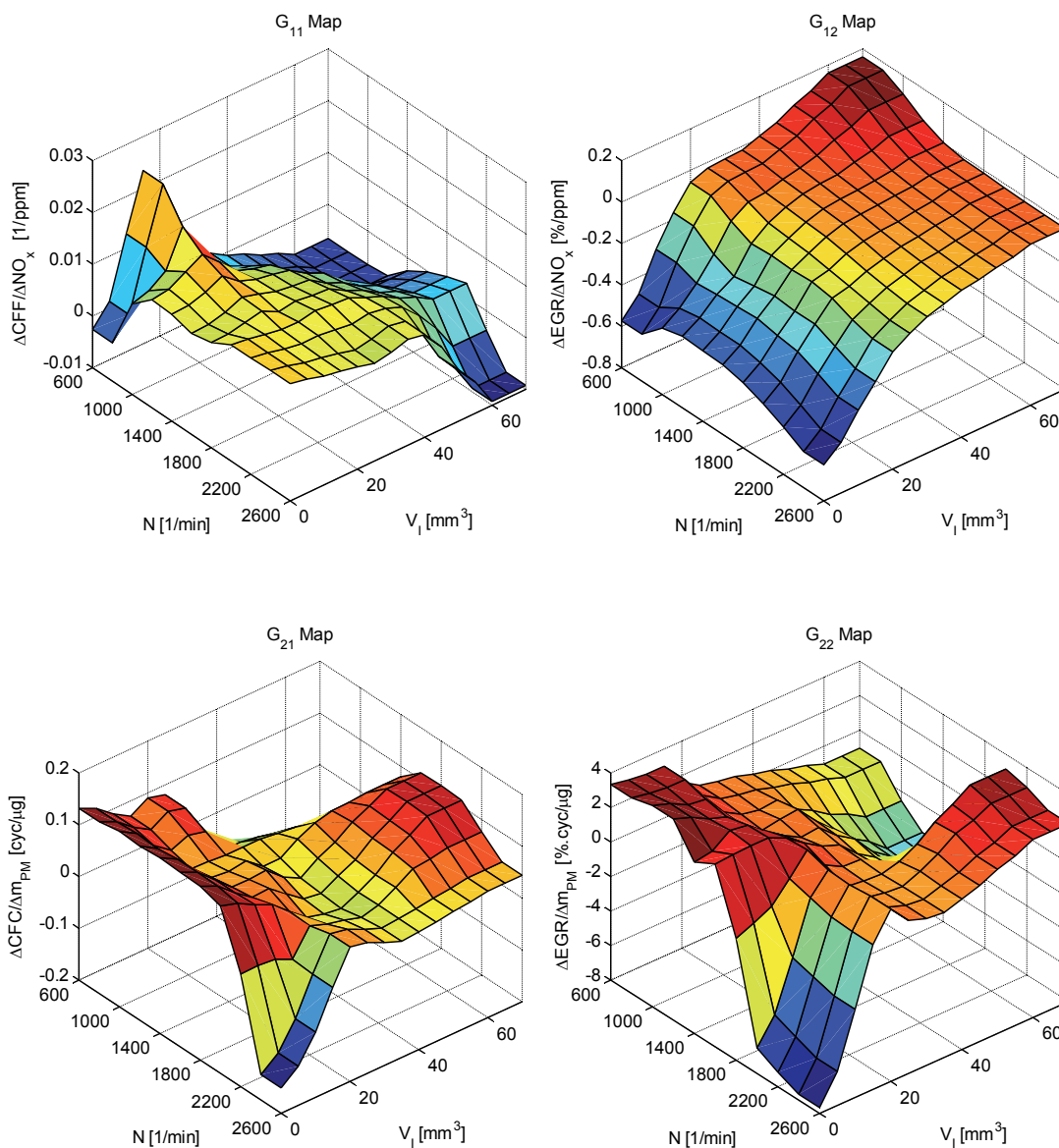


Figure 5.10 Inverse gain maps K_{11}^{-1} , K_{12}^{-1} , K_{21}^{-1} and K_{22}^{-1} for the transfer functions G_{11} , G_{12} , G_{21} and G_{22} .

5.2.3 Implementation & Tests

PM estimator and emissions controller has been implemented in *Matlab/Simulink*. This *Simulink* model has been compiled automatically into a C code using *Matlab* tools and compiled code was flashed into a test vehicle with rapid prototyping tools (Figure 5.12). In-cylinder data processing unit FI^{2RE} (Kracke, Fengler, Müller, & Barsun, 2001) and bypass control unit *ETAS ES690* are the rapid prototyping tools used in engine research and development.

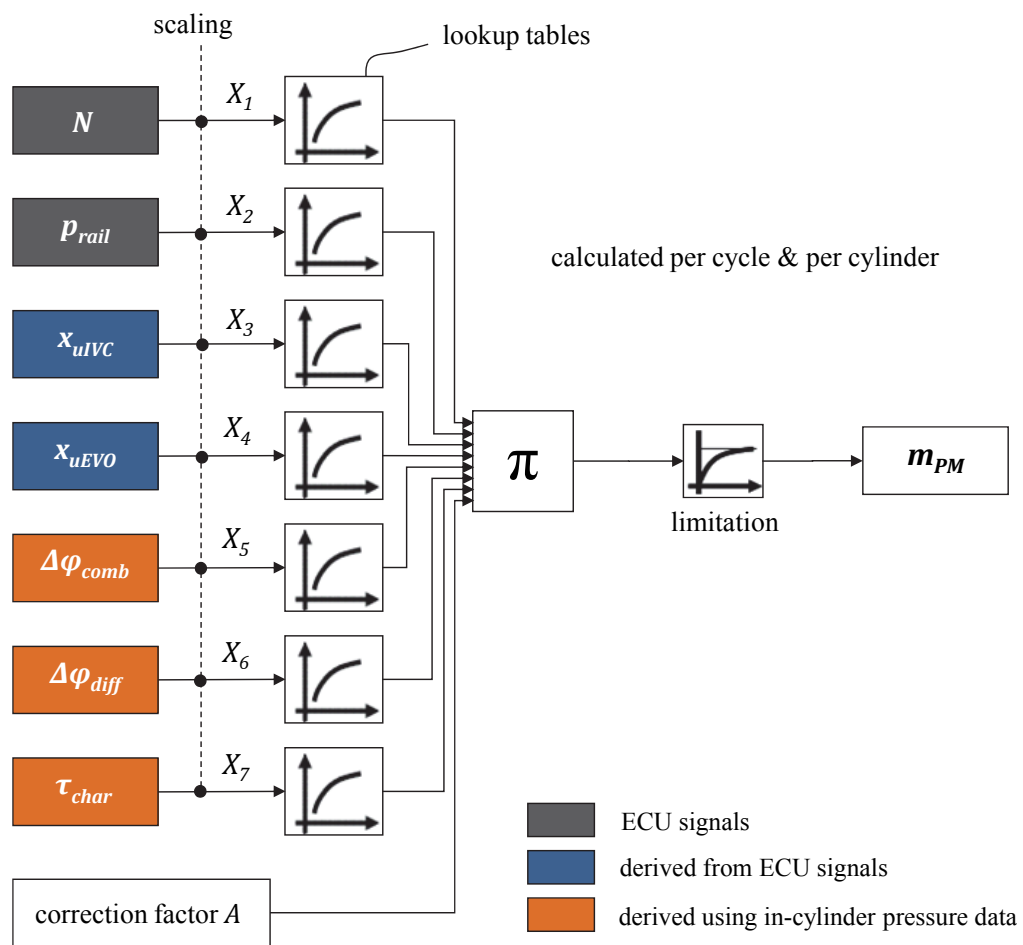


Figure 5.11 Implementation of the developed PM estimator (Çebi & Binder, 2011).

Implementation scheme of PM estimator is seen on Figure 5.11. Last three inputs derived using in-cylinder pressure data (shown in orange) are determined in the in-cylinder data processing unit on Figure 5.12 and sent segment synchronous to the

bypass control unit where the other inputs are calculated and scaled. Here the exponential terms are determined using pre-defined lookup tables as in Figure 5.11 and cycle based mass of PM emissions are calculated.

Within the bypass control unit, output of the PM estimator is received by the emissions controller. Here the emission and actuator signal relationships are decoupled and through inverse system gains ΔEGR and ΔCFF controller inputs are determined (Figure 5.4). Pre-defined lookup tables shown in Figure 5.10 contain these inverse system gains.

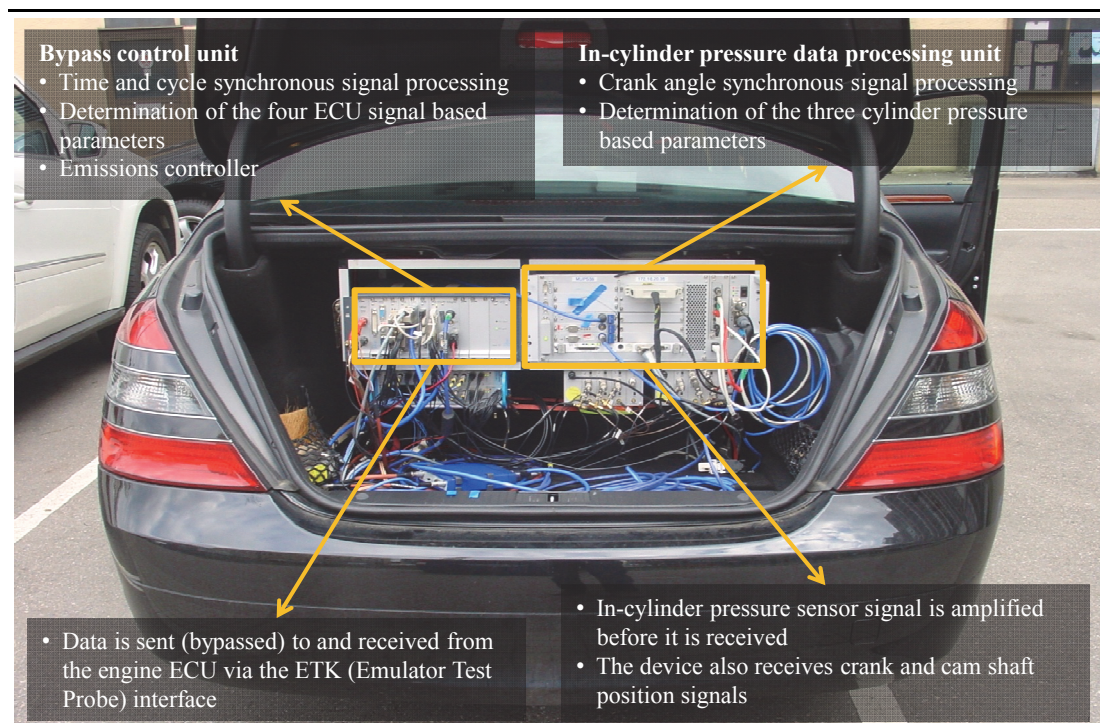


Figure 5.12 Hardware used for vehicle implementation of the developed PM estimator and emissions controller. Shown test vehicle is equipped with engine A.

ΔEGR and ΔCFF controllers are implemented as simple PI controllers. ΔEGR controller is presented in Figure 5.13 and ΔCFF controller has the exact same structure. Anti-windup is used to prevent the control signal from exceeding a certain threshold by freezing the integrator output whilst the max controller threshold is reached. Moreover an integrator reset makes sure integrator gain is reset when the controller has been switched off to guarantee neutral behavior after controller re-

activation.

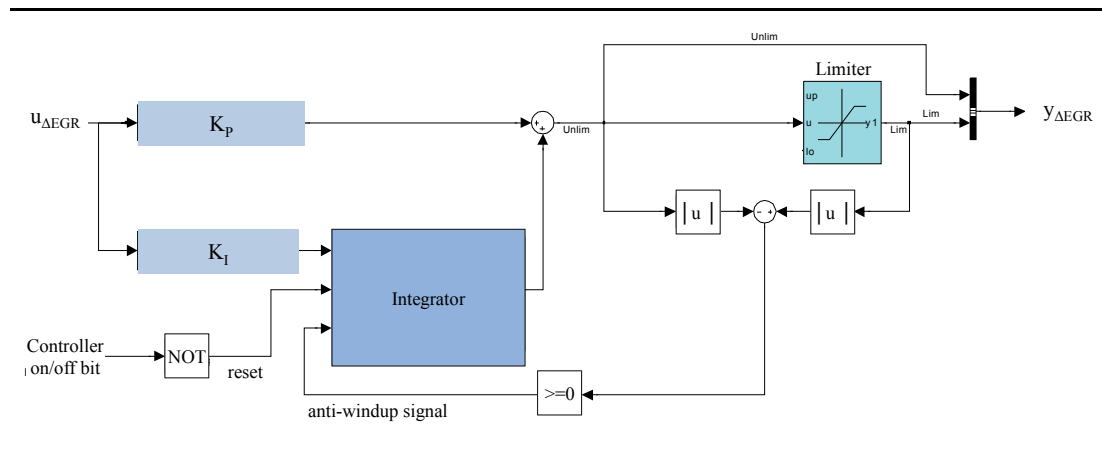


Figure 5.13 Implementation of the ΔEGR controller with anti-windup and integrator reset in. ΔCFF controller implementation is analogous.



Figure 5.14 Connections to the rapid prototyping system in the rear trunk of the test vehicle are enabled by a control panel built in the glove compartment.

Development and calibration of emissions controller has been carried out with the aid of the test vehicle equipped with engine A shown in Figure 5.12 and Figure 5.14. Communication with the bypass ECU is established through an Ethernet connection and through a USB interface with the in-cylinder pressure data processor.

Real time display and the recording of relevant signals in the bypass ECU during development is enabled by the rapid prototyping software *ETAS INCA*. Moreover it is possible to alter the constants defined within the *Simulink* model for the bypass ECU.

5.2.4 Results

Figure 5.15 depicts measurements at constant driving speeds.

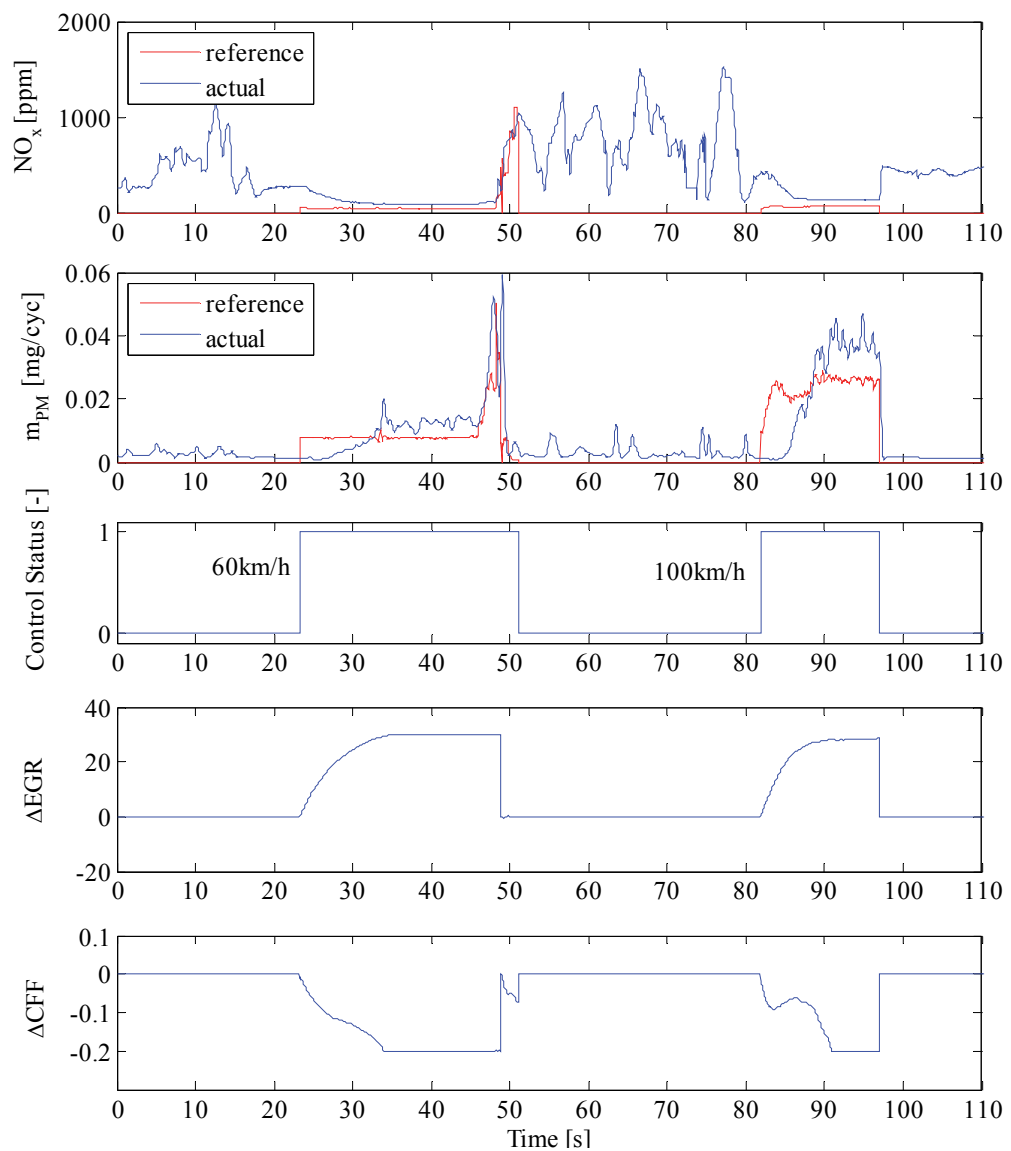


Figure 5.15 Testing of emissions controller during quasi-steady free driving conditions.

At both speeds 60km/h and 100km/h emissions controller has been turned on after quasi-steady-state driving conditions were reached in both cases the typical PM-NO_x tradeoff is observed.

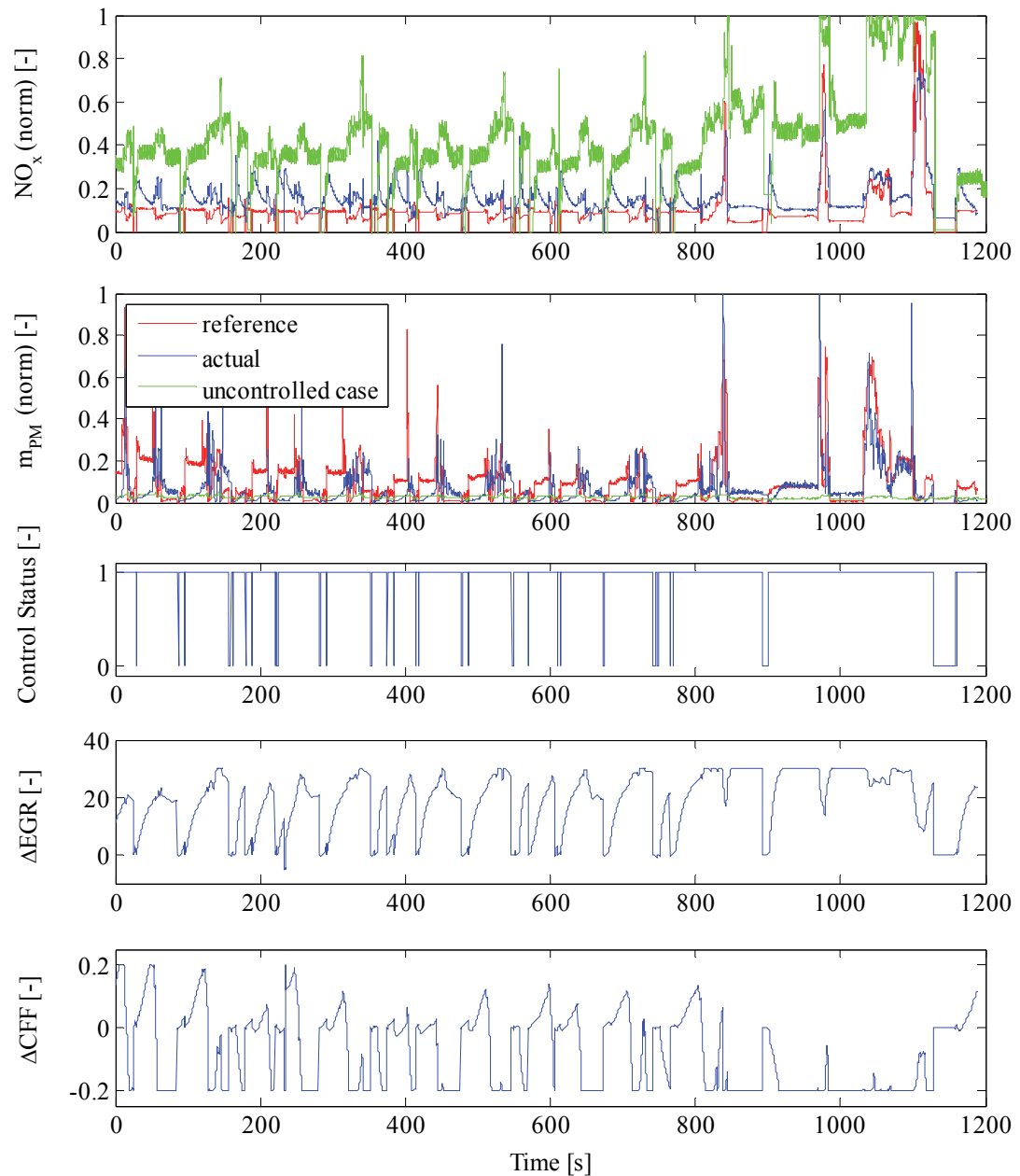


Figure 5.16 Testing of emissions controller on vehicle test bench using NEDC test procedure. First two diagrams above depict two measurements, i.e. controlled and uncontrolled cases. Last three refer only to the controlled case.

Furthermore, it is seen that controller limits are reached and an error remains on both PM and NOx at steady state. PM values estimated by the model may not be accurate as the output is more prone to errors at such low emission values. However, that could not be measured on board. In order to obtain reproducible results, further measurements were carried out on vehicle test bench using standard emission test cycles defined in section 3.3.

Similar to Figure 5.15, emission reference and actual values, controller signal and outputs are depicted. In Figure 5.16 and Figure 5.18 these can be seen for NEDC and US06 emission test cycles respectively. Additionally, uncontrolled measurements were carried out on the same cycles their emission outputs are depicted on the corresponding figures (denoted with "uncontrolled case"). NEDC being a rather steady test cycle in terms of engine dynamics, the controller could adapt faster to operating mode changes (Figure 5.16).

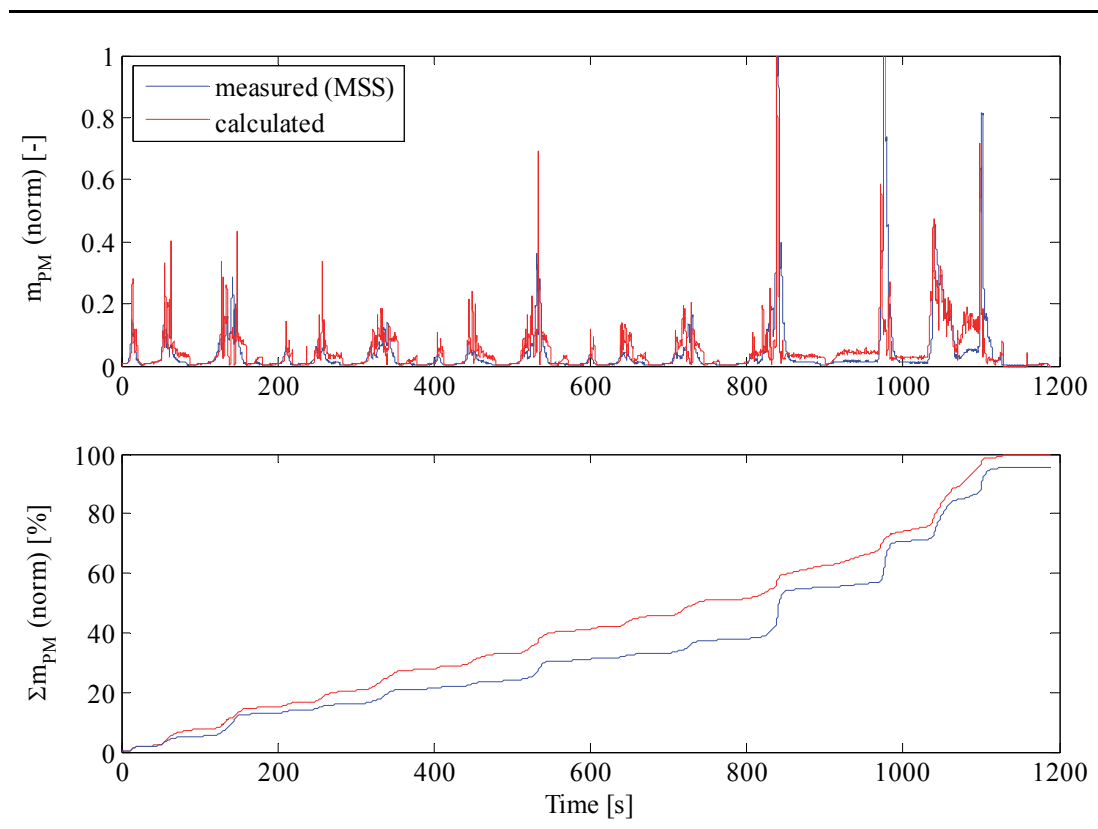


Figure 5.17 Comparison of MSS measurement versus PM estimator calculation in NEDC test procedure on vehicle test bench. Controlled case.

Since external measuring equipment was available on the test bench, accuracy of the PM estimator could be assessed. Figure 5.17 shows real time and integral values of measured (MSS) and calculated PM emissions.

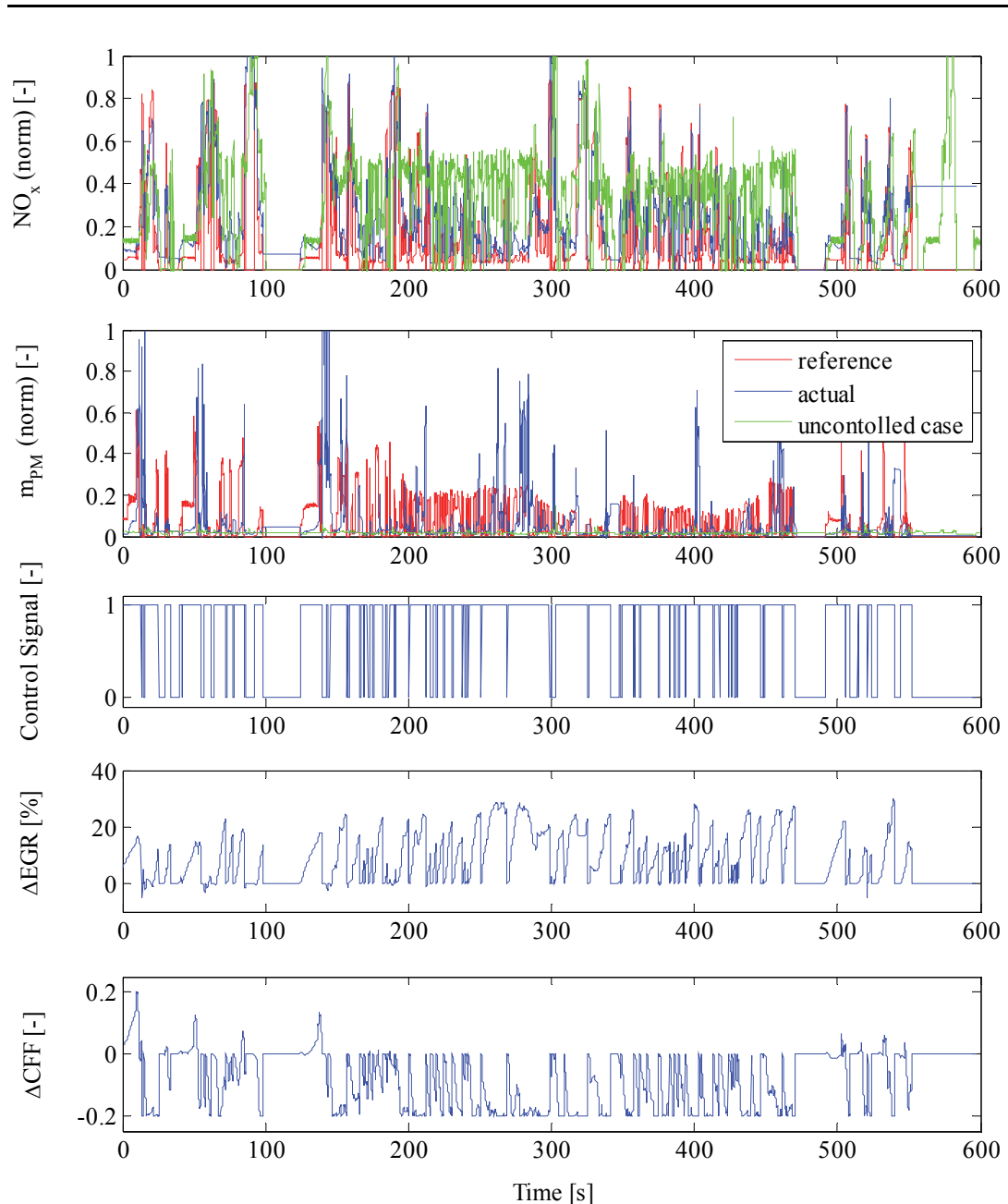


Figure 5.18 Testing of emissions controller on vehicle test bench using US06 test procedure. First two diagrams above depict two measurements, i.e. controlled and uncontrolled cases. Last three refer to the controlled case.

Modeled value tends to overestimate the emissions in the first phase ($t < 800\text{s}$) and underestimate in the second phase ($t > 800\text{s}$) where the engine speed is higher and a more dynamic driving behavior is existent.

Numerous emission peaks seen in Figure 5.18 in the top two plots are associated to the aggressive driving behavior during US06 test cycle. Similar to NEDC, higher EGR rates utilized to decrease NO_x emissions caused very high PM peaks at some intervals.

It can be seen that the controller reaction is faster in US06. This is due to the different gains produced by gain scheduling maps. However it can be concluded that proportional gains used in ΔEGR and ΔCFF controllers on Figure 5.13 can be increased to have faster response to transient changes.

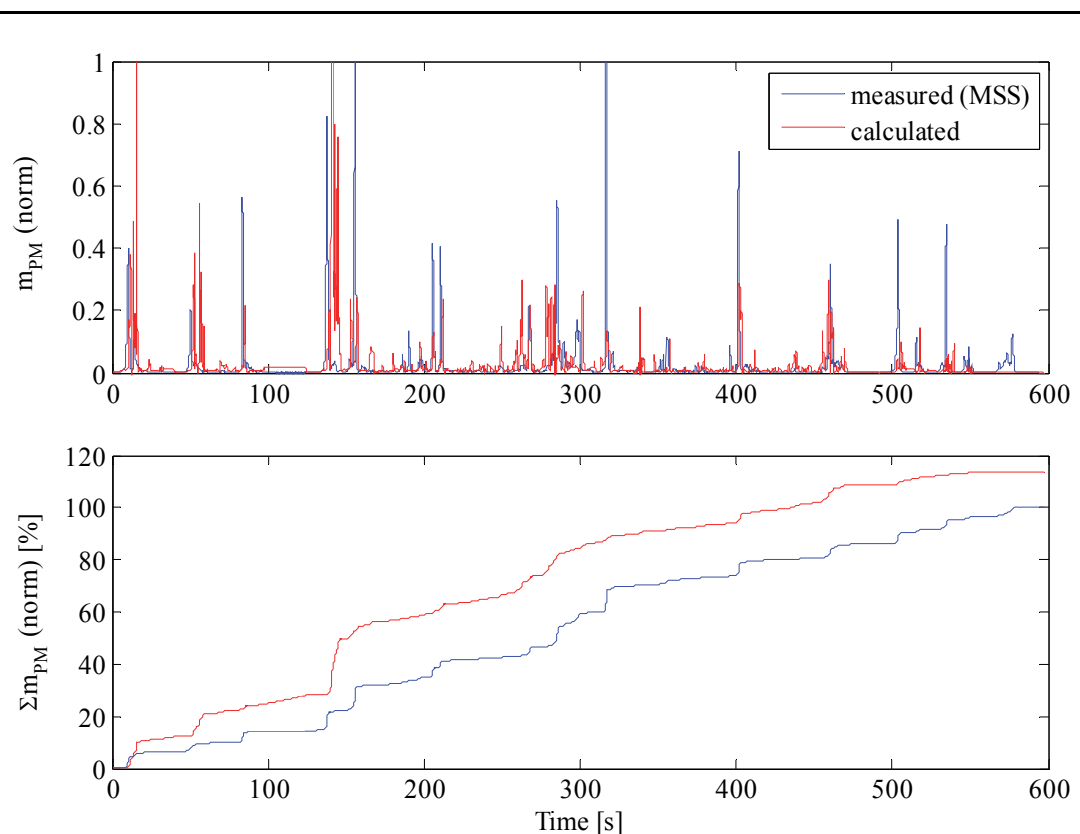


Figure 5.19 Comparison of MSS measurement versus PM estimator calculation in US06 test procedure on vehicle test bench. Controlled case.

Similarly for the controlled case in US06 test procedure, the estimator and MSS measurement results have been compared on Figure 5.19. It is seen that the model tends to overestimate emissions. It has been observed that in NEDC test the model was usually in region 3 whereas in US06 test region 4 was more dominant because of the higher engine speeds during rapid acceleration phases at lower gears.

PM estimator responds worse to higher transients. This could be a signal filtering issue since after the peak at around $t=140s$ the measured and calculated lines run in parallel.

5.3 Discussion on overall performance

Summarizing the four measurements done presented in Figure 5.16 and Figure 5.18 cumulative PM mass emissions on these cycles are presented in Figure 5.20.

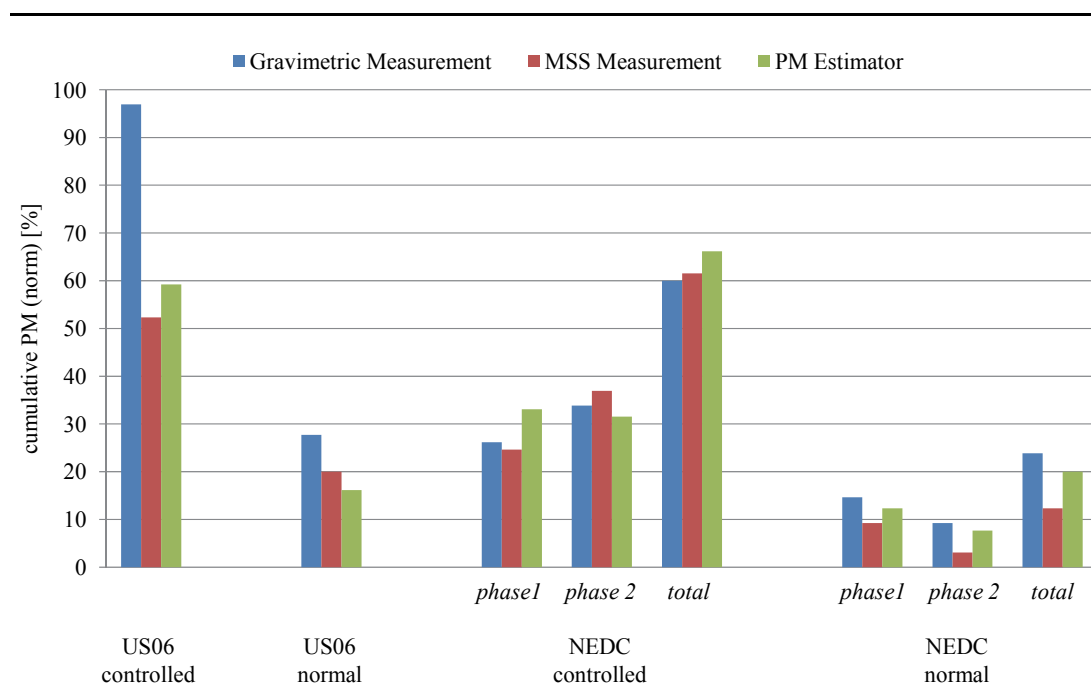


Figure 5.20 Comparison of test results of the PM estimator with two different measurement techniques, gravimetric (particle sampler) and MSS.

First thing to be observed is that PM emissions are higher for controlled cases due to higher EGR rates utilized in order to decrease NO_x emissions. Secondly the more

dynamic test cycle US06 yields more PM than NEDC if the gravimetric measurement is taken as reference.

Furthermore there is a great output difference between MSS and gravimetric measurements. The relevance of PM measurement output to measurement technique portrayed in Figure 3.4 has made it clear that this is an expected outcome. Hence, it can be inferred that gravimetric measurement would result in higher PM emissions than MSS and since the calibration of PM estimator has been done with FSN measurement data, the model is expected to deliver lower values. Nevertheless, for some cases in Figure 5.20 the gravimetric measurement yields nearly two times of what is measured with MSS.

Unfortunately there is no information on the quantity of SOF (Soluble Organic Fraction) for the test engine and the aforementioned discrepancy in measured PM may look unrealistic. Nonetheless, after measurements on a DI diesel engine. Horiuchi, Saito, & Ichiara (1990) have attributed up to more than 50% of the PM composition to SOF at lower loads and this ratio dropped to under 5% at higher loads. This might explain the trend in Figure 5.20 but no solid conclusions can be made since measurements related to SOF are not available at this point. Since the gravimetric measurement is used for certification and is already a well established technique, its output values are considered to be accurate.

Performance of the PM estimator is considered to be good regarding the correlation with MSS measurements. As mentioned already, since FSN measurements are used for calibration, the model is probably estimating PM values based on the solid fraction of PM which is mostly black carbon. Furthermore, as discussed in section 4.5 the effects of in-cylinder pressure sensor error should be investigated as it could have vast effects on the modeled emissions.

Emissions controller can follow certain reference emission values, however it is relatively slow at adapting to transient changes and physical limits were often reached regarding the PM-NO_x tradeoff and limits set for the Δ EGR and Δ CFF

controllers.

Impact of the emissions controller for the presented test cases is shown in Figure 5.21. Increasing EGR leads to a vast increase in PM and a considerable decrease in NO_x emissions. The reason for the different outcome for the two emissions test cycles might be due to NEDC being rather steady and US06 being aggressive cycles and as a result, high EGR rates yielded higher PM emissions in US06.

Additionally, for controlled cases a decrease in fuel consumption for both cycles has been observed, possibly due to the general decrease in pilot injection quantities. This decrease is higher for NEDC and may therefore also be explained with the tradeoff between NO_x and consumption. Since NO_x has not been decreased as much in US06 a smaller decrease in consumption has been realized.

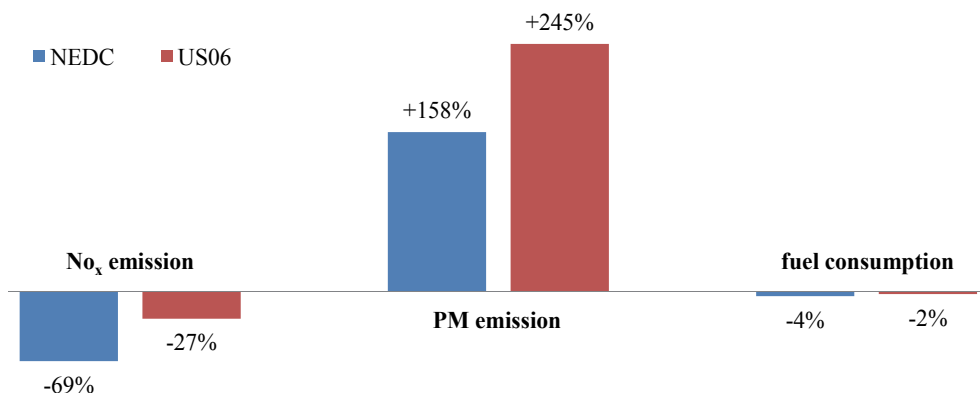


Figure 5.21 Effect of the emissions controller on emissions and fuel consumption. Controlled case is compared to the uncontrolled case for US06 and NEDC tests. PM is based on gravimetric measurement.

It shall be stressed that gain scheduling on the emissions controller has been done based on data originating from engine B and the controller has been implemented on a test vehicle equipped with engine A. Since there was no appropriate data available from engine A that could be used for calibrating inverse system gains (Figure 5.10) of the controller, engine B data has been used. Although the engines are completely different, a great difference between two engines regarding these system gains has not been expected.

After all it is observed from the measurements that given that certain logical reference emission values exist, the emissions model is capable of manipulating the engine actuators in order to achieve the desired PM and NO_x emissions. Therefore the concept is considered to be successful.

CHAPTER SIX

CONCLUSIONS & OUTLOOK

The developed PM estimator has proven to be an efficient tool for real-time PM emissions calculation. Results are not only qualitatively satisfying but also quantitatively promising. Ability of the model to estimate the PM emissions particularly in transient emission cycles such as NEDC and US06 with a relatively high accuracy is the most important achievement. Primary strength of the PM estimator lies in its simplicity. Firstly, the simple configuration leads to negligible calculation effort. Secondly, it makes the application relatively easy, considering that only automotive industry standard test bench setup is required for measurements to generate calibration data.

Nevertheless, further work on the model should be done towards determination of a standard method for the model parameterization, so that the application effort is minimized and model reliability is assured under all circumstances. If the accuracy of the PM estimator is to be increased by introducing new variables, one should concentrate on deriving variables which would describe the local conditions during combustion (e.g. local lambda, temperature etc.). Additionally, determination of cylinder pressure based model variables could be improved so that the model is more robust against in-cylinder pressure sensor errors.

According to Kennedy (1997), back then the fundamental processes involved in soot processes still have uncertainties due to limited knowledge. This is still an existing problem as it has been reported recently by Karataş & Gülder (2012) who have presented a review on soot formation in laminar diffusion flames that the details associated to chemical and physical soot mechanisms in combustion still remain unclear. A lack of understanding persists in the understanding of relationship of physical quantities with soot mechanisms. Therefore the elusive soot mechanisms are subject of ongoing research, within and as well as outside the automotive industry and diesel soot emissions modeling remains a challenge (Lakshminarayanan & Aghav, 2010).

Taking these into account and considering that the diffusive flame in diesel engine combustion has a rather turbulent nature than laminar, the results achieved with the developed PM estimator are significant. Soot models present in the literature are usually capable of predicting trends so far but majority need future improvements to produce more accurate models. The developed PM estimator is seen as a one step forward in the category of empirical emission models that delivers promising qualitative and quantitative results.

In-cylinder pressure data is considered to be compulsory for estimating PM emissions with high accuracy. Engines equipped with in-cylinder sensors is not the state of the art yet, therefore other methods could be investigated to determine in-cylinder pressure or heat release rate during combustion or at least to determine certain variables related to these without having in-cylinder pressure sensors on board. There are already some examples in literature such as in Decker, Hintz, Nobis, Joerres, & Gühmann (2011), Weißenborn, Bossmeyer, & Bertram (2011) and Weymann (2009).

The MIMO controller designed based on gain scheduling concept to control raw emissions has been successful in controlling PM and NO_x emissions simultaneously over EGR and pilot injection quantity. Gain scheduling has eliminated the need for an inverse combustion model. EGR and injector actuators were manipulated in a cascaded controller structure where the Δ EGR and Δ CFF controllers altered reference values of the actual EGR and CFF controllers that were already present in the system.

Calibration of the controller requires variation measurements of EGR and pilot injection quantity versus PM and NO_x emissions on the engine map. This introduces considerable calibration effort but since a complex combustion model is eliminated by this means, computational effort within the ECU is very little using lookup tables.

Emissions controller performance could have been increased if variation

measurements for calibrating the gain maps were available on the same engine type used for testing controller. Furthermore, the P and I factors of Δ EGR and Δ CFF controllers need further optimization in order to achieve better transient response.

Implementation of emission model and controller has been done in a test vehicle equipped with a rapid prototyping system and in-cylinder pressure sensors. By this means, it has been shown that with the availability of in-cylinder pressure sensors and an ECU capable of cylinder pressure data acquisition and processing in real time, it is possible to implement the PM estimator as a virtual sensor on serial production engines along with the emissions controller to have the desired emission characteristics at any time.

In the future further work can be done on an engine test bench to optimize the emissions model and controller. This way, better reproducible measurements can be obtained for better calibration results. Moreover certain strategies for optimal control of emissions in accordance with the exhaust gas aftertreatment system need to be developed and corresponding reference values for emissions controller should be determined.

As pointed out by Dec (2009) advanced combustion systems with increased injection pressures, EGR, improved construction favoring better flow and mixing have allowed great reductions in emissions over the past decade. Despite these advances, he still argues that it still appears unlikely that the conventional diesel combustion will meet the stringent future emission limits without the use of expensive exhaust aftertreatment systems. Besides, in literature, emissions control is commonly referred to as usage of these aftertreatment systems and closed loop control of in-cylinder emissions is underrepresented (Johnson, 2010; Neeft, Makkee, & Moulijn, 1996; Prasad & Bella, 2010; Walker, 2004).

Yet, it is strongly believed that the developed PM emissions model closed loop PM and NO_x emissions controller during this work will still prove useful, provided that mentioned enhancements are done, especially on the emissions controller.

Hereby, this work has introduced a relatively simple emission model utilizing physical quantities based on in-cylinder pressure yielding top results and a simple emissions controller based on gain scheduling that is an add-on solution to the existing controllers in the ECU in a cascaded structure. In the following publications that have resulted from this project are listed:

- Lay (2009) supervised diploma thesis.
- Özel (2009) supervised internship report
- Demirer (2009) supervised internship report
- Çebi & Binder (2011) patent application
- Çebi, Rottenkolber, & Uyar (2011) technical paper and conference
- Çebi, Uyar, & Rottenkolber (2011) symposium proceedings
- Çebi, Uyar, & Rottenkolber (2012) journal publication, submitted

REFERENCES

- Abbass, M. K., Andrews, G. E., Ishaq, R. B., Williams, P. T., & Bartle, K. D. (1991). A comparison of the particulate composition between turbocharged and naturally aspirated D. I. diesel-engines. *SAE Technical Paper, 910733*.
- Akihama, K., Takatori, Y., Inagaki, K., Sasaki, S., & Dean, A. M. (2001). Mechanism of smokeless rich diesel combustion by reducing temperature. *SAE Technical Paper, 2001-01-0655*.
- Alfieri, E. (2009). *Emissions-controlled diesel engine*. Zurich: ETH Zurich, Ph.D. thesis.
- Anastasia, C., & Pestana, G. (1987). A cylinder pressure sensor for closed loop engine control. *SAE Technical Paper, 870388*.
- Andersson, M., Johansson, B., Hultqvist, A., & Nöhre, C. (2006). A real time NOx model for conventional and partially premixed diesel combustion. *SAE Technical Paper, 2006-01-0195*.
- Aronsson, U., Chartier, C., Andersson, Ö., Egnell, R., Sjöholm, J., Richter, M., et al. (2009). Analysis of the correlation between engine-out particulates and local equivalence ratio in the lift-off region of a heavy duty diesel engine using raman spectroscopy. *SAE Technical Paper, 2009-01-1357*.
- Arregle, J., Bermúdez, V., Serrano, J. R., & Fuentes, E. (2006). Procedure for engine transient cycle emissions testing in real time. *Experimental Thermal and Fluid Science* 30 , 485-496.
- Åström, K. J., & Wittenmark, B. (1994). *Adaptive Control, 2nd ed.* Redding - Massachusetts, New York, Bonn, Tokyo, Paris, Milan: Prentice Hall.
- Atkinson, C., & Mott, G. (2005). Dynamic model-based calibration optimization: An

introduction and application to diesel engines. *SAE Technical Paper, 2005-01-0026*.

AVL List GmbH. (2012a). *AVL Micro Soot Sensor*. Retrieved August 2012, from <https://www.avl.com/micro-soot-sensor>

AVL List GmbH. (2012b). *AVL Opacimeter*. Retrieved August 2012, from <https://www.avl.com/opacimeter>

AVL List GmbH. (2012c). *AVL PSS i60 Particulate Sampler*. Retrieved August 2012, from <https://www.avl.com/pss-i60-particulate-sampler>

AVL List GmbH. (2012d). *AVL Smoke Meter*. Retrieved August 2012, from <https://www.avl.com/smoke-meter>

AVL List GmbH. (2005, June). *Smoke value measurement with the filter-paper-method*. Retrieved August 2012, from https://www.avl.com/c/document_library/get_file?uuid=2b39210c-6937-43e4-b223-b5c2c11f91ac&groupId=10138

Badami, M., Mallamo, F., Millo, F., & Rossi, E. E. (2003). Experimental investigation on the effect of multiple injection strategies on emissions, noise and brake specific fuel consumption of an automotive direct injection common-rail diesel engine. 299-314.

Barba, C. (2001). *Erarbeitung von Verbrennungskennwerten aus Indizierdaten zur verbesserten Prognose und rechnerischen Simulation des Verbrennungsablaufes bei PKW-DE Dieselmotoren mit Common-Rail-Einspritzung*. Zurich: ETH Zurich, Ph.D. thesis.

Barro, C., & Tschanz, F. (2010). Soot controlled diesel engine. *FVV Herbsttagung, Band Nr. R551*, Bamberg, 195-218.

- Barths, H., Pitsch, H., & Peters, N. (1999). 3D simulation of DI diesel combustion and pollutant formation using a two-component reference fuel. *Oil & Gas Science and Technology*, 54 (2), 233-244.
- Beasley, M., Cornwell, R., Fussey, P., King, R., Noble, A., Salamon, T., et al. (2006). Reducing diesel emissions dispersion by coordinated combustion feedback control. *SAE Technical Paper*, 2006-01-0186.
- Bergin, M. J., Reitz, R. D., Oh, S., Miles, P. C., Hildingsson, L., & Hultqvist, A. (2007). Fuel injection and mean swirl effects on combustion and soot formation in heavy duty diesel engines. *SAE Technical Paper*, 2007-01-0912.
- Birmili, W., & Hoffmann, T. (2006). Particulate and dust pollution, inorganic and organic compounds. In G. Laurent, & S. Shapiro, *Encyclopedia of Respiratory Medicine*. Elsevier.
- Bobba, M. K., Genzale, C. L., & Musculus, M. P. (2009). Effect of ignition delay on in-cylinder soot characteristics of a heavy duty diesel engine operating at low temperature conditions. *SAE Technical Paper*, 2009-01-0946.
- Böhm, H., Bönig, M., Feldermann, C., Jander, H., Rudolph, G., & Wagner, H. G. (1994). Pressure dependence of formation of soot and PAH in premixed flames. In H. Bockhorn, *Soot Formation in Combustion - Mechanisms and Models*, Berlin, Heidelberg, New York: Springer-Verlag, 145-161.
- Carlucci, P., Ficarella, A., & Laforgia, D. (2003). Effects of pilot injection parameters on combustion for common rail diesel engines. *SAE Technical Paper*, 2003-01-0700.
- Çebi, C., & Binder, S. (2011). *Patent No. P820609/DE pending*. Germany.
- Çebi, E. C., Rottenkolber, G., & Uyar, E. (2011). In-cylinder pressure based real-time estimation of engine-out particulate matter emissions of a diesel engine. *SAE*

Technical Paper, 2011-01-1440.

Çebi, E. C., Uyar, E., & Rottenkolber, G. (2012). An empirical model based approach to in-cylinder diesel engine emissions control. *International Journal of Automotive Technology, manuscript submitted for publication.*

Çebi, E. C., Uyar, E., & Rottenkolber, G. (2011). Modern dizel motorların emisyonlarının modellenmesi ve kontrolü. *TOK 2011 : Otomatik Kontrol Türk Milli Komitesi 2011 Ulusal Toplantısı.* İzmir.

Chen, S. K. (2000). Simultaneous reduction of NO_x and particulate emissions by using multiple injections in a small diesel engine. *SAE Technical Paper, 2000-01-3084.*

Chmela, F. G., & Orthaber, G. C. (1999). Rate of heat release prediction for direct injection diesel engines based on purely mixing controlled combustion. *SAE Technical Paper, 1999-01-0186.*

Chmela, F. G., Werlberger, P., & Cartellieri, W. P. (1992). Parameters affecting in-cylinder soot and NO_x formation in a direct injection diesel engine. *XXIV FISITA Congress London: IMechE, 17-24.*

DaimlerChrysler AG. (2006, February). Effective engine control. *High Tech Report , 44-47.*

de Ojeda, W., Zoldak, P., Espinosa, R., & Kumar, R. (2009). Development of a fuel injection strategy for partially premixed compression ignition combustion. *SAE Technical Paper, 2009-01-1527.*

Dec, J. E. (1997). A conceptual model of DI diesel combustion based on laser-sheet imaging. *SAE Technical Paper, 970873.*

Dec, J. E. (2009). Advanced compression-ignition engines - understanding the in-

- cylinder processes. *Proceedings of the Combustion Institute*, 32, 2727-2742.
- Decker, M., Hintz, K., Nobis, J., Joerres, M., & Gühmann, C. (2011). Noise-controlled diesel engine. *MTZ Worldwide*, 72 (03), 58-65.
- Demirer, O. N. (2009). *Empirical soot emission modeling of OM642LS diesel engine*. Ankara: Middle East Technical University, Internship report.
- DieselNet. (n.d.). *Emission standards: Europe: cars and light trucks*. Retrieved June 2012, from <http://www.dieselnet.com/standards/eu/ld.php#stds>
- DieselNet. (n.d.). *Emission test cycles*. Retrieved September 2010, from http://www.dieselnet.com/standards/cycles/ece_eudc.html
- Egnell, R. (2001). *On zero-dimensional modelling of combustion and NOx formation in diesel engines*. Lund: Lund University, Ph.D. thesis.
- Ehleskog, M., Gjirja, S., & Denbratt, I. (2009). Effect of high injection pressure, EGR and charge air pressure on combustion and emissions in a HD single cylinder diesel engine. *SAE Technical Paper*, 2009-01-2815.
- Elsäßer, A., Braun, R., & Jensen, H. (2000). Luftversorgungsmodule für die neuen Common-Rail-Dieselmotoren OM611 und OM612 von DaimlerChrysler. *MTZ 61* (3).
- Ericson, C., Westerberg, B., Andersson, M., & Egnell, R. (2006). Modelling diesel engine combustion and NOx formation for model based control and simulation of engine and exhaust aftertreatment systems. *SAE Technical Paper*, 2006-01-0687 .
- Fischer, S. (2011). *Bewertung relevanter Einflussgrößen beim Pkw-Dieselmotor auf die Emissionsreduktion durch Höchstdruckeinspritzung*. Universität Rostock, Ph.D thesis.
- Fischer, S., & Stein, J.-O. (2009). Investigation on the effect of very high fuel

- injection pressure on soot-NO_x emissions at high load in a passenger car diesel engine. *SAE Technical Paper*, 2009-01-1930.
- Frenklach, M. (2002, February). Reaction mechanism of soot formation in flames. *Phys. Chem. Chem. Phys.*, 4, 2028-2037.
- Gao, Z., & Schreiber, W. (2001). A phenomenologically based computer model to predict soot and NO_x emission in a direct injection diesel engine. *International Journal of Engine Research*, 2 (3), 177-188.
- Gärtner, U. (2001). *Der Simulation der Stickoxid-Bildung in Nutzfahrzeug-Dieselmotoren*. Universität Darmstadt, Ph.D. thesis.
- Hadler, J., Rudolph, F., Dorenkamp, R., Kösters, M., Mannigel, D., & Veldten, B. (2008). Volkswagen's new 2.0l TDI engine for the most stringent emission standards - Part 1. *MTZ Worldwide*, 69 (05), 12-18.
- Hall, M. J., Diller, T., & Matthews, R. D. (2008). Fast-response electric particulate matter sensor for diesel engine control and DPF failure detection. *8th International Symposium on Combustion Diagnostics*, Baden Baden, 71-86.
- Hawley, J. G., Brace, C. J., Wallace, F. J., & Horrocks, W. R. (1998). Combustion related emission in CI engines. In E. Sher, *Handbook of air pollution from internal combustion engines - Pollutant formation and control*,. Elsevier, 280-357.
- Herden, W., & Kusell, M. (1994). A new combustion pressure sensor for advanced engine management. *SAE Technical Paper*, 940379.
- Herzog, P. L., Bürgler, L., Winklhofer, E., Zelenka, P., & Cartellieri, W. (1992). NO_x reduction strategies for D.I. diesel engines. *SAE Technical Paper*, 920470.
- Heywood, J. B. (1988). *Internal combustion engine fundamentals*. New York:

McGraw Hill.

- Hiroyasu, H., & Kadota, T. (1983). Development and use of a spray combustion modeling to predict diesel engine efficiency and pollutant emissions (part 1, combustion modeling). *Bulletin of JSME*, 26 (214), 569-575.
- Hohenberg, G. (1982). Der Verbrennungsberlauf - ein Weg zur Beurteilung des motorischen Prozesses. 4. *Wiener Motorensymposium*, 6 (103) Düsseldorf: VDI-Fortschrittsberichte.
- Hopp, M. (2001). *Untersuchung der Rußoxidation unter Dieselmotorischen Randbedingungen*. Aachen: RWTH Aachen University, Ph.D. thesis.
- Hopp, M., & Pungs, A. (1998). *Rußoxidationsmodell*. FVV Project Nr. 659, Band R 497.
- Horiuchi, M., Saito, K., & Ichiara, S. (1990). The effects of flow through type oxidation catalysts on the particulate reduction of 1990's diesel engines. *SAE Technical Paper*, 900600.
- Huang, Y., Yang, F., Ouyang, M., Chen, L., & Yang, X. (2011). Optimal feedback control with in-cylinder pressure sensor under engine start conditions. *SAE Technical Paper*, 2011-01-1422.
- Husted, H., Kruger, D., Fatic, G., Ripley, G., & Kelly, E. (2007). Cylinder pressure-based control of pre-mixed diesel combustion. *SAE Technical Paper*, 2007-01-0773.
- Ishida, M., Chen, Z., Luo, G., & Ueki, H. (1994). The effect of pilot injection on combustion in a turbocharged D.I. diesel engine. *SAE Technical Paper*, 941692 .
- Ishikawa, N., Uekusa, T., Nakada, T., & Hariyoshi, R. (2004). DI diesel emission control by optimized fuel injection. *SAE Technical Paper*, 2004-01-0117.

- Jippa, K. (2002). *Onlinefähige thermodynamikbasierte Ansätze für die Auswertung von Zylinderdruckverläufen*. Braunschweig: TU Braunschweig, Ph.D. thesis.
- Johnson, T. V. (2008). Diesel emission control in review. *SAE Technical Paper*, 2008-01-0069.
- Johnson, T. V. (2010). Review of diesel emissions and control. *SAE International Journal of Fuels and Lubricants*, 3 (1), 16-29.
- Kagawa, J. (2002). Health effects of diesel exhaust emissions - a mixture of air pollutants of worldwide concern. *Toxicology*, 181-182.
- Kamimoto, T., & Bae, M. (1988). High combustion temperature for the reduction of particulate in diesel engines. *SAE Technical Paper*, 880423.
- Karataş, A. E., & Gülder, Ö. L. (2012). Soot formation in high pressure laminar diffusion flames. *Progress in Energy and Combustion Science*, 38, 818-845.
- Kennedy, I. M. (1997). Models of soot formation and oxidation. *Progress in Energy and Combustion Science*, 23, 95-132.
- Kim, H. M., Cho, W. J., & Lee, K. H. (2008). Effect of injection condition and swirl on D.I. diesel combustion in a transparent engine system. *International Journal of Automotive Technology*, 9 (5), 535-541.
- Kirchen, P., & Boulouchos, K. (2009). Development and validation of a phenomenological mean value soot model for common-rail diesel engines. *SAE Technical Paper*, 2009-01-1277.
- Kistler. (n.d.). *High temperature pressure sensor for combustion engine measurements*. Retrieved September 2010, from <http://www.kistler.com>
- Koyanagi, K., Öing, H., Renner, G., & Maly, R. (1999). Optimizing common rail-injection by optical diagnostics in a transparent production type diesel engine.

SAE Technical Paper, 1999-01-3646.

- Kozuch, P. (2004). *Ein phänomenologisches Modell zur kombinierten Stickoxid- und Rußberechnung bei direkteinspritzenden Dieselmotoren*. Stuttgart: Fakultät Maschinenbau, Universität Stuttgart, Ph.D. thesis.
- Kracke, T., Fengler, H. -P., Müller, P., & Barsun, N. (2001). FI2RE - A development control unit for flexible injection and ignition. *MTZ Worldwide*, 62 (01), 10-12.
- Krijnsen, H. J., van Leeuwen, J. C., Bakker, R., Calis, H. P., & van den Bleek, C. M. (2001). Inferential NOx emission prediction in feedforward reductant control for SCR. *Topics in Catalysis*, 16/17 (1,4), 337-341.
- Kuo, T., Henningsen, S., & Wu, K. (1988). Evaluation of four mixing correlations for performance and soot emission characteristics for a small open-chamber diesel engine. *SAE Technical Paper, 880599* .
- Kweon, C.-B., Okada, S., Stetter, J. C., Christenson, C. G., Shafer, M. M., Schauer, J. J., et al. (2003). Effect of injection timing on detailed chemical composition and particulate size distributions of diesel exhaust. *SAE Technical Paper, 2003-01-1794*.
- Lakshminarayanan, P. A., & Aghav, Y. V. (2010). Phenomenology of diesel combustion and modelling. In P. A. Lakshminarayanan, & Y. V. Aghav, *Modeling Diesel Combustion - Mechanical Engineering Series*, Springer, 9-21.
- Lay, H. (2009). *Zylinderdruckbasierte Ermittlung von Verbrennungscharakteristiken eines Dieselmotors*. Esslingen: Hochschule Esslingen, Diploma thesis.
- Leonhard, R. (2009). Clean diesel technology - efficient emission reduction. *Near Zero Emission Vehicle Conference*. Jeju, Korea.
- Leonhardt, S., Müller, N., & Isermann, R. (1999, September). Methods for engine

- supervision and control based on cylinder pressure information. *IEEE/ASME Transactions on Mechatronics*, 4 (3), 235-245.
- Li, X., & Wallace, J. S. (1995). In-cylinder measurement of temperature and soot concentration using the two-color method. *SAE Technical Paper*, 950848.
- MacLean, H. L., & Lave, L. B. (2003). Evaluating automobile fuel/propulsion system technologies. *Progress in Energy and Combustion Science*, 29, 1-69.
- Majewski, W. A., & Khair, M. K. (2006). *Diesel emissions and their control*. Warrendale, PA: SAE International.
- Maricq, M. M. (2007). Chemical characterization of particulate emissions from diesel engines: a review. *Journal of Aerosol Science*, 38, 1079-1118.
- Martinot, S., Beard, P., & Roesler, J. (2001). Comparison and coupling of homogeneous reactor and flamelet library soot modeling approaches for diesel combustion. *SAE Technical Paper*, 2001-01-3684 .
- McEntee, J. C., & Ogneva-Himmelberger, Y. (2008). Diesel particulate matter, lung cancer, and asthma incidences along major traffic corridors in MA, USA: A GIS Analysis. *Health&Place*, 14, 817-828.
- Merker, G. P., & Stiesch, G. (1999). *Technische Verbrennung, Motorische Verbrennung*. Stuttgart: B. G. Teubner.
- Meyer-Salfeld, S. (2004). *Piezogesteuertes Forschungseinspritzsystem für direkteinspritzende PKW-Dieselmotoren*. Hannover: Universität Hannover, Ph.D. thesis.
- Minami, T., Takeuchi, K., & Shimazaki, N. (1995). Reduction of diesel engine NOx using pilot injection. *SAE Technical Paper*, 950611.
- Mladek, M. (2003). *Cylinder pressure for control purposes of spark ignition engines*.

- Zurich: ETH Zurich, Ph.D. thesis.
- Mohr, M., Jaeger, L. W., & Boulouchos, K. (2001). Einfluss von Motorparametern auf die Partikelemission. *MTZ* 62, 686-692.
- Mollenhauer, K., & Tschöke, H. (2007). *Handbuch Dieselmotoren*. Berlin: Springer Verlag.
- Neeft, J. P., Makkee, M., & Moulijn, J. A. (1996). Diesel particulate emission control. *Fuel Processing Technology*, 47, 1-69.
- Ochs, T., Schittenhelm, H., Genssle, A., & Kamp, B. (2010). Particulate matter sensor for on board diagnostics (OBD) of diesel particulate filters (DPF). *SAE Technical Paper*, 2010-01-0307.
- Otto, F. *Stömungsmechanische Simulation zur Berechnung motorischer Prozesse*. Hannover: Universität Hannover, Lecture Notes.
- Otto, S., Pfaff, R., Liebscher, T., Bogachik, Y., & Binder, S. (2006). *Patent No. DE102010052951*. Germany.
- Özel, M. (2009). *Literaturrecherche über die innenmotorische Beeinflussung der Emissionen und weiterer Zielgrößen*. Daimler AG, Internship report.
- Pasternak, M., Mauss, F., Janiga, G., & Thévenin, D. (2012). Self-calibrating model for diesel engine simulations. *SAE Technical Paper*, 2012-01-1072.
- Poorghasemi, K., Ommi, F., Yaghmaei, H., & Namaki, A. (2012). An investigation on effect of high pressure post injection on soot and NO emissions in a DI diesel engine. *Journal of Mechanical Science and Technology*, 26 (1), 269-281.
- Prasad, R., & Bella, V. R. (2010). A review on diesel soot emission, its effect and control. *Bulletin of Chemical Reaction Engineering & Catalysis*, 5 (2), 69-86.

- Rajkumar, S., Pramod, S. M., & Bakshi, S. (2011). Parametric investigation for NO_x and soot emissions in multiple-injection CRDI engine using phenomenological model. *SAE Technical Paper, 2011-01-1810*.
- Renner, G., & Maly, R. R. (1998). Moderne Verbrennungsdiagnostik für die Dieselmotorische Verbrennung. In U. Essers, *Dieselmotorentechnik 98*, Renningen, Malmsheim: Expert-Verlag, 174-188.
- Richards, P., Jouaneh, R., & Bradley, J. (2003). A cost effective solution to reduce particulate emissions. *SAE Technical Paper, 2003-26-0006*.
- Schiefer, D., Maennel, R., & Nardoni, W. (2003). Advantages of diesel engine control using in-cylinder pressure information for closed loop control. *SAE Technical Paper, 2003-01-0364*.
- Schmidt, M. (2007). *Bestimmung des Druckoffsets im Zylinderdrucksignal und des Polytropenexponenten mit estimationstheoretischen Methoden*. Karlsruhe: Hochschule Karlsruhe, Diploma thesis.
- Schnorbus, T., Pischinger, S., Körfer, T., Lamping, M., Tomazic, D., & Tatur, M. (2008). Diesel combustion control with closed-loop control of the injection strategy. *SAE Technical Paper, 2008-01-0651*.
- Schommers, J., Leweux, J., Betz, T., Huter, J., Jutz, B., Knauel, P., et al. (2008). The new Mercedes-Benz four-cylinder diesel engine. *MTZ Worldwide, 69* (12), 4-10.
- Schten, K., Ripley, G., Punater, A., & Erickson, C. (2007). Design of an automotive grade controller for in-cylinder pressure based engine control development. *SAE Technical Paper, 2007-01-0774*.
- Schubiger, R. A. (2001). *Untersuchungen zur Rußbildung und-oxidation in der Dieselmotorischen Verbrennung: Thermodynamische Kenngrößen, Verbrennungsanalyse und Mehrfarbenendoskopie*. Zurich: ETH Zurich, Ph.D.

thesis.

- Schubiger, R., Boulouchos, K., & Eberle, M. (2002). Soot emission from diesel combustion. *MTZ Worldwide*, 62 (05), 2-5.
- Sellnau, M. C., Matekunas, F. A., Battiston, P. A., Chang, C. F., & Lancaster, D. R. (2000). Cylinder-pressure-based engine control using pressure-ratio management and low-cost non-intrusive cylinder pressure sensors. *SAE Technical Paper*, 2000-01-0932.
- Sonntag, R. E., Borgnakke, C., & Van Wylen, G. J. (1998). *Fundamentals of Thermodynamics*. New York, Chichester, Weinheim, Brisbane, Singapore, Toronto: John Wiley & Sons, Inc.
- Stebler, H. (1998). *Luft- und brennstoffseitige Massnahmen zur internen NOx-Reduktion von schnell laufenden direkt eingespritzten Dieselmotoren*. Zurich: ETH Zurich, Ph. D. thesis.
- Stegemann, J., Meyer, S., Rölle, T., & Merker, G. P. (2004). Injection system for fully variable control of the shape. *MTZ Worldwide*, 65 (02), 13-16.
- Steuer, J., Mladek, M., Dengler, C., Mayer, W., Kracke, T., Jakubek, P., et al. (2009). Flexible engine control system for the development of innovative combustion processes. *ATZ Worldwide*, 4 (05).
- Stewart, G. E., Kolavennu, S. N., Borrelli, F., Hampson, G. J., Shahed, S. M., & Rhodes, M. L. (2006). *Patent No. US 7,155,334 B1*. United States of America.
- Stölting, E., Seeboda, J., Gratzke, R., & Behnk, K. (2008). Emission-based engine management for heavy-duty applications. *MTZ Worldwide*, 12.
- Stumpf, M., Velji, A., Spicher, U., Jungfleisch, B., Suntz, R., & Bockhorn, H. (2005). Investigations on soot emission behavior of a common-rail diesel engine

- during steady and non-steady operating conditions by means of several measuring techniques. *SAE Technical Paper*, 2005-01-2154.
- Sung, N., Lee, S., Kim, H., & Kim, B. (2003). A numerical study on soot formation and oxidation for a direct injection diesel engine. *Proceedings of the Institution of Mechanical Engineers, Part D: Journal of Automobile Engineering*, 217 (5), 403-413.
- Tao, F. G., & Chomiak, J. (2004, February). A phenomenological model for the prediction of soot formation in diesel spray combustion. *Combustion and Flame*, 136 (3), 270-282.
- Tree, D. R., & Svensson, K. I. (2007). Soot processes in compression ignition engines. *Progress in Energy and Combustion Science*, 33, 272-309.
- Tschöke, H., & Hieber, D. (2010). Verbrennungsverfahren für Dieselmotoren. In R. van Basshuysen, & F. Schäfer, *Handbuch Verbrennungsmotor, Grundlagen, Komponenten, Systeme, Perspektiven*, Wiesbaden: Vieweg+Teubner, 649-666.
- Vander Wal, R. L., & Tomasek, A. J. (2004, January). Soot nanostructure: dependence upon synthesis conditions. *Combustion and Flame*, 136 (1,2), 129-140.
- Vortmeier, A. (1998). *User guide DIESEI version 1.5, Internal Document*. Stuttgart: DaimlerChrysler.
- Vouitsis, E., Ntziachristos, L., & Samaras, Z. (2003). Particulate matter mass measurements for low emitting diesel powered vehicles: what's next? *Progress in Energy and Combustion Science*, 29, 635-672.
- Walker, A. P. (2004, April). Controlling particulate emissions from diesel vehicles. *Topics in Catalysis*, 28 (1-4), 165-170.

- Warey, A., Hendrix, B., Hall, M. J., & Nevius, T. A. (2004). A new sensor for on-board detection of particulate carbon mass emissions from engines. *SAE Technical Paper, 2004-01-1840*.
- Warth, M. (2005). *Comparative investigation of mathematical methods of modeling and optimization of common-rail DI diesel engines*. Zurich: ETH Zurich, Ph.D. thesis.
- Warth, M., Koch, P., & Boulouchos, K. (2003). Voarusberechnung von Brennverlauf NO- und Russemissionen beim Dieselmotor - Optimierung und Validierung eines neuen Ansatzes. *9. Tagung der Arbeitsprozess des Verbrennungsmotors*, Graz, 115-133.
- Weißborn, E., Bossmeyer, T., & Bertram, T. (2011). Adaptation of zero-dimensional cylinder pressure model for diesel engines using the crankshaft rotational speed. *Mechanical Systems and Signal Processing*, 25, 1887-1910.
- Wenzel, S. P. (2006). *Modellierung der Ruß- und NOx-Emissionen des Dieselmotors*. Magdeburg: Fakultät Maschinenbau, Otto-van-Guericke-Universität Magdeburg, Ph.D. thesis.
- Werner, P., Schommers, J., Breitbach, H., & Spengel, C. (2011). The new V6 diesel engine from Mercedes-Benz. *MTZ Worldwide*, 72 (05), 22-28.
- Weymann, H. (2009). *Neuronales Berechnungsmodell zur Bestimmung des Brennraumdruckverlaufes aus motorischen Messgrößen*. Siegen: Universität Siegen, Ph.D. thesis.
- Willems, F., Cloudt, R., van den Eijnden, E., van Genderen, M., Verbeek, R., de Jager, B., et al. (2007). Is closed-loop SCR control required to meet future emission targets? *SAE Technical Paper, 2007-01-1574*.
- Willems, F., Doosje, E., Engels, F., & Seykens, X. (2010). Cylinder pressure-based

control in heavy-duty EGR diesel engines using a virtual heat release and emission sensor. *SAE Technical Paper*, 2010-01-0564 .

Wimmer, A., & Glaser, J. (2002). *Indizieren am Verbrennungsmotor*. Graz: AVL List GmbH, User guide.

Xiaobei, C., Hongling, J., & Zhaowen, W. (2008). A numerical modeling and experimental study on soot formation for a direct injection diesel engine. *SAE Technical Paper*, 2008-01-1794 .

Zhijian, H., Ma, J., & Huang, H. (2011). In-cylinder optimal combustion with ADHDP method for diesel engines emission control. *Procedia Engineering* 15, 1051-1055.

APPENDICES

A.1 Specifications of In-Cylinder Pressure Sensors

Below are the specifications of the used cylinder pressure sensor used on engine test bench and vehicle application.

Table A.1 Cylinder pressure sensor specifications (Kistler).

Meas. range	0-250 bar
Sensitivity	~45 pC/bar
Sensitivity shift 250°C ± 100°C	≤±0.7 %
Thermal shock error (at 1500 1/min, imep = 9bar)	
Δp (short-term drift)	≤±0.3 bar
$\Delta imep$	≤±1.5 %
Δp_{max}	≤±1 %

A.2 Specifications of PM Measurement Instrumentation

In the following, some relevant specifications of the PM measurement devices presented in Table 3.3 are listed. For further information, please refer to the references.

Table A.2 Smoke Meter specifications (AVL List GmbH, 2012d).

Meas. value output	FSN pollution level or mg/m^3
Meas. range	0-10 FSN
Detection limit	0.002 FSN or $0.02 \text{ mg}/\text{m}^3$
Display resolution	0.001 FSN or $0.01 \text{ mg}/\text{m}^3$
Repeatability	~3% of meas. value

Table A.3 Opacimeter specifications (AVL List GmbH, 2012b).

Meas. value output	Opacity % or absorption m^{-1}
Meas. range	0-100% or 0-10 m^{-1}
Detection limit	0.1% opacity
Rise time	0.1 s

Table A.4 Micro Soot Sensor specifications (AVL List GmbH, 2012a).

Meas. value output	Concentration of soot in mg/m^3 in the diluted exhaust gas
Meas. range	0-50 mg/m^3
Detection limit	~0.005 mg/m^3
Display resolution	0.001 mg/m^3
Rise time	$\leq 1 \text{ s}$
Accuracy of DR (dilution ratio) display	max $\pm 3\%$ in the range of DR [2..10] max $\pm 10\%$ in the range of DR [10..20]

B.1 Nomenclature

Abbreviations

BDC	Bottom Dead Center
CA	Crank Angle
CFF	Combustion Form Factor
DPF	Diesel Particulate Filter
DI	Direct Injection
ECU	Engine Control Unit
EGR	Exhaust Gas Recirculation
EVO	Exhaust Valve Opening
FSN	Filter Smoke Number
HCCI	Homogeneous Charge Compression Ignition
HFM	Hot-Film Air-Mass Meter
HSDI	High Speed Direct Injection
IVC	Inlet Valve Closing
MAE	Mean Absolute Error
LNT	Lean NO _x Trap
MSS	Micro Soot Sensor
NEDC	New European Driving Cycle
NO _x	Nitrogen Oxides
OBD	On-Board Diagnostics
OPAC	Opacity
US06	US Supplemental Test Procedure
PAH	Polycyclic Aromatic Hydrocarbon
PM	Particulate Matter
PM10	Particulate Matter with diameter < 10μm
SCR	Selective Catalytic Reduction

SOI	Start of Injection
TDC	Top Dead Center
VTG	Variable Turbine Geometry

Variables

$\Delta\varphi_{comb}$	$^{\circ}\text{CA}$	main combustion duration
$\Delta\varphi_{diff}$	$^{\circ}\text{CA}$	diffusive combustion duration
λ_e	-	measured exhaust lambda
φ	$^{\circ}\text{CA}$	crank angle
τ_{char}	$^{\circ}\text{CA}$	characteristic time
A	-	model constant
B	-	model constant
C	-	model constant
dQ_{max}	-	max heat release rate
f	-	cost function
G_{XX}	-	system transfer function
K_{XX}	-	transfer function gain
$m_{air,in}$	mg/cyc	inducted air mass per cycle
$\dot{m}_{air,HFM}$	kg/h	air mass flow rate
m_{EGR}	mg/cyc	EGR mass per cycle
$m_{EGR,b}$	mg/cyc	burned EGR mass
$m_{EGR,u}$	mg/cyc	unburned EGR mass
$m_{u,IVC}$	mg/cyc	unburned air mass at IVC
m_{PM}	mg/cyc	particulate matter mass per cycle
m_{res}	mg/cyc	residual gas mass
$m_{res,u}$	mg/cyc	unburned residual gas mass
$m_{tot,IVC}$	mg/cyc	total cylinder charge mass at IVC
n	-	number of cylinders or polytropic exponent

n_X	-	model exponents
N	rpm	engine speed
p_3	Pa	exhaust gas pressure before turbine
p_{rail}	Pa	rail pressure
Q	J	cumulative net heat release
Q_{avail}	J	energy of injected fuel that is yet available for combustion
Q_{max}	J	max. cumulative net heat release
Q_{fuel}	J	chemical energy of injected fuel
Q_{XX}	J	xx% cumulative heat release point
R	-	correlation factor
R_{air}	J/kg-K	specific gas constant of dry air
T_3	K	exhaust gas temperature before turbine
V_c	m ³	min. cylinder volume
x_{EGR}	-	EGR ratio
x_{uEVO}	-	unburned gas concentration at EVO
x_{uIVC}	-	unburned gas concentration at IVC
X	-	model input
Y	-	model output

B.2 List of Figures

Figure 1.1 U.S. PM10 emission inventory in 1997. PM10 data include exhaust, brake, and tire wear emissions. “Mobile sources, diesel nonroad vehicles” includes railway locomotives, marine vessels and aircraft (Majewski & Khair, 2006). With PM10 it is referred to the particles with less than 10 μ m in diameter.	2
Figure 1.2 Exhaust manifold and the exhaust gas aftertreatment elements on an exemplary state of the art passenger car diesel engine designed to conform to the latest emission norms.	3
Figure 1.3 Methods of decreasing diesel engine emission levels according to the legislative emission limits	7
Figure 2.1 HSDI engine system layout without the exhaust gas aftertreatment. Extended from Schmidt (2007).	12
Figure 2.2 Effect chain of fuel injection (lower left) and charge movement parameters in the diesel engine combustion process and pollutant formation (Renner & Maly, 1998).	15
Figure 2.3 Types of combustion in internal combustion engines and their allocation to engine types (Otto F.).	16
Figure 2.4 Diffusive and premixed portions of the heat release rate approximated by Schubiger (2001) on a heat release rate curve for a single injection. Heat release rate of combustion can be calculated using in-cylinder pressure as described in section 3.2.1.	17
Figure 2.5 Approximated diffusive to total combustion ratio in terms of burned fuel mass fractions (Lay, 2009). Isometric view (left), diffusive portion ratio vs. bmep view (right).	18
Figure 2.6 (a) Qualitative representation of diesel engine combustion and pollutant formation regions (Merker & Stiesch, 1999). (b) Quasi steady diesel combustion plume displaying the NO production and soot concentration distribution (Dec, 1997).	19
Figure 2.7 Phases of soot formation and oxidation in diesel engine combustion, depicted over crank angle. Adapted from Hopp (2001).	23

Figure 2.8 A general look into soot formation and oxidation mechanisms. Adapted from Martinot, Beard, & Roesler (2001).	24
Figure 2.9 Soot yield map adapted from Warth, Koch, & Boulouchos (2003).	26
Figure 3.1 Operating points of calibration and validation datasets for the two engines.	39
Figure 3.2 Heat release calculation.	44
Figure 3.3 Installation of an exhaust gas sampling valve for measurements with MSS.	46
Figure 3.4 Particle emissions and their reference to different measuring principles. Adapted from AVL List GmbH (2005).	47
Figure 3.5 Fuel injection rate curve approximation (Barba, 2001).	49
Figure 3.6 Fuel injection rate curve calculation. Injector actuator signal and injection and estimated curve (top). Cumulative theoretical injected fuel energy (bottom)	52
Figure 3.7 NEDC (New European Driving Cycle) used for emissions testing and certification in Europe.	53
Figure 3.8 US06 driving cycle used for emissions testing and certification in USA.	53
Figure 4.1 Empirical approach to PM raw emissions modeling.	57
Figure 4.2 Mass composition in the cylinder at IVC	60
Figure 4.3 Determination of overall combustion duration (top) and diffusive combustion duration (bottom) variables.	62
Figure 4.4 Determination of the characteristic time: Available fuel energy (top), heat release rate curve (middle), characteristic time curve (bottom).	64
Figure 4.5 Measured vs. calculated PM mass per cycle for the steady state calibration data set from engine A. Polynomial model.	68
Figure 4.6 Measured vs. calculated PM mass per cycle for the steady state validation data set from engine A. Polynomial model.	69
Figure 4.7 Measured and calculated PM mass per cycle for the steady state validation data set from engine A. Polynomial model.	70
Figure 4.8 Measured vs. calculated PM mass per cycle for the steady state calibration data set from engine A.	74

Figure 4.9 Measured and. calculated PM mass per cycle for the steady state validation data set from engine A.....	74
Figure 4.10 Measured vs. calculated PM mass per cycle for the steady state validation data set from engine A.....	75
Figure 4.11 Measured and. calculated PM mass per cycle for the steady state validation data set from engine A.....	75
Figure 4.12 Load, EGR (top) and SOI (bottom) values for the steady state validation data set from engine A.....	76
Figure 4.13 PM Estimator input values for the steady state validation data set from engine A.....	77
Figure 4.14 Measured vs. calculated PM mass per cycle for the steady state calibration data set from engine B.....	78
Figure 4.15 Measured and calculated PM mass per cycle for the steady state calibration data set from engine B.....	78
Figure 4.16 PM emission from engine B during NEDC for transient validation data set. Please note that the emission values are normalized.....	79
Figure 4.17 Cumulative PM emission from engine B during NEDC for transient validation data set.....	79
Figure 4.18 Model variables from engine B during NEDC for transient validation data set. Please note that the emission values are normalized.....	80
Figure 4.19 Variable sensitivities for Region 1 Engine A.	81
Figure 4.20 Variable sensitivities for Region 2 Engine A.	82
Figure 4.21 Variable sensitivities for Region 3 Engine A.	82
Figure 4.22 Variable sensitivities for Region 4 Engine A.	83
Figure 4.23 Variable sensitivities for Region 1 Engine B.	84
Figure 4.24 Variable sensitivities for Region 2 Engine B.	84
Figure 4.25 Variable sensitivities for Region 3 Engine B.	85
Figure 4.26 Variable sensitivities for Region 4 Engine B.	85
Figure 4.27 Effect of deviations of in-cylinder pressure signal on model outputs for engine B. Interval from transient validation dataset.....	86
Figure 4.28 Effect of deviations of in-cylinder pressure signal on model outputs for engine B. Interval from transient validation dataset.....	87

Figure 4.29 Effect of deviations of in-cylinder pressure signal on cumulative model output for engine B. Transient validation dataset.....	87
Figure 5.1 Schematic representation of a model based raw emissions controller.	90
Figure 5.2 Relationship between CFF (Combustion Form Factor) and ratio of pilot injection to main injection amount.....	92
Figure 5.3 Cascaded controller structure.	92
Figure 5.4 In-cylinder emissions controller.	93
Figure 5.5 Operating points of engine B where the measurements were done for controller calibration.....	95
Figure 5.6 Variation of mPI at five different EGR rates for determining the linear gain $K11$ value (NOx/CFF) at two different operating points, low load (left), high load (right) on engine B.....	96
Figure 5.7 Variation of EGR at three different mPI rates for determining the linear gain $K12$ value (NOx/EGR) at two different operating points, low load (left), high load (right) on engine B.....	96
Figure 5.8 Variation of mPI at five different EGR rates for determining the linear gain value $K21$ (mPM/CFF) at two different operating points, low load (left), high load (right) on engine B.....	97
Figure 5.9 Variation of EGR at three different mPI rates for determining the linear gain value $K22$ (mPM/EGR) at two different operating points, low load (left), high load (right) on engine B.....	97
Figure 5.10 Inverse gain maps $K11 - 1$, $K12 - 1$, $K21 - 1$ and $K22 - 1$ for the transfer functions $G11$, $G12$, $G21$ and $G22$	98
Figure 5.11 Implementation of the developed PM estimator (Çebi & Binder, 2011).....	99
Figure 5.12 Hardware used for vehicle implementation of the developed PM estimator and emissions controller. Shown test vehicle is equipped with engine A.	100
Figure 5.13 Implementation of the ΔEGR controller with anti-windup and integrator reset in. ΔCFF controller implementation is analogous.....	101
Figure 5.14 Connections to the rapid prototyping system in the rear trunk of the test vehicle are enabled by a control panel built in the glove compartment.	101

Figure 5.15 Testing of emissions controller during quasi-steady free driving conditions.	102
Figure 5.16 Testing of emissions controller on vehicle test bench using NEDC test procedure. First two diagrams above depict two measurements, i.e. controlled and uncontrolled cases. Last three refer only to the controlled case.	103
Figure 5.17 Comparison of MSS measurement versus PM estimator calculation in NEDC test procedure on vehicle test bench. Controlled case.	104
Figure 5.18 Testing of emissions controller on vehicle test bench using US06 test procedure. First two diagrams above depict two measurements, i.e. controlled and uncontrolled cases. Last three refer to the controlled case.	105
Figure 5.19 Comparison of MSS measurement versus PM estimator calculation in US06 test procedure on vehicle test bench. Controlled case.	106
Figure 5.20 Comparison of test results of the PM estimator with two different measurement techniques, gravimetric (particle sampler) and MSS.	107
Figure 5.21 Effect of the emissions controller on emissions and fuel consumption. Controlled case is compared to the uncontrolled case for US06 and NEDC tests. PM is based on gravimetric measurement.	109

B.3 List of Tables

Table 1.1 EU emission standards for passenger cars with compression ignition (diesel) engines. Taken from DieselNet (2012).	3
Table 3.1 Specifications of the engines that are used for the model development (Werner, Schommers, Breitbach, & Spengel, 2011; Schommers, et al., 2008).	38
Table 3.2 Further information on the calibration and validation datasets.....	40
Table 3.3 Devices used for PM emissions measurement.....	45
Table 4.1 Empirical model inputs. Second column from the left shows the indices of the variables after scaling.	58
Table 4.2 Empirical models are calibrated for these four engine operating regions separately.	66
Table 4.3 Model parameterization constraints used in calibration.	72
Table 4.4 Model parameterization, engine A.....	73
Table 4.5 Model parameterization, engine B.	73
Table A.1 Cylinder pressure sensor specifications (Kistler).....	131
Table A.2 Smoke Meter specifications (AVL List GmbH, 2012d).	132
Table A.3 Opacimeter specifications (AVL List GmbH, 2012b).	132
Table A.4 Micro Soot Sensor specifications (AVL List GmbH, 2012a).	132

*“Hayatta en hakiki mürşit ilimdir, fendir,
ilim ve fenden başka yol gösterici aramak
gaflettir, dalalettir, cehalettir.”*

M. Kemal Atatürk